Thermochemical and topological studies of systems constituted by transition metals (Co, Ni) with Sn and Bi

Kristina Lilova

Nancy-Université
Université Henri Poincaré

FACULTE DES SCIENCES & TECHNIQUES **FACULTE DE CHIMIE**

U.F.R. Sciences & Techniques de la Matière et des Procédés
Ecole Doctorale EMMA

Département de Formation Doctorale PCMM

Thèse

présentée pour l'obtention du titre de

Docteur de l'Université Henri Poincaré, Nancy-I

en Physique et Chimie de la Matière et des Matériaux

par Kristina Ilcheva LILOVA

Thermochemical and topological studies of systems constituted by transition metals (Co, Ni) with Sn and Bi

Soutenance publique: 7 juin 2007

Membres du jury :

Rapporteurs :	Ljuben Terziev	Prof. dr., Université de Sofia, Bulgarie
	Jacques Rogez	DR. CNRS, Université P. Cezanne, Marseille
Examinateurs :	Jean-Claude Tédenac	Professeur, Université de Montpellier 2
	Nina Dimcheva	Ass. Prof. dr, Université de Plovdiv, Bulgarie
	Gueorgui Vassilev	Pr. dr. Université de Plovdiv, Bulgarie codirecteur du travail
	Jean-Claude Gachon	Professeur, U.H.P., Nancy I codirecteur du travail

Gratitudes

I would like to express my deepest gratitude to Professor Jean-Claude Gachon and to Professor Gueorgui Vassilev for their excellent supervision, guidance, reviewing and editing of the manuscript, continuous encouragement and support throughout my work.

I am sincerely in debt to Prof. Gachon who has introduced me to the areas of calorimetry in practice by motivating perfectly. I also would like to thank him for hospitality and valuable help for any-related problems.

I am also extremely grateful to Prof. Vassilev for his enormous patience and support through every stage of my Ph. D studies, for everything he taught me during these three years.

I also would like to thank to whole laboratory team from LCSM, Nancy for giving me the opportunity to do the research and for their help in my experimental work.

Finally, I would like to show my very special thanks and appreciation to my family for unbelievable support, continuous motivation and patience.

Summary

Introduction

A phase diagram is the shortest and the most essential representation of the phase equilibria in a system. The knowledge of the phase diagram and the stabilities of the pertinent phases is mandatory for the understanding and the control of processes like crystallization, solid-state transformations and the accompanying microstructure formation (changes). The control of the microstructures is often essential for the design of mechanical or other (magnetic, electric) properties. That is why such a studies are fundamentally related with the development of new materials.

Moreover, with the progress of the computers the thermodynamic modelling of various systems becomes easier. The thermodynamic descriptions achieved for the stable or unstable phases can be used for quantitative assessment of the moving forces for the phase transitions, chemical reactions or diffusion processes. Some physico-chemical properties (e.g. surface tension and viscosity of the liquid phases) can also be modeled using thermodynamic descriptions of the respective phases.

An example related with the investigations presented in this work is the design of lead-free solders. Their development is closely linked with environmental and health concerns because lead is rather toxic for human beings.

The construction of phase diagrams is important for the investigation of alloys systems. Knowledge of phase equilibria, phase stability and phase transformation is essential for the description and understanding both of the fundamental properties of the alloys and of their possible technological applications. In order to obtain accurate data, it is obligatory to carry out research on binary and ternary systems. Experimental studies, in combination with a thermodynamic optimization, allow a complete evaluation of mechanical, physical and chemical proprieties and also a modeling of different processes (diffusion, crystallization, etc.). The results, given by appropriate models can be used to modify the microstructure of different materials, to assess the viscosity and surface tension of liquid.

Increasing interest to phase diagram science is clearly evident, for example, by the growth in the number of publications, books and journals, in which data, relevant to phase diagrams are systematically reported and assessed. Another clear indication of the relevance of these data and of their reliability is given by the growing number of different actions, often organized on an international basis, devoted to the assessment and critical evaluation of phase equilibria data.

Solders, providing the ohmic contacts (joining electronic components to circuit boards) in almost all of electronic devices are based, typically, on Pb-Sn eutectic. The main risk of lead contamination is due to electronic waste (e-waste) - a waste type consisting of any broken or unwanted electrical or electronic appliance. It is a point of concern considering that many components of such equipment are toxic.

Once in the environment, the lead from electronic equipment migrates from soil into groundwater and afterwards bioaccumulates in the food chain. Probably these processes are connected with some reactions between lead containing solders and oxygen, carbon dioxide, chlorides in the water.

Due to the high toxicity and environmental impacts of lead, research and development of alternative, lead-free solders have become a necessity. The European Commission adopted proposals for a Directive on Waste Electrical and Electronic Equipment (WEEE) and the Directive on the Restriction of the Use of Certain Hazardous Substances in Electrical and Electronic Equipment (RoHS) in 2002. The objectives of these proposals are to prevent waste, promote reuse and recycling of electrical and electronic equipment and to substitute lead and other heavy metals in electrical and electronic equipment by January 1, 2007.

COST Action 531 is a part of Framework Program 6 of the European Union. The main objective of Action 531 is generating and systematizing information of thermochemistry, phase relations and physical properties of alloy systems that can be used as lead-free solder materials in order to replace the currently used lead-containing solders in the future. One of the aims is creating a Thermodynamic database, including elements Ag, Au, Bi, Cu, In, Ni (P), Pb, Pd, Sb, Sn and Zn.

Various research groups out of COST 531 became partners in the FP6 Coordination Action ELFNET (European Lead-Free Soldering Network), which consists of universities, research institutions, as well as industrial partners from 19 European countries.

The aim of the present work is to contribute to the knowledge of prospective lead-free solder systems based on tin and with participation of transition metals (namely Co–Sn, Ni–Sn and Ni–Sn–Bi). It was done in the frame of the European action for development of lead-free solders COST 531. For this purpose thermochemical and topological studies had to be performed. Moreover critical assessment of literature data was planned.

In the scope of this work are also included verifications of previous experimental results and thermodynamic optimizations, acquiring of new information about phase equilibria, enthalpies of formation, phase transformations and re-optimization of phase diagrams where appropriate (i.e. Co–Sn system).

In the thesis various experimental techniques were employed: Direct Reaction and Drop Solution Calorimetry; CALPHAD method, Differential Scanning Calorimetry, Differential Thermal Analyses, X-ray diffraction, Scanning Electron Microprobe Analyses, etc. Special attention was given to the first techniques thus they are described in Chapter One

Chapter I

Experimental Techniques and Computational Thermodynamics

I.I Experimental Techniques

Enthalpies of formation ($\Delta_f H$) are commonly used to characterize alloy formation and stability and they are a primary source of data for alloy theory. $\Delta_f H$ is generally measured using high temperature techniques such as solution calorimetry or direct reaction calorimetry. In the case of transition elements, temperatures in excess of 1273 K are often needed to complete formation reactions. Accurate determination of $\Delta_f H$ at these temperatures is experimentally demanding, and great care must be taken to avoid environmental contamination. Many of the oxidations due to environmental contamination are highly exothermic, so small amounts of contamination, even in relatively pure atmosphere, may result in large errors in measured heats. Such difficulties have limited the availability of enthalpies of formation for transition metal systems [1].

➢ Calorimetry

Calorimetry has developed historically within bounds imposed by available measurement technology and by the spectrum of construction materials. The first calorimetric measurements of heat content were made in the easily accessible temperature range and were based on some variation of the "method of mixture". For practical reasons, this is usually done by physically dropping a specimen into a calorimeter; hence, the terms "drop calorimetry" and "drop calorimeter", etc.

Generally, the specimen temperature is equal to or lower than that of the calorimeter. The heat content of the specimen is inferred from the measured signal of the calorimeter through the independent application of some energy-calibration procedure to the calorimeter, either before or after the specimen experiment. Joule effect can be used for calibration.

The introduction of improved construction materials and fabrication techniques, along with electronic power supply, temperature control, and data recording, has greatly expanded the temperature range in so-called “drop calorimetry” and simultaneously lowered the levels of imprecision and inaccuracy of this method. The term “drop solution calorimetry” will be preferred in the present work in order to distinguish two used methods: solution and direct reaction calorimetry.

In a calorimetric determination, many factors have to be considered. Their influence varies according to the type of DTA, DSC or calorimeter that is used for the measurement. The main influencing factors are:

Temperature: one of the main influencing factors, as thermal analysis techniques cover a wide range, from very low to very high temperature. Temperature will affect the sensitivity of the detector, the stability of the baseline, the choice of container and type of sample to be investigated (e.g. solid or liquid). Heat capacity also varies with temperature.

Sample mass: The choice of sample mass depends on the type of calorimetric detector used for the test. For DTA and plate DSC types, a small sample mass (some mg) has to be used in order to guarantee a good heat transfer through the bottom of the crucible. By increasing the mass, the heat leakages are more important and the detector has to be recalibrated.

Sample type: Both solid and liquid samples are investigated with calorimetric techniques. When a solid sample is heated in a closed and tight container, an internal pressure can build up in the crucible, produced by moisture from the sample or its decomposition. Care is needed to prevent explosion of the container. With a liquid sample in a tight crucible, the problem is identical. If the crucible is not tight, heating the liquid sample will generate a leak of vapour, producing an endothermic effect that can possibly mask the transition to be measured.

Crucible: The nature of the crucible (aluminium, stainless steel, glass, ceramic) has to be selected according to different parameters: good thermal conductivity; no interaction between the sample and carrier gas; type of closing (tight or not tight); pressurisation.

Carrier gas: Different carrier gases can be selected: inert, oxidative, reducing. As the thermal conductivities of gases differ, the calibration factor can be affected. It is also necessary to check that there is no interaction between gas and detector or crucible [2].

I.I.1. Direct Reaction Calorimetry

The formation reaction itself (the synthesis of the alloys from the pure metals) takes place into the calorimeter. The main difficulty is to start the reaction inside the component mixture and have it running in a controlled manner inside the calorimeter.

The direct synthesis of the alloys (exothermic and also endothermic) from a component mixture can be conveniently carried out in high-temperature calorimeters.

According to the heating regime we may have:

– continuous heating mode when the sample is continuously heated up to the reaction temperature, as in the DTA technique (scanning calorimetry, DTA, etc)

– high temperature isothermal calorimeters. A typical calorimeter pertaining to this category is the drop calorimeter. The sample (for instance a pellet of the component mixture) is dropped from a lower temperature thermostat (often room temperature) into the high temperature calorimetric cell. The calorimetric cell is maintained at a temperature high enough to ensure that the reaction occurs [5].

In our case, direct reaction calorimetry has been employed by means of a calorimeter designed and built [9] in a Setaram furnace (called further Gachon–calorimeter) and by Setaram–Calvet 800 C calorimeter. In all the manuscript RT means room temperature and CT means calorimeter temperature.

➢ Details about the manipulations

Direct reaction experiments were performed by inserting pellets (initially at room temperature) in a calorimeter crucible, kept at constant temperature. It has been maintained within an interval of ±2 K (Setaram–Calvet 800 C) and ±3 K (Gachon–calorimeter). The number of sample pellets is always equal to the number of α–Al_2O_3 pellets, mainly used for a calibration.

After introducing a specimen at room temperature into the calorimeter, a large endothermic peak appears due to heat adsorption. An (usually) exothermic chemical reaction between the pure constituents starts while the specimen temperature increases. That is why, after some time, the signal sign changes (i.e. an exothermic part of the curve appears) when the sample temperature becomes higher than that of the crucible and finally returns to the baseline value after the reaction is finished or when its kinetics has become such slow that there is no remaining

detectable heat effect. . The exothermic part appears only if the negative formation enthalpy is negative and if its quantity is high enough to overcome the endothermic contribution. No exothermic part appears if the enthalpy of formation is positive). This could also happen if the quantity of heat produced is not large enough to compensate the endothermic flux (e.g. when the reaction is incomplete). The reaction could start around 8–10 s after introducing the sample and be completed in around 11 – 15 minutes (depending on the mass of the sample) in the Gachon–calorimeter. Reactions times in Setaram – Calvet apparatus vary quite a lot, depending on the temperature, masses, reactivity, etc, of the metals. In general, they exceed 1 hour and occasionally prolong up to 6 hours or more. These long times are due to slow reactions and not to the time constant of the calorimeter. In the Calvet, this is not a source of uncertainty, because the baseline is stable at the microvolt level for weeks.

In order to avoid oxidation of the materials, all the samples have been prepared in a glove box under argon atmosphere (99.9995% Ar). The initial compositions were calculated depending on the compound, which has to be obtained. Powdered metals (325 mesh for Co, Sn, Bi and 200 for Ni) were weighed, and then mixed and the mixture homogenized in a porcelain mortar for about 30 – 40 minutes. Afterwards pellets with 1.5 mm thickness and 5 mm of diameter have been prepared with a manual press (Fig. II.I.1.1). The mixture of metals is supposed to be homogeneous and five pellets are prepared. Generally, calorimetric results confirm the homogeneity, but we check the composition of one pellet after the measurements. If one of the five calorimetric results is different from the others, it is discarded. It is impossible during the preparation of samples to check visually the homogeneity of the mixture, because the different powders are absolutely of the same aspect. Only one system, studied in the laboratory, allowed to check homogeneity during preparation: ZrAu, because of the different colors. In this case, obviously pouring the mixture into the press induced a separation between gold and zirconium. The difficulty was overcome by mixing carefully small quantities and preparing one pellet from this mixture.

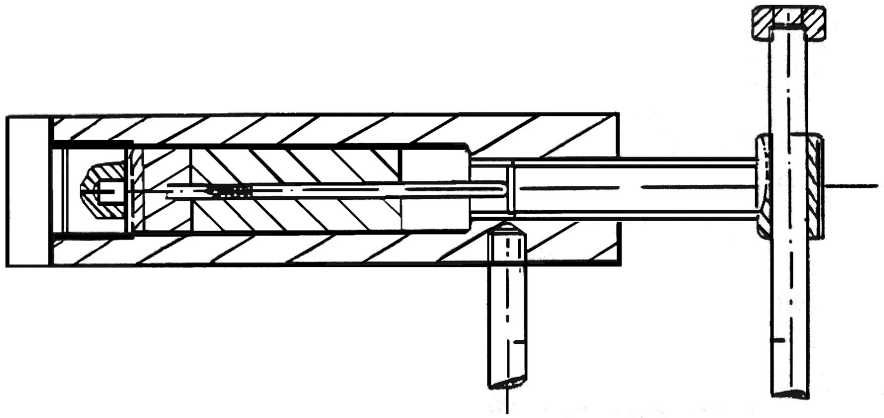

Fig. I.I.1.1 Manual press

The specimens were weighed and sealed hermetically under argon in the distributor to be transported and dropped into the calorimeter together with pieces of α–Al_2O_3, which have been used for calorimeter calibrations.

Literature data for the heat capacity of α–Al_2O_3 is used for the calculation of the calorimetric constant (KEM). We use ordinary α–Al_2O_3 as the comparison between this commercial α–Al_2O_3 and the standard reference material 720 of the NBS did not show a noticeable difference. Thermal curves, obtained as a result of the change in the equilibrium state of the specimen have only an endothermic part, which due to heat adsorption. This peak is proportional to the quantity of heat, interchanged between the calorimeter crucible and its environment. The exact definition of the baseline as a part of the recorded curve without any reactions or transitions is very important, but easy in the Calvet, because it is stable for weeks, so we admitted that the baseline was the same during the reaction as before and after. In the high-temperature calorimeter the definition is less obvious, because the baseline is less stable. At high temperatures (more than 1300 ^{0}C) the baseline is different after dropping an alumina piece or a metallic sample. In this case, we compared two different possibilities: first a straight line joining the two points selected as beginning and end of the signal; second a curve computed with the constraints of having the same tangents as the baselines at the points selected as beginning and end of the reaction. In case of noticeable difference between the signal before and after reaction the second possibility gave better results than the first. Fig. I.I.1.2 represents a real calorimetric curve, obtained by direct reaction between pure Co and Sn at 356^{0}C using Setaram–Calvet 800 C apparatus.

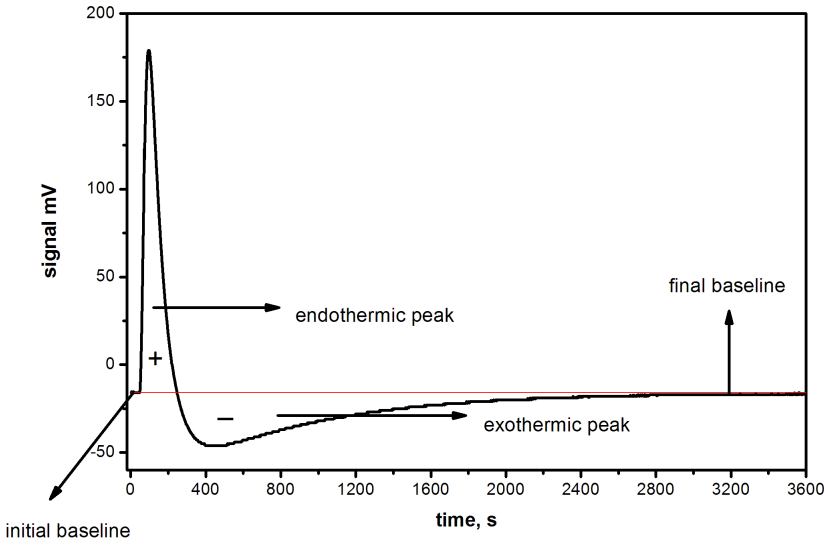

Fig. I.I.1.2 Example of a calorimetric curve, obtained by direct reaction calorimetry.

In both Calvet and Gachon calorimeters, the value (electric signal at instant minus base line level) is proportional to the thermal power exchanged between the sample and its surroundings. Thus, integrating this quantity on the total duration of the reaction gives, after calibration, to the heat effect of the sample inside the crucible. Following the principle of initial and final states, this heat effect can be considered as the sum of two contributions: the enthalpy increments of the pure metals from room to calorimeter temperatures and the enthalpy of reaction at the calorimeter temperature.

Peak area (area enclosed between the peak and the interpolated baseline) is calculated by means of Origin software. Thus, the expression for the calculation of the calorimetric constant is:

$$KEM = \frac{n * \left[(H_{\sup} - H_{RT}) + (H_{\inf} - H_{RT}) + Cp_{\inf} * (T_{CT} - T_{\inf}) - Cp_{\sup} * (T_{\sup} - T_{CT}) \right]}{2 * S} \quad \text{(I.I.1.1)}$$

where S is the peak area; n – mole fraction; $(H_{\sup} - H_{RT})$ – enthalpy increment of α–Al_2O_3 from room temperature (RT) to T_{sup}; $(H_{\inf} - H_{RT})$ – enthalpy increment of α–Al_2O_3 from room temperature to T_{inf}; T_{CT} – temperature of the measurement (CT); $Cp_{\sup}$ – heat capacity of α–Al_2O_3 at $T_{sup,}$ that is the closest tabulated temperature, but greater than T_{CT} ; $Cp_{\inf}$ – heat capacity of α–Al_2O_3 at T_{inf}, that is the closest tabulated temperature, but lower than T_{cal} temperature;

The enthalpies and specific heat values ($(H_i - H_{RT})$ and C_P) are taken from the reference [3]. Standard deviations of the calorimetric constant measurements are around 2 to 3 %,

The measured molar enthalpy of formation could be associated with a chemical reaction, when it occurs completely:

$$xA(s)^{RT} + yB(s)^{RT} = A_xB_y(s)^{T_{CT}} + H_{total} \qquad \text{(I.I.1.2)}$$

x, y are the molar fraction of components A and B (x + y = 1).

The enthalpies of formation ($\Delta_f H$) are calculated (per mole of atoms) using the expressions (with CT – calorimeter temperature, RT – room temperature):

$$\Delta_f H = H_{total} - H_{RT}^{CT} \qquad \text{(I.I.1.3)}$$

where the total enthalpy change, measured during the manipulation is:

$$H_{total} = \frac{S.KEM}{n} \qquad \text{(I.I.1.4)}$$

where n is the quantity of moles of A_xB_y

and the enthalpy change due to the temperature increase from T_{RT} to T_{CT} (temperature of the measurement) is:

$$H_{RT}^{CT} = xH_{RT}^{CT}(A) + yH_{RT}^{CT}(B) \qquad \text{(I.I.1.5)}$$

$$H_{RT}^{CT}(A) = \frac{(H_{\sup} - H_{RT}) + (H_{\inf} - H_{RT}) + Cp_{\inf}(A) * (T_{CT} - T_{\inf}) - Cp_{\sup}(A) * (T_{\sup} - T_{CT})}{2}$$

(I.I.1.6)

Here S is peak area, KEM – calorimetric constant, A and B – elements; x and y are the molar fraction of components A and B; $Cp_{\sup}$ – heat capacity of pure element A at $T_{sup,}$ closest tabulated temperature, but greater than T_{CT}; $Cp_{\inf}$ – heat capacity of pure element A at T_{inf}, that is the closest tabulated temperature, but lower than T_{CT} temperature; $H_{\sup} - H_{RT}$ – enthalpy increment of the pure element A from room temperature to T_{sup}.

The peak area is calculated by means of Origin software in the same way, described above.

➢ Description of Gachon calorimeter

The furnace, which provides the desired temperature in the interval between 300 and 1800 K, is a commercial Setaram model ("2400"), built for calorimetry and differential thermal analysis. A graphite resistor assures a zone without thermal gradient about 10 cm of height (in fact the temperature variation is roughly 10^{-3}*CT). That resistor is disposed around a vertical laboratory tube made of alumina with 22 mm internal diameter and 50 cm height. It is surrounded by a thick layer of graphite felt (≈6 cm) contained inside a double wall jacket, where cooling water circulates. The whole furnace interior is protected by an argon flow, which avoids graphite oxidation.

The resistor receives energy from a Setaram TGC 85 electronic controller, which provides a maximum power of 3 kW. The temperature information is received from a Pt – Pt – PtRh10% thermocouple, settled in the laboratory tube just beneath the calorimetric sensor in the zone without thermal gradient. The TGC 85 electronic controller possesses three actions: proportional, integral and differential (P.I.D.), which are separately adjustable by means of a keyboard at the front. That kind of control provides an easy and simple adjustment of the parameters, but do not allow their change during the experiment without seriously perturbing the system. The values of the three actions depend on the type of experiment: isothermal (measurements of the enthalpies of formation or mixing) and anisothermal (differential thermal analysis) temperature range and heating rate. The TGC 85 electronic controller allows to link up 10 sequences, each one composed of an isotherm (duration between 0 and 9999 s), followed by a ramp (heating or cooling). Rates between 0.1 and 99.99 deg/min are theoretically possible. In fact, real heating and cooling rates are limited by the furnace characteristics.

The calorimetric cell has been conceived by Gachon [9] with the purpose to obtain a robust apparatus, easy repairable in the laboratory (Fig. I.I.1.3).

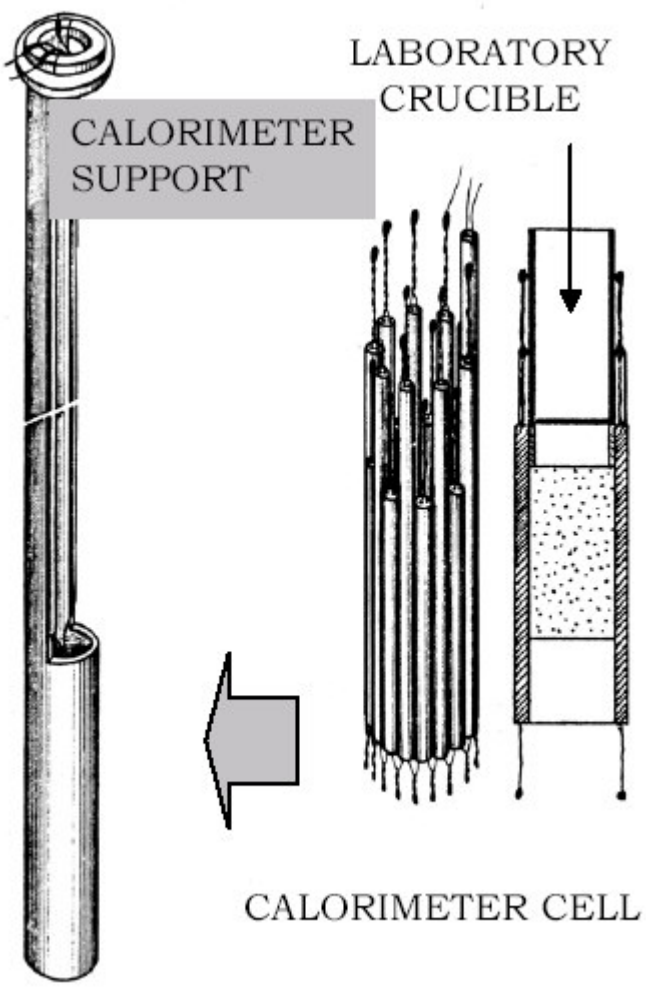

Fig. I.I.1.3 The calorimeter scheme

The main part represents a solid support, made of a modified alumina tube with exterior diameter of 20 mm and interior of 15 mm. The lower part of the support has a cylindrical shape with 9 cm length, which assures a radial symmetry for the thermal exchange on all levels. The upper part consists of a semi-cylinder cut along opposed generatrixes. The opening gives access to the cylindrical part for placing the thermopile and the crucible.

The thermopile is made of a series of thermocouples; hold by alumina two bore tubes, which are kept together by refractory cement. The junctions are 1 cm long and they are situated on two different levels around the crucible in order to minimize the thermal resistance between thermocouples and crucible and to limit sensitivity variation when filling the laboratory crucible. When DTA measurements are performed, all the junctions should be at the same level.

It's possible to use different kinds of wires to build the sensor: pure Pt and PtRh10%, PtRh6%–PtRh30%, or Ni/Cr–Al/Cr. We made two piles, preferring Ni/Cr–Ni/Al thermocouples

instead of Pt/Rh 10 %. They are cheaper and more sensitive, but their upper temperature limit is about 1400 K.

The laboratory crucibles are alumina hollow cylinders with exterior diameter 10 mm, interior 9 mm and 40 mm height. During one single experiment, the level of samples, dropped into the crucible, do not exceed 1 cm, i.e. the thermal effects remain always in the zone covered by the thermocouples.

Dropping of the sample from a distributor at the top of the furnace into the crucible is realized through a thin alumina tube (0.5mm thick) placed in the semi-cylindrical part of the support.

The whole calorimeter is tightly closed and works under a permanent argon flow during experiments. Samples, prepared in a glove box under purified argon, are introduced by means of a tight distributor, which ties together with the upper part of the calorimeter. That device consists of twelve sections. Generally, half of them are used for alumina pieces and the other half for the samples.

Two signals are registered at the same time: calorimetric signal from the thermopile and temperature from a thermocouple, placed at the crucible level, near to the sample. The thermopile signals are saved as a file on the hard disk of a PC, connected to the calorimeter. The second signal allows verifying the real temperature inside the furnace during the experiments.

➢ Description of Setaram–Calvet 800 C calorimeter

Setaram–Calvet 800 C calorimeter was used both for direct reaction and drop solution calorimetry. It is a heat exchanging (heat flux) calorimeter (Fig. I.I.1.4). In a heat exchanging calorimeter, the specimen surroundings (generally the furnace and detector) are at constant temperature (isothermal mode) or at a variable temperature (scanning temperature mode). The amount of heat flowing (heat flow rate) is determined on the basis of the temperature difference along a thermal resistance between the specimen and its environment.

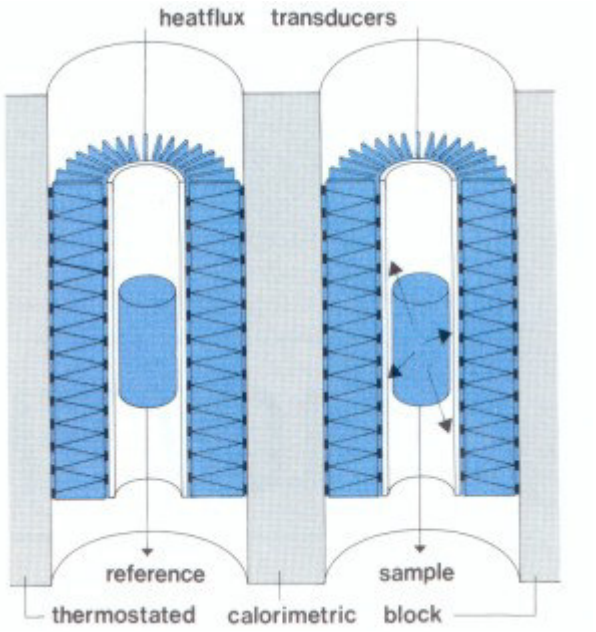

Fig. I.I.1.4 A heat flux calorimeter scheme

Sample and reference containers are surrounded by thermopiles, each one made of 400 thermocouples. The temperature differences between the internal and external surfaces of sensors are proportional to both the EMF of each thermocouple and the thermal power which is transmitted by the thermocouple wires which means that the total electrical signal of a thermopile is proportional to the thermal power which is exchanged between inside (crucible) and outside (calorimeter block) through the thermopile. Such a design guarantees the measurement of the nearly total heat exchange between the sample and the surroundings through the calorimetric detector, except for the two solid angles (top and bottom), which are not covered by the thermocouples.

Contrary to the DSC plate detection principle, the sensitivity of the calorimeter does not depend heavily on the nature of the experimental vessel, the nature of the gas around the sample or the sample size.

This type of calorimetric technique allows the development of calorimeters for investigating large samples and the development of specific vessels for mixing and reactions.

The Calvet principle is typical for microcalorimetry (μC) but it is also used in DSC, and in some cases in Reaction Calorimetry (RC). The instruments based on this principle are the most sensitive. However, they are usually limited to low heating rates and moderate temperatures.

Setaram–Calvet 800 C apparatus is characterized with very stable signal and respectively very stable baseline. Because of its high sensitivity, a small and sudden change in the environment temperature can affect strongly the baseline. Preliminary experiments have shown that the temperature fluctuations could be less than $\pm 1\ ^{0}C$ for some weeks provided that the conditions are kept approximately constant. This high level of stability is necessary when slow reactions are studied. When the calorimeter temperature is relatively low, reaction times increase and can reach more than 7 hours (solid phase reaction). In such a case, a measurement can be significant only if the baseline is the same after the reaction is finished as it was before its beginning, which is the case for our experiments.

I.I.2 Drop Solution Calorimetry

Drop calorimetry is the method by which most of the high-temperature heat capacity data in the literature have been determined. Drop calorimetry has few temperature limitations and can use any type of sample container. On the other hand, it is extremely slow, makes only one measurement of sensible heat at a time. The need to determine heat capacities as the derivative of a sensible-heat curve reduces accuracy [4].

In all drop calorimetry experiments, the specimen, first brought to an initial thermodynamic equilibrium state (state while outside the calorimeter), is dropped inside the calorimeter, at a different (higher for us) temperature. As a result of this change, the calorimeter proceeds from its own initial thermodynamic equilibrium state prior to adding the specimen to some final state while containing the specimen. The specimen proceeds at the same time to its final equilibrium state within the calorimeter. In the ideal experiment, the specimen and the calorimeter each have the same temperature throughout in their final states. The physical quantity which one aims to obtain through this measurement is the enthalpy change of the specimen upon entering the calorimeter. To achieve this, at least one additional experiment (calibration) is needed. In this calibration, one measures the amount of heat, Q_{calib}, required to produce the identical change in state of the calorimeter as the specimen.

Consider now the specimen in the calorimeter and the thermodynamic definition of its enthalpy:

$$H = U + pV \qquad \text{(I.I.2.1)}$$

For an infinitesimal change in the equilibrium state of the specimen,

$$dH = dU + pdV + Vdp \qquad \text{(I.I.2.2)}$$

However, the heat dQ transferred between the specimen and calorimeter in this change,

$$dQ = dU + pdV \qquad \text{(I.I.2.3)}$$

Therefore

$$\frac{dH}{dT} = \frac{dQ}{dT} + V\frac{dp}{dT} \qquad \text{(I.I.2.4)}$$

where dT is the infinitesimal change in the thermodynamic temperature of the specimen that is associated with the change of state.

Under isobaric conditions which apply in all drop calorimetry, except measurements on volatile liquids

$$\left(\frac{dH}{dT}\right)_p = \left(\frac{dQ}{dT}\right)_p = C_p \qquad \text{(I.I.2.5)}$$

where C_P denotes the specific heat

Thus, the change in specimen enthalpy under these conditions is equal to the heat transferred between the calorimeter and the specimen

$$\int_{T_c}^{T_i} dH = H_{T_i} - H_{T_c} = Q = \int_{T_c}^{T_i} C_p dT \qquad \text{(I.I.2.6)}$$

where T_i is the initial specimen temperature and T_c – the final temperature common to both specimen and calorimeter.

Further, the entropy and Gibbs energy can be calculated [2]:

$$S_{T_i} = S_{T_c} + \int_{T_c}^{T_i} \frac{C_p}{T} dT \qquad \text{(I.I.2.7)}$$

and

$$-\frac{(G_{T_i}-H_{T_c})}{T_i}=S_{T_i}-\frac{(H_{T_i}-H_{T_c})}{T_i} \qquad \text{(I.I.2.8)}$$

➢ Details about the manipulations

Regarding the preparation of the samples, pieces of solid Sn (4N) were used. They were weighed and sealed in a distributor under argon. Sn pieces were used both for calorimeter calibrations and to create a liquid bath.

The calorimeter manipulations and calibration are done in the same way as described in I. 1. The only difference is replacing the α–Al_2O_3 with pure tin.

Compared to the direct reaction calorimetry, the duration of trials are longer, especially if a big difference between the melting temperatures of the components exists.

The partial enthalpy of mixing ($\Delta_f \bar{H}_B^L$) at the mean concentration between beginning and end of sample dissolution is identical with the heat of dissolution for one mole of atoms:

$$\Delta_f \bar{H}_B^L=\frac{S.KEM}{n_B}-H_{RT}^{CT}(B) \quad \text{(I.I.2.9)}$$

and

$$H_{RT}^{CT}(B)=\frac{(H_{\sup}-H_{RT})+(H_{\inf}-H_{RT})+Cp_{\inf}(B)*(T_{CT}-T_{\inf})-Cp_{\sup}(B)*(T_{\sup}-T_{CT})}{2}$$

(I.I.2.10)

where S is peak area; KEM – calorimetric constant; H_{RT}^{CT} – enthalpy change due to the temperature increase from T_{RT} to T_{CT} (temperature of the measurement); $(H_{\sup}-H_{RT})$ - enthalpy increment of the pure element B from room temperature to T_{sup} ; T_{CT} – temperature of the measurement; heat capacity of pure element B at $T_{sup,}$ closest tabulated temperature, but greater than T_{CT}; heat capacity of pure element B at T_{inf}, that is the closest tabulated temperature, but lower than T_{cal} temperature; T_{RT} – room temperature

The integral enthalpy of mixing of both components A and B is calculated, using the expression:

$$\Delta_f H^L = \frac{\sum_i \Delta_f \bar{H}^L_{B_i} n_B}{n_A + n_B} \qquad \text{(I.I.2.11)}$$

and

$$n_j = \frac{m_j}{M_j}; \qquad \text{(I.I.2.12)}$$

n_j – quantity of j^{th} sample, m_j – mass of the j^{th} sample.

Whatever the calorimetric techniques used may be (room, high temperature, etc.), an accurate check of the state, composition, etc. of the synthesized alloy is necessary (for instance by X–ray diffraction, optical and electronic microscopy, electron–probe microanalysis, etc.) [5]

The Electron Probe Micro Analysis (EPMA) measurements were carried out on a Cameca SX 100 instrument using wavelength dispersive spectroscopy (WDS) for quantitative analyses and employing pure metals as standard materials at 15 kV with a beam current of 20nA. Scanning Electron Microscope (SEM) images are made in Back Scattered Electrons (BSE), which are high-energy electrons that rebound from the sample surface. They ca be used to detect contrast between areas with different chemical compositions. The quantity of electrons backscattered from a given surface is proportional to the mean atomic number (Z) of the sample material.

Samples to be examined by scanning electron microscope (SEM) techniques were embedded in a resin and polished to obtain a smooth surface. The apparatus, used for X–ray diffraction (XRD) is X`Pert Philips with Cu $K_{\alpha 1}$ rays.

The products of all reaction were reduced to a fine powder by means of a mortar in order to obtain a X-ray pattern immune of orientation effects.

I.I.3. Differential Scanning Calorimetry

Differential scanning calorimetry (DSC) is a thermoanalytical technique in which the difference in the amount of heat required to increase the temperature of a sample and a reference is measured as a function of temperature. Both sample and reference are maintained at nearly at the same temperature throughout the experiment. Generally, the temperature program for a DSC analysis is designed such that the sample holder temperature increases linearly as a function of time. The reference sample should have a well-defined heat capacity over the range of temperatures to be scanned. The basic principle underlying this technique is that, when the

sample undergoes a physical transformation such as phase transitions, more (or less) heat will flow to it compared to the reference to maintain both at the same temperature. Whether more or less heat must flow to the sample depends on whether the process is exothermic or endothermic. For example, as a solid sample melts it will require more heat flowing to the sample to increase its temperature at the same rate as the reference. This is due to the absorption of heat by the sample as it undergoes the endothermic phase transition from solid to liquid. Likewise, as the sample undergoes exothermic processes such as crystallization less heat is required to raise the sample temperature. By observing the difference in heat flow between the sample and reference, differential scanning calorimeters are able to measure the amount of energy absorbed or released during such transitions. DSC may also be used to observe more subtle phase changes, such as glass transitions. DSC is widely used in industrial settings as a quality control instrument due to its applicability in evaluating sample purity and for studying polymer curing [6 – 8].

There are two types of DSC systems in common use. In power - compensation DSC (e. g. DSC 7 Perkin Elmer) the temperatures of the sample and reference are controlled independently using separate, identical furnaces. The temperatures of the sample and reference are made identical by varying the power input to the two furnaces; the energy required to do this is a measure of the enthalpy or heat capacity changes in the sample relative to the reference. In heat – flux DSC (g.e. Calvet – type calorimeters, described above), the sample and reference are connected by a low - resistance heat - flow path. The assembly is enclosed in a single furnace. Enthalpy or heat capacity changes in the sample cause a difference in its temperature relative to the reference; the resulting temperature difference is small compared with that in differential thermal analysis (DTA) because the sample and reference are in good thermal contact. This temperature difference is recorded and related to enthalpy change in the sample using calibration experiments.

The result of a DSC experiment is a heating or cooling curve, usually represented as the change of the signal versus temperature. The first step is the baseline definition. The most common approximation of the baseline is a straight line, connecting the start and the finish of the transformation. The transition temperature (T_{tr}, Fig. I.3.1) is determined from intersection point of the peak slope with the baseline. The integrated area under the peak yields the enthalpy of given transition and can be expresses using the following equation:

$$\Delta H = E^{*}A \qquad \text{(I.I.3.1)}$$

where ΔH is the enthalpy of transition, E is the calibration constant, and A is the area under the curve.

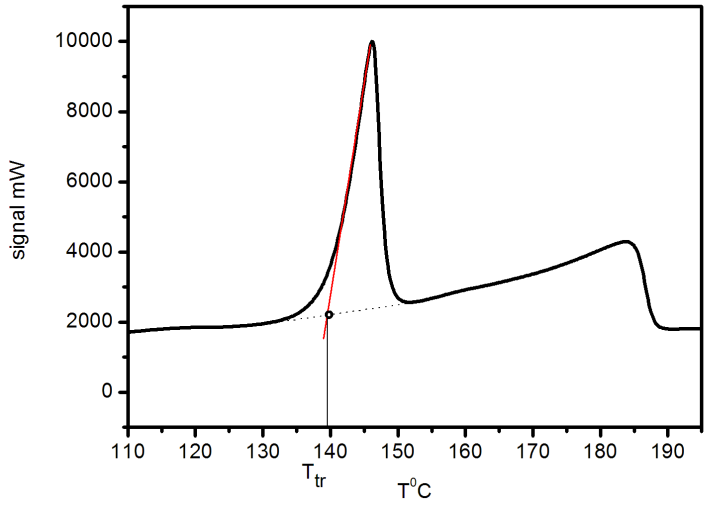

Fig. I.I.3.1 Example of a DSC curve. The dotted line represents one conventional baseline, the red line is the tangent at the inflection point of the peak; T_{tr} is the transition temperature (eutectic, next peak on the right - liquidus).

The DSC 111 SETARAM, which has been used for most of the experiments, is characterized with a temperature range: from -120 up to 830°C. The measurements are independent of experimental parameters such as sample's shape, nature of crucibles or atmosphere. The surrounding transducer (Fig. II.1.6) is made up of two opposite thermopiles in the central section of two refractory-material tubes. The assembly is fitted in a heating, metal block. The crucible is completely surrounded by the thermopile, ensuring that nearly all the heat exchanges are measured (only two solid angles at the top and bottom of the sensors are not covered by the thermopiles).

➢ Differential scanning calorimetry of pure Co

We have exemplified the Differential scanning calorimetry with one experiment, verifying the allotropic transformation of pure cobalt [10].

Cobalt occurs in two crystalline forms, hcp (ε) and fcc (α). Both of them coexist at room temperature, because of kinetic reasons [11]. A compilation and review of the physical, chemical and mechanical properties of elemental cobalt has been given by T. Nishizawa and K. Ishida [12]. Cobalt undergoes an allotropic transformation from hcp to fcc on heating near 673 K. The temperature and hysteresis associated with this martensitic - type reaction depends on the impurity content, thermal and mechanical history, and grain size. According to A. E. Ray and S. R. Smith [13] the transformation temperatures range from 702 to 718 K on heating, A_s, and from 673 to 692 on cooling, M_s, investigated with Perkin–Elmer PC Series DSC 7. The reported enthalpy changes of the transformation range from 464 to 511 $J.mol^{-1}$ on heating and –351 to –376 $J.mol^{-1}$ on cooling.

The allotropic transformation of cobalt was investigated with a DSC Setaram 111. The system was calibrated, using empty crucible and Al_2O_3 standard. The cobalt was obtained from Goodfellow (5N purity). It was cut from the same 5mm rod of cobalt, utilized for drop solution calorimetry experiments of Co–Sn binary system. The DSC measurements were made on a small piece of Co weighting 2.31032 g. The allotropic transformation was observed at heating and cooling rate of 10 $K.min^{-1}$. The cobalt sample was cycled through the transformation temperature 5 times.

According to [13] the enthalpies of transformation increase with each cycle and the peaks narrow and deepen. The cycle-to-cycle differences decreased with increasing number of cycles. We managed to mention this phenomenon only after five cycles. One can take into consideration the values, obtained by the second and fifth run.

The expected A_s transformation temperature ($\varepsilon \rightarrow \alpha$) is about 723 K. During the second cycle, the phase transformation was observed at about 701 K. During the fifth run it extrapolated to 731 K. The differences with reported values [13] can be due to the higher heating rate, which produces a displacement toward higher temperatures. The hysteresis associated with the phase transformation also widens with increasing the heating rate [10].

The expected M_s transformation ($\alpha \rightarrow \varepsilon$) during the cooling is about 673 K [13]. The observed temperatures are from 671 to 674 K. (Fig. I.I.3.2). The enthalpies of phase transformation during the heating were 0.289 and 0.327 $kJ.mol^{-1}$ for the second and the fifth run,

respectively. In contradiction with [13], no remarkable differences in the enthalpies were observed during the cooling (0.280 and 0.286 J.mol^{-1}), which can be due to the smaller number of implemented cycles.

Table I.I.3.1 represents the allotropic transformation temperatures and associated enthalpy changes of cobalt [10].

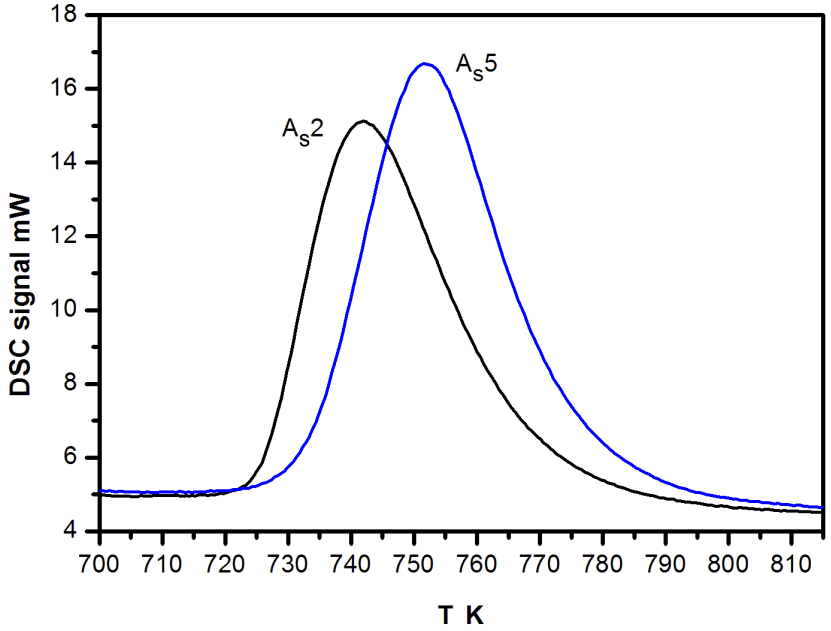

Fig. I.I.3.2 DSC curves of Co at heating (second and fifth run). The working interval is between 300 and 1080 K and the heating rate is 10 K.min^{-1}. The first peak A_s2 is at around 721 K and A_s5 around 731 KC. The signal (mW) of the DSC calorimeter is plotted along the ordinate and the temperature (K) along the abscissa.

Table I.I.3.1 (unpublished) Allotropic transformation temperatures and associated enthalpy changes of cobalt. Notes: last run is equal to fifth in our work and to 30th in [13].

Transformation	Onset Temperature second run K	Onset Temperature last run K	Enthalpy of phase transformation, second run kJ.mol^{-1}	Enthalpy of phase transformation, last run kJ.mol^{-1}	Reference
A_s ($\varepsilon \rightarrow \alpha$)	699	718	0.265	0.476	[13]
	694	713	–	–	[12]

	721	731	0.289	0.327	This work [10]
M_s ($\alpha \rightarrow \varepsilon$)	673	692	0.256	0.499	[13]
	674	693	–	–	[12]
	671	674	0.280	0.286	This work [10]

Although we have performed a smaller number of DSC cycles (5 runs) in comparison with [13] (30 runs), the tendency to increase for allotropic transformation temperatures (A_s, M_s) and the enthalpies of transformation with the number of DSC cycle was confirmed, which is the signature of martensitic transformation. Each thermal cycle increases the quantity of material, which transforms and so reduces the constraints that remain during cooling. During the next cycle the transformation starts later but is more complete.

The obtained A_s and M_s temperatures are respectively 22 to 26 K higher or 2 and 3 K lower, than previously reported. The disparity may be due to the differing thermal histories of the cobalt specimen, its purity and utilized apparatus.

Previous investigators [13] have reported larger enthalpies for $\varepsilon \rightarrow \alpha$ transformation than to $\alpha \rightarrow \varepsilon$, which is in agreement with our results, and demonstrate that α is not and equilibrium state.

➢ Bibliography

[1] Weihs T. P., T. W. Barbee, Jr., M. A. Wall J. Mater. Res., Vol. 11, No. 6, Jun 1996

[2] Ditmars D.A., S. Ishihara, S.S. Chang, J. of Research of the N.B.S., 87, (1982), 159

[3] Barin I., Thermochemical Data of Pure Substances, vol. I, VCH, Weinheim, 1993

[4] Toffolon C., Journal of Phase Equilibria, 134 – 139, Vol. 23, No 2, 2002

[5] Borzone G., R. Raggio, R. Ferr, Journal of Mining and Metallurgy, 38 (3–4) B (2002) 249 – 272

[6] Dean, J. A. The Analytical Chemistry Handbook. New York. McGraw Hill, Inc.1995. pp. 15.1 – 15.5

[7] Pungor, E. A Practical Guide to Instrumental Analysis. Boca Raton, Florida. 1995. pp. 181 – 191

[8] Skoog, D. A., F. James Holler and Timothy Nieman. Principles of Instrumental Analysis. Fifth Edition. New York. 1998. pp. 905 – 908

[9] Gachon J.C., State thesis, University of Nancy, Nancy, 1986

[10] Lilova K.I., G.P. Vassilev, J.C. Gachon, Enthalpies of formation of Co–Sn solid alloys, VIII International Workshop of Associated Phase Diagram and Thermodynamic Committee (APDTC), Kosice, Slovakia, 19 November 2005, Proceedings, Editor W. Zakulski, ISBN 83–921845–5–6, Published by: Institute of Metallurgy and Materials Science, Polish Academy of Sciences, Krakow, Poland, p. 35 – 43

[11] Hultgren R., P.D. Desai, D.T. Hawkins, Handbook of Materials Science, 126, Vol.2, 1973

[12] Nishizawa T., K. Ishida, Bull. Alloy Phase Diagrams, 4(4), 387–390, 420 (1980)

[13] Ray A. E., S. R. Smith, Journal of Phase Equilibria, 644–647, Vol. 12, No 6, 1991

I.II. Computational Thermodynamics. Calphad Method

A fundamental goal in materials science is to be able to control the final physical, mechanical or chemical properties of a material. In order to do that one must understand the interrelations between the raw materials and their chemical composition, the processing conditions, the microstructure (in a wide sense) thus produced and the properties of the final material. During processing, and often also during use, most materials undergo one or more heterogeneous reactions, or rather phase transformations. This is particularly obvious in melt processing where the material is completely or partially melted and then solidified.

To aid understanding of the interrelation between chemical composition, processing conditions and microstructure phase diagrams are used extensively in the development and processing of metals and ceramics and also in geochemistry. Experimentally determined phase diagrams are usually only available for binary systems, to some extent for ternary systems and very rarely for higher order systems. Since a phase diagram is a representation of the equilibrium thermodynamic properties of a system it is in principal possible to calculate the phase diagram if the thermodynamic properties are known. It is then also possible to extrapolate to multicomponent systems [1].

Computational thermodynamics is a phenomenological scientific discipline that enables metallurgical engineers and materials scientists to calculate phase diagrams and to numerically simulate and study phase equilibria and phase transformations. The thermodynamic properties as a function of composition and temperature can also be calculated.

By combining knowledge on the phase diagram and the thermodynamic properties, a model description of the system suitable for phase diagram calculations can be created. Descriptions of low order systems can be combined to make extrapolations to higher order systems. For this purpose the Gibbs energy of each phase is described by a suitable model containing a relatively small number of variable coefficients. These coefficients are optimised using experimental information on phase equilibria such as melting temperatures, other transformation temperatures, solubilities, and on thermodynamic properties such as enthalpies of formation, chemical potentials from EMF or pressure measurements, heat capacities. Most of this information is taken from the literature, but one can also do own phase equilibria studies using typically light optical microscopy, Scanning Electron Microscope (SEM), Electron Probe Micro Analysis (EPMA), X–ray diffraction (XRD) and Differential Scanning Calorimetry (DSC), Differential Thermal Analyses (DTA). There is a large number of thermodynamic models available and we

normally use the very general "compound energy formalism" for solid solution phases and the "two-sublattice model for partially ionic liquids" for liquid phases [1].

➢ Thermodynamic Descriptions and Models

For the calculation of phase equilibria in a multicomponent system, it is necessary to minimize the total Gibbs energy, G, of all the phases that take part in this equilibrium:

$$G = \sum_{i=1}^{p} n_i G_i^{\phi} = \text{minimum} \qquad \text{(I. II.1)}$$

where n_i is the number of moles and G_i the Gibbs energy of phase i.

A thermodynamic description of a system requires assignment of thermodynamic functions for each phase. The CALPHAD method employs a variety of models to describe the temperature, pressure and concentration dependencies of the free energy functions of the various phases. The contributions to the Gibbs energy of a phase can be written:

$$G^{\phi} = G_T^{\phi}(T,x) + G_p^{\phi}(p,T,x) + G_m^{\phi}(T_C, \beta_0, T, x) \qquad \text{(I. II.2)}$$

where $G_T(T,x)$ is the contribution to the Gibbs energy by the temperature, T, and the composition, x, $G_p(p,T,x)$ is the contribution of the pressure, p, and $G_m(T_{C,0},T,x)$ is the magnetic contribution of the Curie or temperature, T_C, and the average magnetic moment per atom, $ß_0$.

The temperature dependence of the concentration terms of G_T is usually expressed as a power series of T:

$$G = a + b \cdot T + c \cdot T \cdot \ln(T) + \sum d_n \cdot T^n \qquad \text{(I. II.3)}$$

where a, b, c and d_n are coefficients and n are integers.

In each of the equations in the following models describing the concentration dependence, the G coefficients on the right hand side can have such a temperature dependence. Frequently only the first two terms are used for the representation of the excess Gibbs energy. Pressure dependence for condensed systems at normal pressures is usually ignored.

For multicomponent systems it has proven useful to distinguish three contributions from the concentration dependence to the Gibbs energy of a phase, G:

$$G^{\phi} = G^{0} + G^{ideal} + G^{xs} \qquad \text{(I. II.4)}$$

The first term, G^0, corresponds to the Gibbs energy of a mechanical mixture of the constituents of the phase, the second term, G^{ideal}, corresponds to the entropy of mixing for an ideal solution and the third term, G^{xs}, is the so-called excess term [2]. Since Hildebrand introduced the term "regular solution" to describe interactions of different elements in a random solution, a series of models have been proposed for phases which deviate from this "regularity", i.e. show a strong compositional variation in their thermodynamic properties, to describe the excess Gibbs energy, G^{xs}. For ordered solid phases, Wagner and Schottky [3] introduced the concept of defects on the crystal lattice in order to describe deviations from stoichiometry. A description of order/disorder transformations proposed by Bragg and Williams [4]. Since then many other models have been proposed. Today the most commonly used models are those for stoichiometric phases, regular solution type models for disordered phases, and sublattice models for ordered phases having a range of solubility or exhibiting an order/disorder transformation.

The Gibbs energy of a binary stoichiometric phase is given by:

$$G^{\phi} = x_A^0 G_A^0 + x_B^0 G_B^0 + \Delta G^f \qquad \text{(I. II.5)}$$

where $x_A{}^0$ and $x_B{}^0$ are mole fractions of element A and B and are given by the stoichiometry of the compound, $G_A{}^0$ and $G_B{}^0$ are the respective reference states of element A and B, and G^f is the Gibbs energy of formation. The first two terms correspond to G^0 and the third term to G^{xs} . G^{ideal} is zero for a stoichiometric phase since there is no random mixing.

Binary solution phases, such as liquid and disordered solid solutions, are described as random mixtures of the elements by a regular solution type model:

$$G^{\phi} = x_A G_A^0 + x_B G_B^0 + RT\left\{ x_A \ln x_A + x_B \ln x_B \right\} + x_A x_B \sum_{i=0}^{n} G_i \left(x_A - x_B\right)^i \qquad \text{(I. II.6)}$$

where x_A and x_B are the mole fractions and $G_A{}^0$ and $G_B{}^0$ the reference states of elements A and B, respectively. The first two terms correspond to G^0 and the third term, from random mixing, to

G^{ideal} . The G_i of the fourth term are coefficients of the excess Gibbs energy term, G^{xs}. The sum of the terms $(x_A - x_B)^i$ is the so-called Redlich-Kister polynomial [5] which is the most commonly used polynomial in regular solution type descriptions.

The most complex and general model is the sublattice model frequently used to describe ordered binary solution phases. The basic premise for this model is that a sublattice is assigned for each distinct site in the crystal structure. For example, an ordered binary solution phase with two sublattices that exhibits substitutional deviation from stoichiometry can be described by the expression:

$$G^{\phi} = x_A G_A^0 + x_B G_B^0 + RT\left\{a^1\left(y_A^1 \ln y_A^1 + y_B^1 \ln y_B^1\right) + a^2\left(y_A^2 \ln y_A^2 + y_B^2 \ln y_B^2\right)\right\}$$
$$+ y_A^1 y_A^2 G_{AA}^0 + y_A^1 y_B^2 G_{AB}^0 + y_B^1 y_A^2 G_{BA}^0 + y_B^1 y_B^2 G_{BB}^0$$
$$+ y_A^1 y_B^1 y_A^2 \sum_{i=0}^{n_{1A}} G_i^{2A}\left(y_A^1 - y_B^1\right)^i + y_A^1 y_B^1 y_B^2 \sum_{i=0}^{n_{1B}} G_i^{2B}\left(y_A^1 - y_B^1\right)^i$$
$$+ y_A^1 y_A^2 y_B^2 \sum_{i=0}^{n_{1A}} G_i^{1A}\left(y_A^2 - y_B^2\right)^i + y_B^1 y_A^2 y_B^2 \sum_{i=1}^{n_{1B}} G_i^{1B}\left(y_A^2 - y_B^2\right)^i + y_A^1 y_B^1 y_A^2 y_B^2 G^{hp}$$

(I. II.7)

where y_A^1, y_B^1, y_A^2 and y_B^2 are the species concentrations of element A and B on sublattices 1 and 2 with $a^1\ y_A^1 + a^2\ y_A^2 = x_A$, $a^1\ y_B^1 + a^2\ y_B^2 = x_B$ and $y_A^1 + y_B^1 = 1$, $y_A^2 + y_B^2 = 1$. a^1 and a^2 are the site fractions of the sublattices 1 and 2 and are given by the number of sites in the unit cell. The first two terms correspond to G^0 and the third term corresponds to G^{ideal}. The remaining terms are the excess Gibbs energy term, G^{xs}. The coefficients G_{AA}^0 , G_{AB}^0 , G_{BA}^0 and G_{BB}^0 can be visualized as the Gibbs energies of the end-member phases. The end-member phases are formed when each sublattice is occupied only by one kind of species and can be either real ($A_a^1 B_a^2$: A atoms on sublattice 1 and B atoms on sublattice 2) or hypothetical ($A_a^1 A_a^2$, $B_a^1 A_a^2$ and $B_a^1 B_a^2$). The remaining terms of G^{xs} describe interactions between the atoms on one sublattice similar to regular solution type models for disordered solution phases. This model description was first introduced by Sundman and Ågren [6] and later refined by Andersson et al [7]. For the treatment of order/disorder transformations with this model, the coefficients in G^{xs} are not independent of each other. For example, Ansara et al. [8] derived dependencies for the order/disorder transformation of fcc/$L1_2$. This model was later modified by Ansara et al. [9] to allow

independent evaluation of the thermodynamic properties of the disordered phase. Chen et al. [10] have proposed another model for the treatment of ordered phases.

➢ Computer Software Tools and Databases

A variety of software packages can be used for the calculation of phase diagrams making it impossible to list all of them. Frequently used software packages are ChemSage, the so-called Lukas programs, MTDATA and Thermo-Calc. Thermo-Calc has been developed for thermodynamic and phase diagram calculations in the fields of metallurgy, material science, alloy development, chemistry, geochemistry, semiconductors, energy conversation, power production, etc. The software specializes in calculations for multicomponent systems. Thermo-Calc provides better understanding of the factors that affect material behavior and helps reduce costs by quickly identifying control parameters or alloy compositions [2].

Several thermodynamic databases have been constructed from the assessments of binary, ternary and quaternary systems. One of them is COST database, creating within the intergovernmental framework for European Co-operation in the field of Scientific and Technical Research.

➢ Bibliography

[1] Grundy N., M. Chen, Thermodynamic Modeling using the Calphad Method, Departments of Materials, (12) 2005

[2] Kattner U., JOM 49 (12), 1997, 14-19

[3] Wagner C., W. Schottky, Z. phys. Chem., B11 (1930) 163-210

[4] Bragg W.L., E.J. Williams, Proc. Royal Soc. A, London, 145 (1934) 699-730; 151 (1935) 540-566

[5] Redlich O., A.T. Kister, Indust. Eng. Chem., 40 (1948) 345-348

[6] Sundman B., J. Ågren, J. Phys. Chem. Solids, 42 (1981) 297-301

[7] Andersson J., A. Fernández Guillermet, M. Hillert, B. Jansson and B. Sundman, Acta metall., 34 (1986) 437-445

[8] Ansara I., B. Sundman and P. Willemin, Acta metall., 36 (1988) 977-982

[9] Ansara I., N. Dupin, H.L. Lukas and B. Sundman, J. Alloys Compd., 247 (1997) 20-30

[10] Chen S., C.R. Kao and Y.A. Chang, Intermetallics, 3 (1995) 233-242

Chapter II

Experimental Studies of Co–Sn, Ni–Sn and Ni–Sn–Bi Systems

II. 1. Experimental Investigations and Thermodynamic Optimization of the Co–Sn Binary System

It is anticipated that future lead-free solders would be based on tin-containing systems. Thus, the eutectic Sn–Co–Cu alloys have been suggested as potential solders by Liu et al. [1]. Moreover, this work is part of a series of studies concerning prospective binary or ternary systems consisting of low melting metals (Zn, Sn, Bi, In) and elements of the Fourth or Fifth period (Ti, Ni, Co, Cu, Ag). The applications of such alloys could be sought in the field of joining materials (as multicomponent solders or by the transition liquid phase method) [1], in galvanizing technologies [2, 3, 4] or in specific uses. Particularly, Co–Sn–Se phases would be interesting due to the optoelectronic and semiconductor properties of the tin-selenides [5–9].

Co–Sn alloys might be suitable for the production of metallic glasses [10–13] as well. Another application of electro-deposited Sn–Co alloys is sought as electrode materials for lithium batteries [14].

Numerous studies of enthalpies of formations, activities, phase equilibria and thermodynamic optimizations [1, 15–23] of this system have been performed but ambiguities about the thermochemical properties persist. Thus, the purpose of this work is measuring enthalpies of formation of solid and liquid Co–Sn alloys and re-optimization of the phase diagram.

➢ Literature review

Most of the experimental studies of the Co–Sn system [15, 16, 25–29, 30] are taken into account in the compilations of the binary phase diagrams [31, 32] or in the assessments of this system [17, 18]. The commonly accepted phase diagrams are shown in Fig II.1.1 and Fig II.1.2

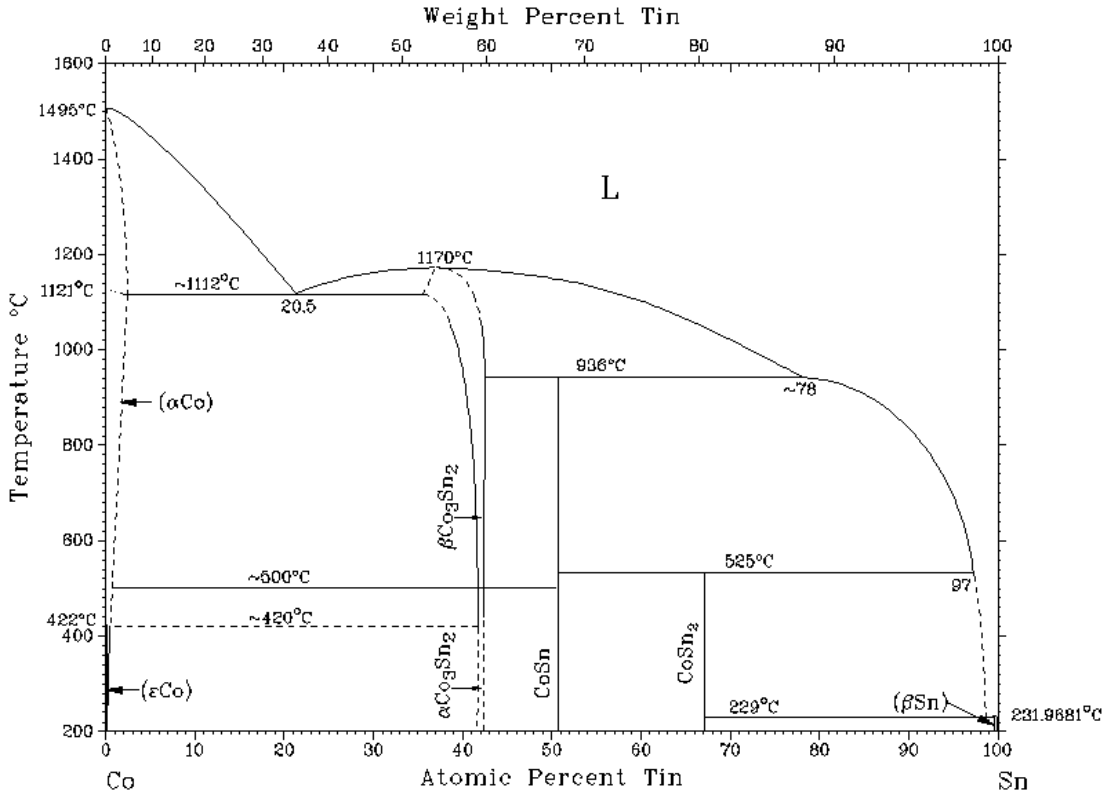

Fig. II.1.1 The Co–Sn phase diagram by T. Massalski [32]

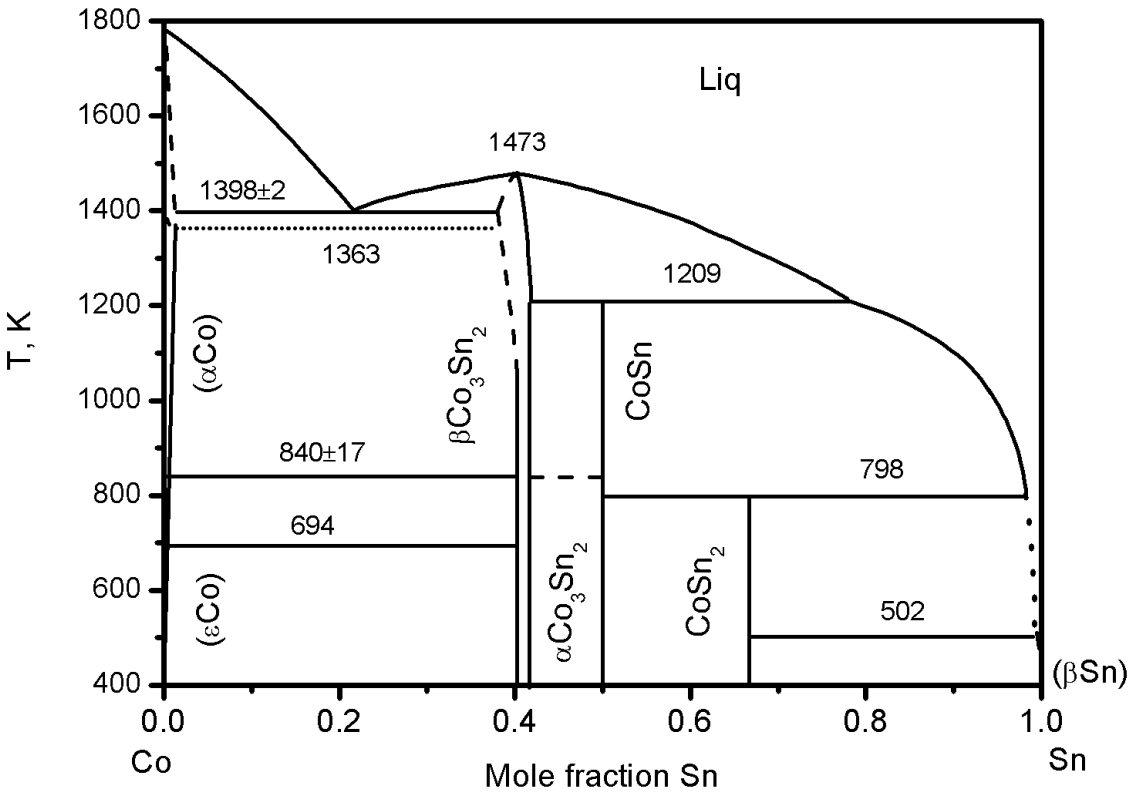

Fig. II.1.2 Revised Co–Sn phase diagram by H. Cömert, J.N. Pratt [16]

As one can see (Fig. II.1.1, II.1.2) the phase $CoSn_3$ has been ignored at that time. It has been revealed recently by Lang and Jeitschko [33], that two modifications exist (Fig. II.1.3.). Another compound (Co_3Sn) has been observed by Schluckebier [29] but it has been found to be metastable [30].

The equilibria between the liquid solution and the solid phases have been studied by Lewkonja [25], Zemczuzny and Belinsky [26], Hashimoto [27], and Darby and Jugle [28]. The latter authors worked in the tin-rich side, where the liquidus is very steep and the determination of the exact equilibrium concentration of the liquid phase is rather complicated.

Actually, Lewkonja [25] has accepted the Co melting point to be at 1440^0C (the presently established value is 1495^0C (1768 K) [22]), while Zemczuzny and Belinsky [26] considered 1502 ^{O}C. The supposed Sn melting point is, respectively, 232^0C [25] and 231.5^0C [26], while the contemporary value is 231.93 (505.078 K) [59]. Thus the most important corrections concerned the experimental points of the Co-rich region of the phase diagram. After the temperature corrections, the high-temperature eutectic is estimated to be at 1414±7 K [25], thus showing a relatively good agreement with the recent measurements of Comert and Pratt [16] giving a value of 1398±2 K. Similar good agreement between both authors is observed for the temperature of the peritectic P1 (1239 K) as well.

The ferromagnetic transition in the cobalt–tin face centered cubic (fcc) solid solutions has been studied by Hashimoto [27] who found that tin diminishes the temperature of the magnetic ordering. Cömert and Pratt [16] contributed largely to the determination of the solvus. Limited tin solubility (around 1 at. % Sn) in fcc cobalt has been found, while there is no data about the tin solubility in the hexagonal cobalt. Anyhow, even more limited solubility in such a lattice is expected, like in the Co–Zn system, already studied in our team, for example [34].

The cobalt solubility in the solid tin (αSn or βSn) is unknown, but it is expected to be negligible. Such behaviour is in agreement with the theoretical considerations taking into account the unfavourable size- and electronegativity- factors (the metallic radii of both kinds of atoms differ by 25 % (r_{Co}=125.2 pm and r_{Sn}=162.3 [35]) while they exhibit similar Pauling electronegativities (1.88 for Co and 1.96 for Sn) [36]).

Both solid solutions (αCo, εCo) and the liquid phase have been modelled as disordered substitutional solutions in the above mentioned recent works [1, 33]. The concentration dependence of the excess Gibbs energy in such phases is described by Redlich–Kister polynomials, while the magnetic contribution to the Gibbs energy is calculated following an expression developed by Hillert and Jarl [37].

The stoichiometric phases (Fig. II.1.2) in the system are: CoSn, $CoSn_2$, $\alpha CoSn_3$, $\beta CoSn_3$, (αSn), (βSn). Linear temperature dependences of their Gibbs energies of formation have been accepted for all of them, except for the $\beta CoSn_3$, where one temperature independent term is used only. (αSn) and (βSn) are considered as identical with the corresponding pure substances.

The intermediate phases denoted as β are high-temperature forms, corresponding to the pertinent α low-temperature forms. All intermediate phases melt peritectically except βCo_3Sn_2 that melts congruently at around 1200 °C [16]. In some previous assessments [17, 31] the temperature of 1170 °C is accepted. Jiang et al. [38] and Liu et al. [1] accept this value (1200 °C) as well. The calculated congruent melting temperature of βCo_3Sn_2 is 1181 °C [38] and 1199 °C [1].

The compound Co_3Sn_2 is nonstochiometric and exhibits two modifications. The high-temperature form (βCo_3Sn_2) is disordered (prototype Ni_3Sn_2(r)), while long-range ordering exists in the low-temperature form (αCo_3Sn_2, prototype NiAs(h) or $B8_1$) [39–41]. The first three compounds are supposed to be stoichiometric. Cömert and Pratt [29, 43] have determined the homogeneity range of the phase Co_3Sn_2 (approximate 40 to 42 at. % Sn) using a variety of techniques (electromotive force measurements, X–rays, metallographic and thermo-analytical methods). They have revealed that the temperature of the transformation $\beta Co_3Sn_2 \leftrightarrow \alpha Co_3Sn_2$ has the value of 567±17 ºC (or 840±17 K) on the Co-rich side of the compound.

The literature data about the crystal structures of the stable Co-Sn phases are compiled in Table II.1.1.

Table II.1.1 Crystal structures of the stable binary Co-Sn phases by literature data.

Phase	Homogeneity range at. %	Pearson symbol	Structurbericht desi4gnation	Space Group	Prototype	Source
1	2	3	4	5	6	7
$(\alpha Co)^{A,D}$	≈100-98 at. % Co	cF4	A1	$Fm\bar{3}m$	Cu	[32]
$(\varepsilon Co)^{C}$	≈100 at. % Co	hP2	A3	$P6_3/mmc$	Mg	[32]
$(\alpha Sn)^{B}$	≈100 at. % Sn	cF8	A4	$Fd\bar{3}m$	C(diam.)	[32]
$(\beta Sn)^{A}$	≈100 at. % Sn	tI_4	A5	$I4_1/amd$	βSn	[32]

Table II.1.1 continuation

1	2	3	4	5	6	7
$\alpha CoSn_3$	75 at. % Sn	…	…	Cmca	$PdSn_3$	[33]
$\beta CoSn_3$ [A]	75 at. % Sn	…	…	$I4_1/acd$	$\beta CoSn_3$	[33]
$CoSn_2$	66.67 at. % Sn	tI12	C16	I4/m	$CuAl_2$	[32]
CoSn	50 at. % Sn	hP6	B35	P6/mmm	PtTl	[32]
αCo_3Sn_2 [E]	≈40 ат. % Sn	oP20	…	Pnma	$Ni_3Sn_2(r)$	[32,39]
βCo_3Sn_2 [A]	≈40-42 ат. % Sn	hP4	$B8_1$	$P6_3/mmc$	NiAs(h)	[32,39]

[A] - high-temperature modification; [B] – modification stable below 286.2 K;

[C] - ferromagnetic phase; [D] - phase, where magnetic transition occurs;

[E] – ordered phase.

- Experimental studies of the enthalpy of formation of liquid Co–Sn alloys

Enthalpies of formation of the cobalt–tin liquid phase were measured [24] by drop solution calorimetry at 991 and 1020 K using Calvet–calorimeter. The method was described in Chapter II. 2. The initial idea was to obtain the enthalpy of dissolution of solid cobalt in liquid tin and then to precipitate the compound CoSn up to the composition of roughly 49 at. % Sn to get the enthalpy of formation of CoSn.

For these experiments, 16 tin pellets with weight from 0.08 g to 0.10 g and total mass of 1.23 g were prepared in a glove box under argon atmosphere using a manual press (Table II.1.2). They have been used for determination of the calorimetric constant initially (as described in Chapter I.2). For this purpose exactly weighed tin pellets were in successively added into the calorimeter and the heat effects were measured at every step. The tin bath formed in this way was used for the further calorimetric measurements. Afterwards, 16 pellets of cobalt with total mass 1.23 g (Table II.1.3) were sequentially dropped in the calorimeter. The heat effects due to the cobalt dissolution were measured for every sample and the integral molar enthalpies of formation of the liquid solutions (Fig. II.1.3) were obtained.

Table II.1.2 Experimental details about Sn specimens, used for the determination of the enthalpy of liquid phase at 991 K (unpublished). No – number of the Sn sample, mass – mass of Sn pellets

Sn N°	mass Sn g	Total mass g
1	0.09989	0.09989
2	0.08391	0.1838
3	0.0771	0.2609
4	0.08225	0.34315
5	0.08637	0.42952
6	0.09909	0.52861
7	0.10615	0.63476
8	0.09965	0.73441
9	0.1023	0.83671
10	0.0874	0.92411
11	0.1071	1.03121
12	0.10234	1.13355
13	0.09873	1.23228
14	0.10395	1.33623
15	0.09755	1.43378
16	0.09165	1.52543
17	0.07851	1.60394
18	0.07766	1.6816
19	0.08985	1.77145
20	0.07858	1.85003
21	0.09241	1.94244
22	0.09105	2.03349
23	0.0907	2.12419
24	0.10355	2.22774

Table II.1.3 Experimental details and results of the determination of the enthalpy of liquid phase at 991 K (unpublished). No – number of the experiment, mass – mass of Co pellets, X_{Co} – molar fraction of Co, $\Delta_f \bar{H}_{Co}^{L}$ – partial enthalpy of mixing; $\Delta_f H^L$ – integral enthalpy of mixing

N^0	m Co g	X_{Co}	$\Delta_f \bar{H}_{Co}^{L}$ kJ.mol^{-1}	$\Delta_f H^L$ kJ.mol^{-1}
1	0.035	0.031	–25.469	–0.779
2	0.0246	0.051	–25.690	–1.304
3	0.0314	0.076	–44.294	–2.431
4	0.0247	0.095	–19.108	–2.767
5	0.0781	0.149	–45.131	–5.309
6	0.1172	0.219	–48.148	–8.847
7	0.0991	0.271	–23.983	–9.835
8	0.0698	0.303	–15.559	–10.087
9	0.1619	0.367	–9.637	–10.045
10	0.1019	0.402	–45.375	–11.990
11	0.1484	0.446	–42.332	–14.241
12	0.0788	0.467	–35.763	–15.057
13	0.1022	0.492	–4.051	–14.541
14	0.0443	0.503	–16.249	–14.575

At the experimental conditions (temperature and composition) the liquidus line is disposed at around 90 at. % Sn. Thus, only integral enthalpies of formation of the liquid binary solutions ($\Delta_f H^{L,T}$) with tin content superior to the above mentioned value are representative for the liquid phase.

A regular solution model (eqns. II.1.1 and II.1.2), using the few data obtained in the liquid phase field, was selected to represent (Fig. II.1.2) the concentration dependence of $\Delta_f H^{L,T}$ (x is the mole fraction of tin):

$$\Delta_f H^{L,991} = x(1-x)\ (-30 \pm 4)\quad kJ/mol \qquad 1 \geq x_{Sn} \geq 0.905 \qquad \text{(II.1.1)}$$

$$\Delta_f H^{L,1020} = x(1-x)\ (-10 \pm 5)\quad kJ/mol \qquad 1 \geq x_{Sn} \geq 0.909 \qquad \text{(II.1.2)}$$

The integral molar enthalpy of formation of CoSn, obtained by drop solution calorimetry (Fig. II.1.3) deviates significantly from the value measured by direct reaction calorimetry. In Fig. II.1.3 it can be seen that our results are not reliable as in the two-phase field L+CoSn the integral enthalpy, which is the weighted mean of the integral enthalpy of formation of the liquid at the concentration limit and CoSn enthalpy of formation should be a straight line. The experimental results are far from that and illustrate the difficulty of the measurements.

Such problems might be due to a variety of reasons. Primary, the dissolution of solid cobalt in liquid tin seems to be incomplete. This was confirmed by EMPA and X–ray analyses of crystallized (after the calorimetric experiments) specimens, where undissolved cobalt has been observed. Another reason might be the formation of Co–Sn associates in the liquid phase and metastable solid phases. These suggestions are backed by some literature data. For example, short-range ordering is observed in amorphous Co–Sn alloys by Nabil et al. [44]. In addition, Mudry et al. [45] reported X–ray investigations of liquid Co–Sn alloys, confirming the "tendency to form complexes or associates in the liquid state" (cited up to Komarnitsky et al. [46]).

Moreover, a (metastable) phase corresponding to the formula Co_2Sn was observed in this work in a sample used for calorimetric experiment at 991 K (Fig. II.1.4A). In the half of the same specimen the phase CoSn has formed (Fig. II.1.4B). X–ray studies of the allow, containing Co_2Sn allowed distinguishing diffraction peaks of ßSn, fcc Co and others that were associated with this phase (Fig. II.1.5). The blue and red curves represent diffraction lines of ßSn and hcp Co simulated by PowderCell2, respectively. Literature data published by Villars [47] has been used.

A phase notified as Co_2Sn was mentioned in the first constitutional work on the Co–Sn system [46] but now it is identified as the stable compound Co_3Sn_2. Another metastable phase (Co_3Sn) has been obtained by Schluckebier et al. [29] by rapid cooling of binary melt. In the case

reported in this work, however, the phase Co_2Sn is obtained by slow cooling of a specimen left in the furnace of the calorimeter.

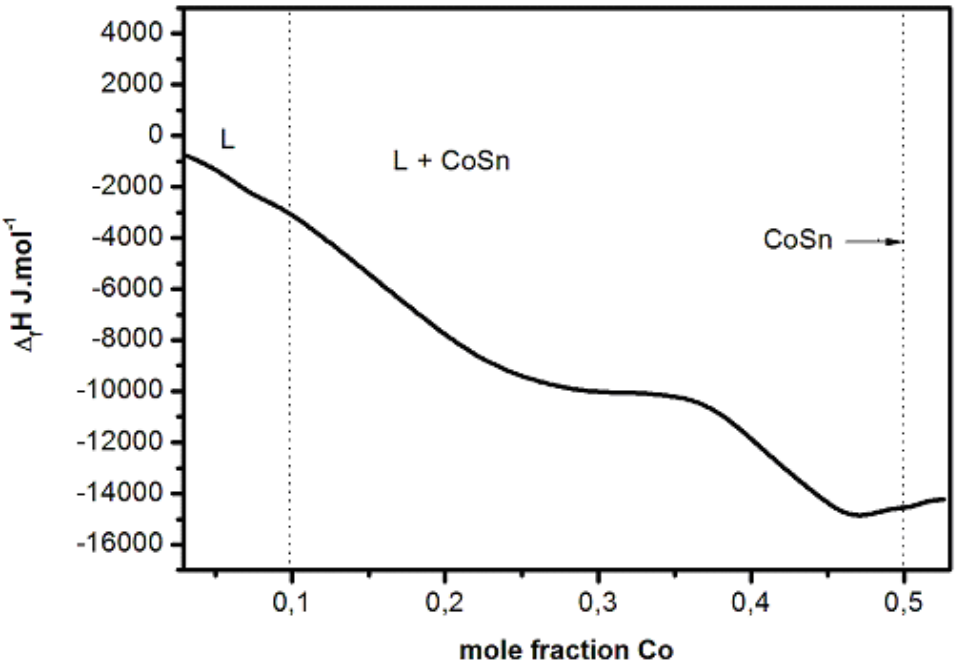

Fig. II.1.3 Integral molar enthalpies of formation of cobalt–tin alloys ($\Delta_f H$) measured by solution calorimetry at 991 K. The solid line corresponds to enthalpies of formation calculated by regular solution approximation. The symbols (L), and (L + CoSn) indicate the monophase and the two-phase regions, in that order. The vertical dashed and dotted lines show, respectively, the approximate positions of the liquidus at the working temperatures and the concentration of the phase CoSn. The reference states are fcc Co and liquid Sn at the corresponding working temperature.

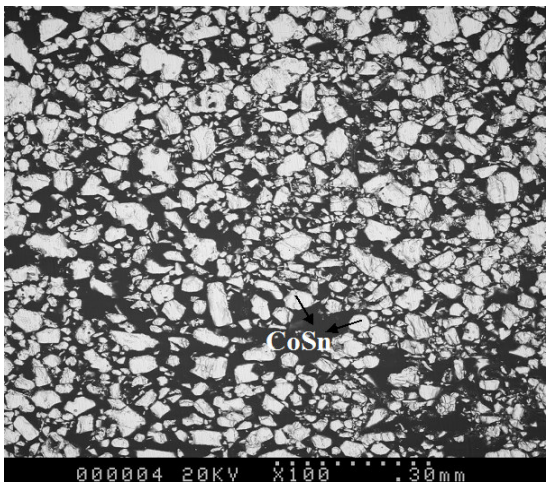

A.

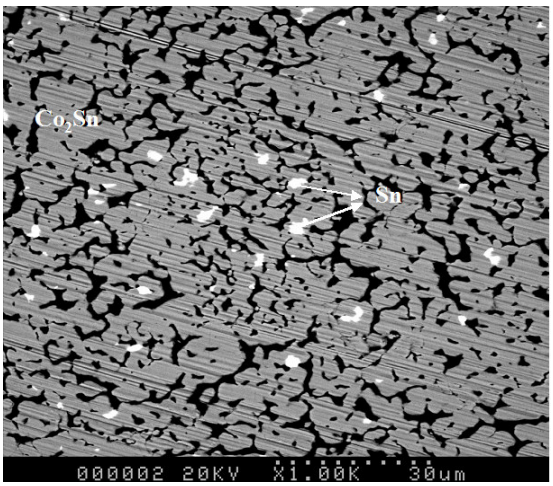

B.

Fig. II.1.4 A. SEM image in BSE of the product of dissolution of Co in liquid Sn at 991 K (unpublished). The white crystals belong to CoSn phase. The black areas represent the resin where the CoSn powder is embedded.

B. SEM image in BSE of the Sn-rich part of the same specimen [24]. The gray matrix corresponds to the formula Co_2Sn. The white areas are of pure Sn

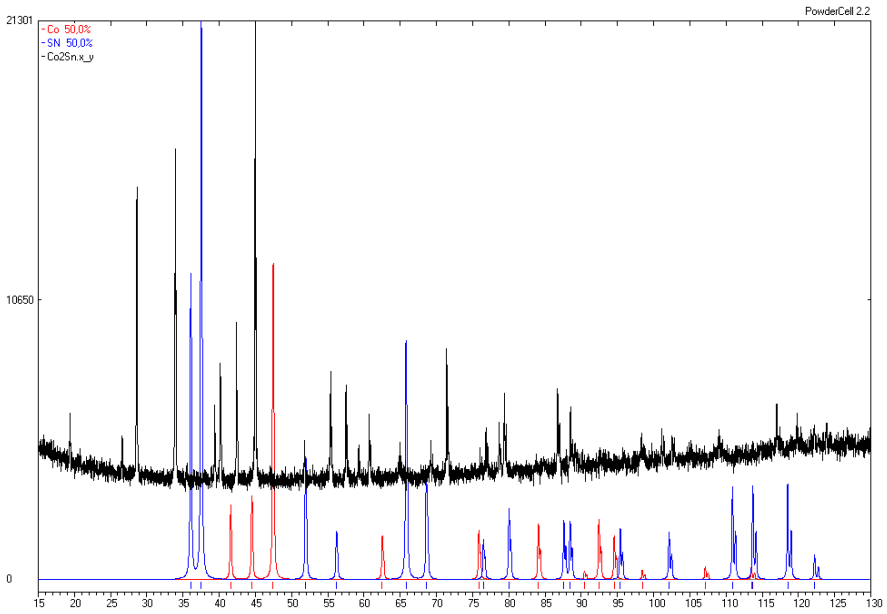

Fig. II.1.5 XRD spectrum of alloy [24], obtained at 991 K, superimposed with theoretical patterns of hcp Co (red curve) and ßSn (blue curve), simulated by PowderCell 2.3, using [48].

In order to verify the existence of Co_nSn metastable phases, eight samples with different composition were prepared and annealed at 993 K for two weeks. (Table II.1.4).

Table II.1.4 Experimental details and results of the experiment, concerning Co_nSn metastable phases

Composition, at. % Co	Initial mass, g	Mass after annealing, g	Phases
1	2	3	4
7.6	0.4905 0.4144	0.9017 (one piece, melted)	pure Sn CoSn
18	0.5195 0.3577	0.8736 (one piece, melted)	pure Sn CoSn
41	0.4648 0.4179	0.4614 0.4153	pure Sn CoSn

Table II.1.4 continuation

1	2	3	4
70	0.3945	0.3870	pure Co
	0.4301	0.4289	Co_4Sn
			Co_3Sn
			Co_2Sn

According to the microprobe analysis, three metastable phases Co_4Sn, Co_3Sn and Co_2Sn have been found in the specimen with nominal composition of 70 at. % Co. The others samples have consisted of only two phases – pure Sn and CoSn compound.

With the purpose to obtain partial and integral enthalpies of dissolution of pure Co in tin liquid bath at higher temperature (1020 K), 12 pellets of pure Sn were prepared (Table II.1.5).

Table II.1.5 Experimental details about Sn specimens, used for the determination of the enthalpy of liquid phase at 1020 K. No – number of Sn sample, mass – mass of Sn pellets

Sn N°	mass Sn g	Total mass g
25	0.1819	0.1819
26	0.17715	0.35905
27	0.19876	0.55781
28	0.19887	0.75668
29	0.15255	0.90923
30	0.16135	1.07058
31	0.17085	1.24143
32	0.20063	1.44206
33	0.16237	1.60443
34	0.15595	1.76038
35	0.1745	1.93488
36	0.18946	2.12434

Afterwards, 28 pellets of Co with total mass 1.06 g were dropped in the calorimeter (Table II.1.6).

Table II.1.6 Experimental details and results of the determination of the enthalpy of liquid phase at 1020 K (unpublished). No – number of the experiment, mass – mass of Co pellets, X_{Co} – molar fraction of Co, $\Delta_f \bar{H}^L_{Co}$ – partial enthalpy of mixing; $\Delta_f H^L$ – integral enthalpy of mixing

N^0	m Co g	X_{Co}	$\Delta_f \bar{H}^L_{Co}$ kJ.mol^{-1}	$\Delta_f H^L$ kJ.mol^{-1}
1	2	3	4	5
15	0.0284	0.0262	–6.428	–0.169
16	0.0307	0.0531	–7.065	–0.359
17	0.0251	0.0739	–10.182	–0.575
18	0.0214	0.0910	–48.447	–1.458
19	0.0324	0.1157	–49.186	–2.754
20	0.0526	0.1531	–38.453	–4.262
21	0.0445	0.1823	–19.715	–4.797
22	0.0398	0.2068	–46.982	–6.059
23	0.0426	0.2314	–38.901	–7.079
24	0.0371	0.2516	–45.511	–8.090
25	0.0378	0.2712	–17.601	–8.339
26	0.0388	0.2902	–20.896	–8.667
27	0.0472	0.3121	–20.694	–9.037
28	0.0578	0.3371	–18.856	–9.393
29	0.0366	0.3520	–21.737	–9.671
30	0.0375	0.3666	–29.929	–10.127
31	0.0503	0.3851	–33.658	–10.817
32	0.032	0.3964	–43.458	–11.414
33	0.0514	0.4137	–1.2538	–11.447
34	0.0508	0.4298	–14.061	–11.518

Table II.1.6 continuation

1	2	3	4	5
35	0.0472	0.4439	–29.179	–11.958
36	0.0392	0.4552	–20.784	–12.137
37	0.0465	0.4680	–24.014	–12.416
38	0.0266	0.4750	–21.547	–12.537
39	0.0288	0.4825	–12.588	–12.537
40	0.0271	0.4892	–6.497	–12.458
41	0.0262	0.4956	–18.925	–12.539
42	0.0194	0.5003	–7.207	–12.490

Fig. II.1.6 represents integral enthalpies of mixing, obtained at this temperature.

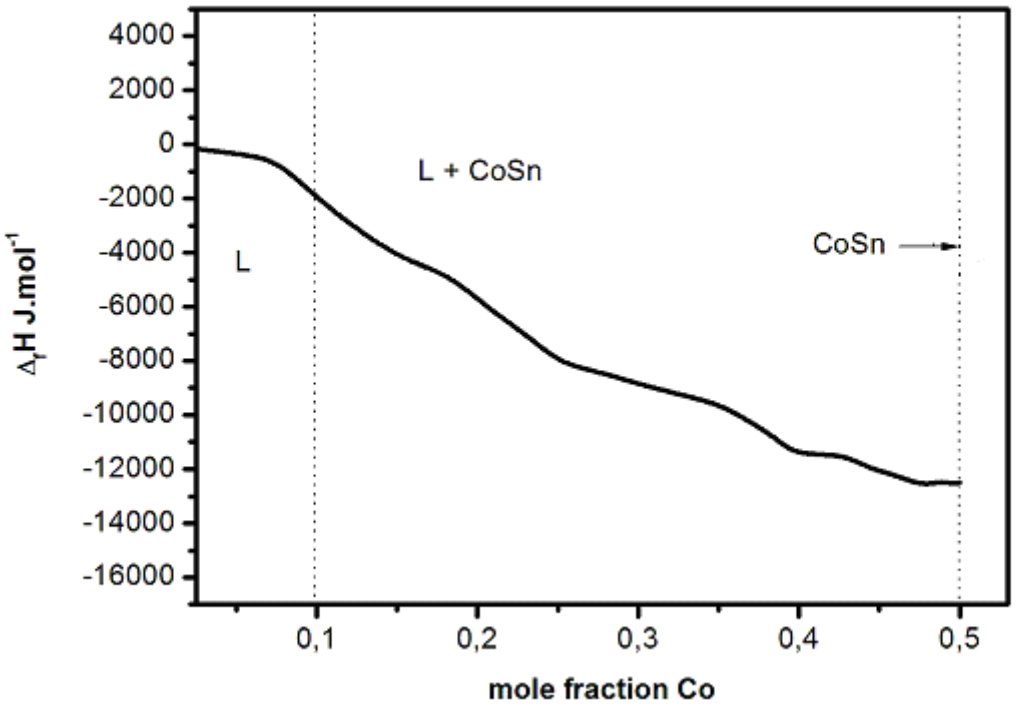

Fig. II.1.6 Integral molar enthalpies of formation of cobalt–tin alloys ($\Delta_f H$) measured by solution calorimetry at 1020 K (unpublished). The solid line corresponds to enthalpies of formation calculated by regular solution approximation in the liquid domain. The symbols (L), and (L + CoSn) indicate the monophase and the two-phase regions, in that order. The vertical dashed and dotted lines show, respectively, the approximate positions of the liquidus at the

working temperatures and the concentration of the phase CoSn. The reference states are fcc Co and liquid Sn at the corresponding working temperature. Like in Fig. II.1.3, in two-phased field the curve should be a straight line.

The mass of every sample was reduced, which should assure complete dissolution in liquid tin. The number of Co samples was increased in order to obtain an exact composition at the end of the whole experiment (about 50 at. % Co). According to the microprobe analysis and x–ray patterns, there are two phases. The main one is CoSn. There is a small light phase – $CoSn_2$ (Fig. II.1.7).

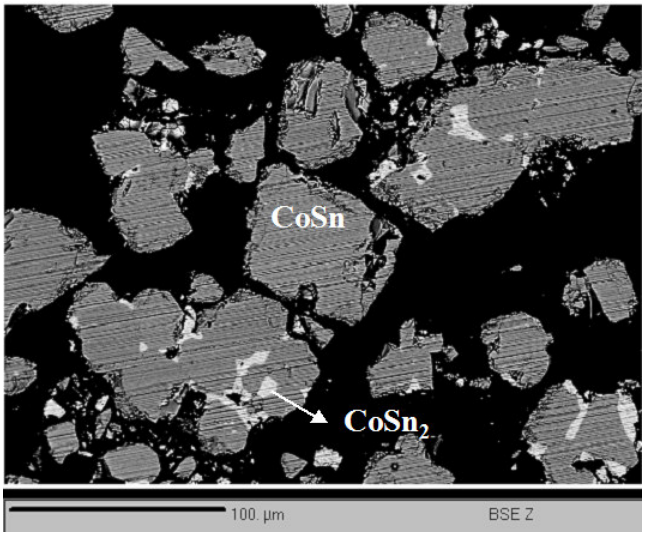

Fig. II.1.7 SEM image in BSE of the end product of the experiment at 1020 K (unpubished). The gray matrix corresponds to the formula CoSn. The white areas are of $CoSn_2$. The black areas represent the resin where the CoSn powder is embedded.

The results cannot rule out significant temperature dependence of the enthalpies of formation. Such a phenomenon has been reported previously by Lück et al. [20]. Thus, transition from positive to negative integral molar enthalpies of formation is expected for the liquid Co–Sn solutions depending on the temperature and the composition.

To help clarifying these problems further measurements of the liquid phase enthalpies of formation were done using direct reaction calorimetry. Namely, pellets containing 9.7 at. % Co and 20.0 at. % Co (five for each composition) were prepared and measurements performed at 1010 and 1303 K, respectively. According to the equilibrium phase diagram (Fig. II.1.3), these specimens are situated in the monophase field of the liquid solutions. The experimental values

obtained for the integral molar enthalpies of formation were –4.3±1.0 kJ.mol^{-1} and +4.9±0.7 kJ.mol^{-1}, correspondingly. The respective regular solution constants (Ω, kJ.mol^{-1}) calculated from these data are –49.1±11.4 kJ.mol^{-1} (at T=1010 K) and +30.6±4.4 kJ.mol^{-1} (at T=1303 K). It is evident (taking also into account the solution calorimetry results at 991 K and 1020 K that temperature dependence of Ω subsists. Thus, the so-called Porter approximation (eqn. II.1.3) suitable for regular solutions with temperature dependent parameter [49, 50] could be applied to describe the experimental results:

$$\Delta_f H^{L,T} = x(1-x)(\Omega + T\,\partial\Omega/\partial T)\ \ kJ/mol \qquad \text{(II.1.3)}$$

The values of the coefficients Ω (–210±20 kJ.mol^{-1}) and $\partial\Omega/\partial T$ (0.185±0.018 kJ.mol^{-1}K^{-1}) were calculated by the least squares method, assuming linear temperature dependence of the parameters Ω assessed at 991, 1020, 1010 and 1303 K.

According to X–ray diffraction of the product, obtained at 1010, there are peaks of CoSn and $CoSn_2$. According to the microprobe, there are four phases: pure Sn, CoSn, $CoSn_2$, $CoSn_3$, which are formed during the cooling of the product. The EMPA of the product, obtained at 1303 K, revels the coexistence of two phases. The main phase (matrix) is almost pure Sn (99.8%). The second phase is gray: Co (19%) and Sn (81%), which was the initial composition of the specimens and the third is pure unreacted Co.

In addition solution calorimetry experiments were done at 1430 K by means of Gachon calorimeter. Positive heat effects have been registered, but we are not definitive about the reliability of the results. Investigation of the final alloy (cooled in the furnace) by EMPA has shown the presence of Co_3Sn_2 (as main phase) and of CoSn. Small amount of $CoSn_2$ and traces of $CoSn_3$ are observed as well. The occurrence of all equilibrium phases confirms the construction of the phase diagram Co–Sn and is indication that the reaction $0.6Co+0.4Sn = 1/5\beta Co_3Sn_2$ has not been completely achieved during the discussed calorimetric experiment.

- Experimental studies of the enthalpies of formation of solid Co–Sn phases

Enthalpies of formation ($\Delta_f H$ per mole of atoms) of cobalt–tin compounds have been measured by direct reaction calorimetry at 1287, 1033, 629 and 605 K, respectively [24]. Table II.1.7 represents details about the working conditions and the experimental results for the direct reaction calorimetry of solid phases and Table II.1.8 – a comparison between experimental and calculated enthalpies of formation of solid cobalt–tin phases. The measured molar enthalpies of formation could be associated with four chemical reactions (eqn. II.1.4 – 7).

$0.6Co+0.4Sn = 1/5\beta Co_3Sn_2$ (II.1.4)

$05Co+0.5Sn = 1/2CoSn$ (II.1.5)

$0.33Co+0.67Sn = 1/3CoSn_2$ (II.1.6)

$0.25Co+0.75Sn = 1/4\beta CoSn_3$ (II.1.7)

The mean statistical values of the enthalpies of formation are: –16.0 ± 1.2, –22.0 ± 0.4, –19.8 ± 1.0 and –13.0 ± 0.4 kJ.mol^{-1} for βCo_3Sn_2, $CoSn$, $CoSn_2$ and $\beta CoSn_3$ phases, respectively. These quantities are referred to the stable forms of the constituents at the corresponding temperatures (i.e. liquid Sn and fcc or hcp Co). In this connection one should be aware that the allotropic transition of the pure Co from hexagonal closed packed (hcp) structure to face centered cubic (fcc) structure occurs at 695 K [32] but the transition temperature depends notably on the cooling (heating) rate [51]. The enthalpy change of this transition is around 0.4 kJ.mol^{-1} [51], thus it is in the frame of the statistical errors of the present measurements. Nevertheless, all pertinent enthalpy values (including literature data) have been converted finally to reference states fcc Co and liquid Sn.

The completeness of the reactions has been verified regularly by checking up the reactions products with electron microprobe analyses (EMPA) and X–ray diffraction. Apparatus Cameca SX 100 and X`Pert Philips were used for these purposes.

Table II.1.7 Details about the working conditions and the experimental results for the direct reaction calorimetry of solid phases [24]: m – mass of the specimens (g); $\Delta_f H$ – enthalpy of formation (kJ·mol^{-1}) per mol of atoms; T – working temperature (K); X_{Sn} –

composition of the specimen (mole fraction Sn); Phase – compound synthesized during the experiment. Reference states are fcc Co and liquid Sn at the corresponding temperatures.

No	X_{Sn}	Phase	T K	Time min	m g	$\Delta_f H$ kJ·mol^{-1}
1	0.397	βCo_3Sn_2	1287	12	0.1221	15.7
2					0.1152	–17.3
3					0.1605	–16.3
4					0.1211	–14.5
5	0.499	CoSn	1032	15	0.1249	–22.6
6					0.1151	–22.0
7					0.1358	–21.8
8					0.1132	–21.7
9	0.670	$CoSn_2$	629	120	0,1498	–18.8
10					0.1614	–18.9
11					0.1222	–19.9
12					0.1805	–20.0
13					0.096	–21.5
14					0.1727	–19.9
15	0.750	$\beta CoSn_3$	604	180	0.1536	–12.7
16					0.1069	–13.3
17					0.1147	–13.4
18					0.1476	–13.1
19					0.1499	–12.6
20					0.1022	–13.4
21					0.1290	–12.7

The experimentally obtained enthalpies are influenced by the formation of other phases (usually adjacent). Thus, the overall experimental errors are surely greater than the statistical inaccuracy, amounting probably to around 2 kJ.mol^{-1} while the uncertainties shown in Table II.1.7 and in the text of the paper are statistical only. Corrections of these values could be done by taking into account the amounts of the impurities (i.e. additional phases). Nevertheless to make such corrections one needs to know exactly two kinds of quantities – mole fractions of all impurities and the enthalpy of formation for every single phase at the corresponding temperature. According to us the second condition could not be reliably enough fulfilled at present. That is why we abstained of making such corrections and the experimental enthalpy of formation values were attributed to the respective main phase obtained in every calorimetric trial.

This consideration should be taken into account when comparisons between literature data are done (Table II.1.8). As one could see, good agreements between our own experimental work, literature experimental [15, 18, 42] and calculated [1, 22, 38] enthalpies of formation are observed for βCo_3Sn_2 and CoSn phases. No literature data for $\beta CoSn_3$ enthalpies of formation are available, while temperature independent value [15] is found for $CoSn_2$ only.

Table II.1.8. Comparison between experimental and calculated enthalpies of formation of solid cobalt–tin phases [24]. The reference states are: fcc Co and liquid Sn, at the respective working temperatures.

Phase	$\Delta_f H$, kJ.mol^{-1}	T K	Source
1	2	3	4
βCo_3Sn_2	–16.0±1.2	1287	This work [24]
	–14.3 to –14.9	Temperature independent	[15]
	–13.6	Temperature independent	[14]
	–15.1 [A]	1287	[22]
	–17.5 [A]		[1]
	–14.6 [A]		[38]
	–15.1 [A]		[22]
CoSn	–22.0±0.4	1032	This work [24]
	–22.1	Temperature independent	[15]
	–21.7	Temperature independent	[14]
	–22.1	874	[23]
	–21.4 [A]	1032	[22]
	–20.8 [A]		[1]
	–21.1 [A]		[38]
	–21.4 [A]		[22]

Table II.1.8 continuation

1	2	3	4
$CoSn_2$	–19.8±1.0	629	This work [24]
	–14.7	Temperature independent; Interpolated value	[15]
	–17.2 [A]	629	[22]
	–14.8 [A]		[1]
	–16.8 [A]		[38]
$\beta CoSn_3$	–13.0±0.4	604	This work [24]
	–13.8 [A]		[22]
	–14.2 [A,B]		[38]

[A] – calculated values of thermodynamic optimizations; [B] – $\alpha CoSn_3$ and $\beta CoSn_3$ are modeled as a single phase by Jiang et al. [38].

Measurements of enthalpy of βCo_3Sn_2 have been done by direct reaction calorimetry at 1287 K. Four pellets with composition 60 at. % Co were prepared. Details about the working conditions and the experimental results are given in Table II.1.7 (nos. 1 – 4). The calorimetric curves from every experiment are plotted in Fig II.1.8. The time of the isothermal heating follows the temperature dependence (shown in Table II.1.7) and the reaction is exothermic. The average value of the enthalpies of formation of βCo_3Sn_2 compound is – 16.0±1.2 $kJ.mol^{-1}$.

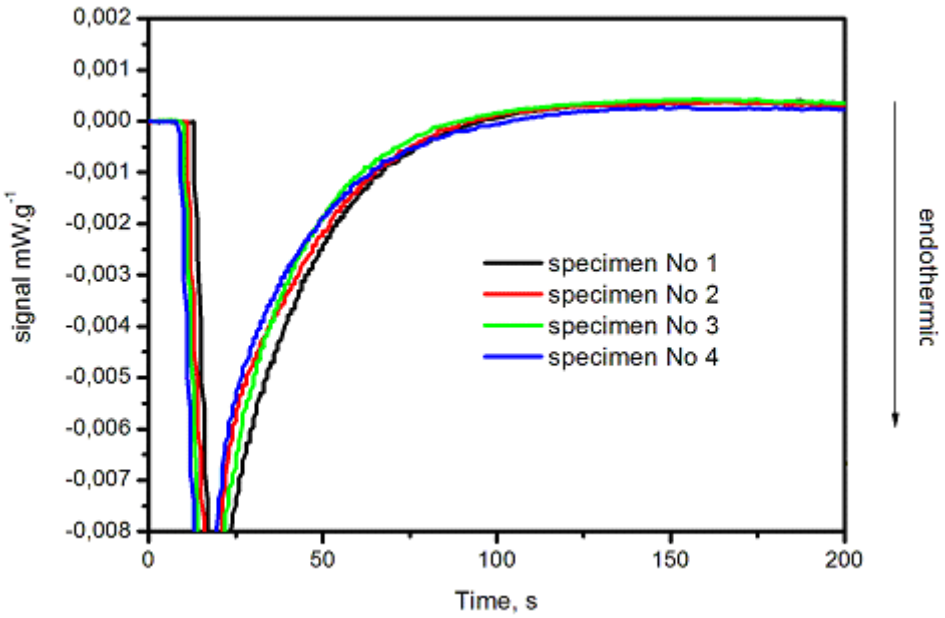

Fig. II.1.8 Calorimetric curves of specimens nos. 1 to 4 (Table II.1.6) [58]. The numbers of the peaks correspond to the number of the specimen. The peaks are due to the reaction between solid Co and liquid Sn to form the compound βCo_3Sn_2. The temperature of the reaction is 1287 K. The time since the introducing of a sample into the calorimeter is plotted along the abscissa and the weight corrected DSC signal ($mW.g^{-1}$) is plotted along the ordinate. The signals' values are proportional to the enthalpy changes. The endothermic peaks show downward. The signal returns to the baseline after more than 600 s, which explains that this is not visible here.

X–ray diffraction of specimen No 1 was performed. It is of worth noting that in specimens nos. 1–4 the low-temperature phase αCo_3Sn_2 was observed only. This fact indicates a rapid transition from the high- to the low-temperature form.

According to the results of microprobe (specimen nos. 2) the main phase is Co_3Sn_2 (94%) as well. There are two more phases: dark one, which is almost pure Co (5%) and light, which is quasi-pure Sn (1%) (Fig. II.1.9). These values are assessed by an empirical quantitative method. Equidistant straight lines are drawn across the picture. On each of these lines the proportion of the different phases is determined and for the picture mean values are computed. It is considered that these values correspond to the phase volume fractions.

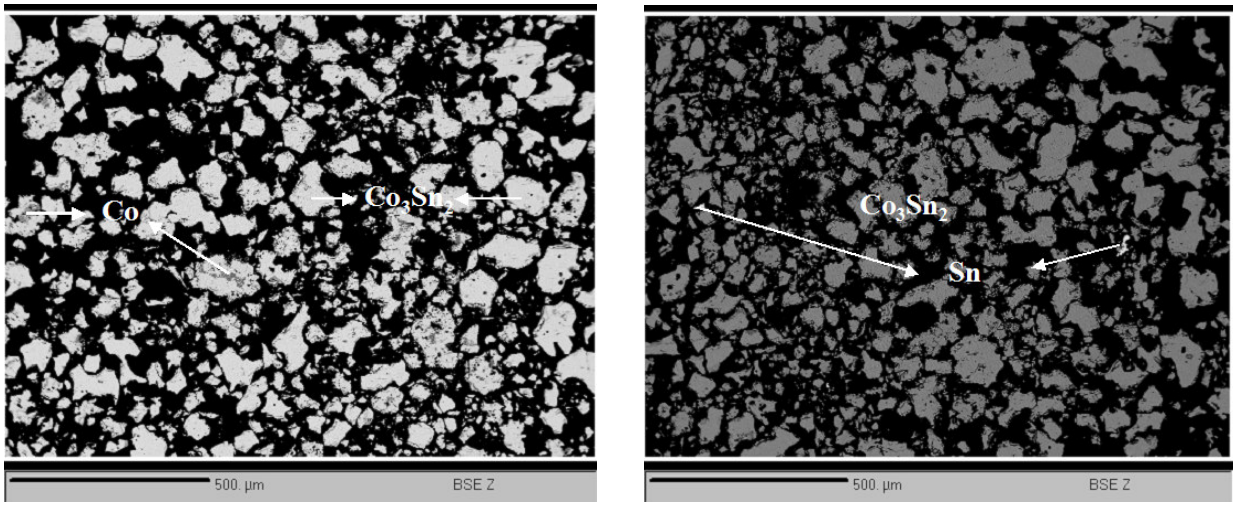

A B

Fig. II.1.9 SEM images in BSE of specimen No 2, obtained by direct reaction calorimetry at 1287 K (unpublished). The gray phase corresponds to the formula Co_3Sn_2. The dark gray phase represents quasi pure Co (II.1.9 A) and the white areas are of pure Sn (II.1.9 B). The black areas represent the resin where the CoSn powder is embedded.

The enthalpy of formation of CoSn compound has been measured by direct reaction at 1033 K. Four pellets with composition 50 at. % Co are prepared. The calorimetric curves show a well-defined exothermic effect. Details about the working conditions and the experimental results are given in Table II.1.7 (nos. 5 – 8). The time of the isothermal heating (Table II.1.7) is relatively short in comparison with preceding experiments (Fig. II.1.10), which due to the higher temperatures. The average value of the enthalpies of formation of CoSn is – 22.0 ± 0.4 kJ.mol^{-1}.

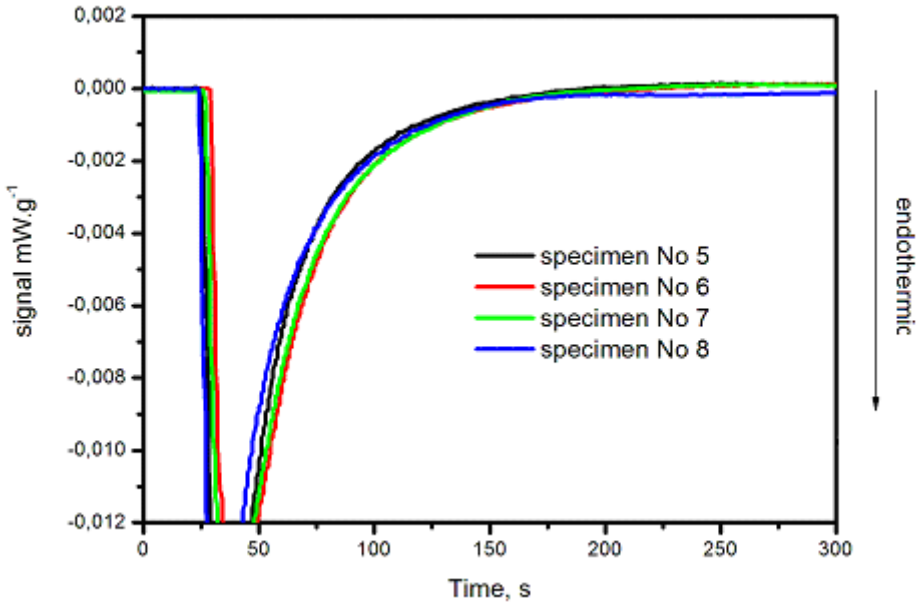

Fig. II.1.10 Calorimetric curves of specimens nos. 5 to 8 (Table II.1.6) (unpublished). The peaks are due to the reaction between solid Co and liquid Sn to form the compound CoSn. The numbers of the peaks correspond to the number of the specimen. The temperature of the reaction is 1033 K. The time since the introducing of a sample into the calorimeter is plotted along the abscissa and the weight corrected DSC signal ($mW.g^{-1}$) is plotted along the ordinate. The signals' values are proportional to the enthalpy changes. The endothermic peaks show downward. The signal returns to the baseline after more than 600 s, which explains that this is not visible here.

After the calorimetric experiments specimen No 6 has been analysed at room temperature by X–ray diffraction and specimen No 5 by EMPA.

The X–ray analyses have confirmed the existence of the phase CoSn. A few reflections corresponding to $CoSn_2$ have been observed as well. The X–ray spectra obtained have been compared with standard (calculated) spectra. These results have been confirmed by EMPA. It is observed a small light phase of $CoSn_2$ about 15% of the whole sample (Fig. II.1.11). These values are assessed by an empirical quantitative method, already explained.

The influence of the second phase on the calorimetric result can be estimated as follows:

$A = \Delta_f H_{experimental} = 0.85\Delta_f H\ (CoSn) + 0.15\Delta_f H\ (CoSn_2)$

$\Delta_f H\ (CoSn) = (A - (0.\ 15\Delta_f H\ (CoSn_2))/0.85 = -22.4\ kJ/mol^{-1}$

The uncertainty of the new result, not considering the fact that the two experiments have been made at different temperatures which means that the temperature effects are neglected and not considering the uncertainty on the phase quantities, is:

$\Delta A/0.85 + \Delta(\Delta_f H(CoSn_2)0.15/0.85$

$\Rightarrow\ 0.4/0.85 + 0.15/0.85 = 0.65$

This justifies the fact that we do not correct the experimental result.

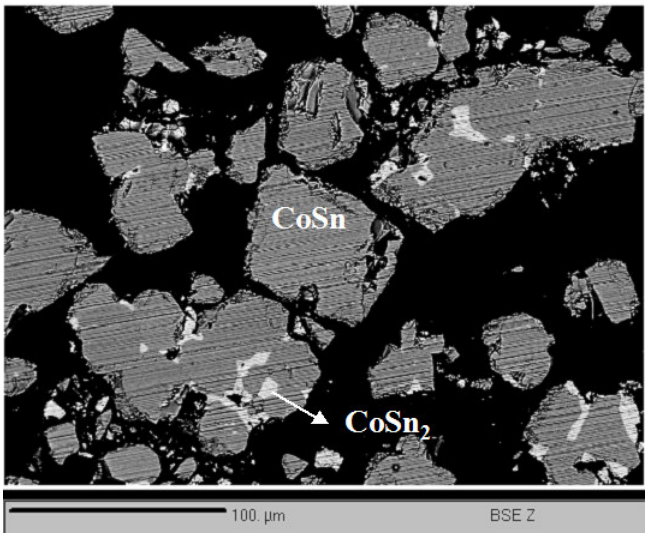

Fig. II.1.11 SEM image in BSE of specimen No 5, obtained by direct reaction calorimetry at 1033 K (unpublished). The gray phase corresponds to the formula CoSn. The small white areas represent $CoSn_2$. The black areas are the resin where the CoSn powder is embedded.

The enthalpy of formation of $CoSn_2$ compound has been measured by direct reaction (apparatus Calvet) at 629 K. Six samples with composition 33 at. % Co were prepared (Table II.1.7, nos. 9–14). The calorimetric curves are plotted in Fig. II.1.12. The time of the isothermal heating is shown in Table II.1.7. The mean value of the enthalpies of formation of $CoSn_2$ compound is -19.8 ± 0.97 kJ.mol^{-1}l..

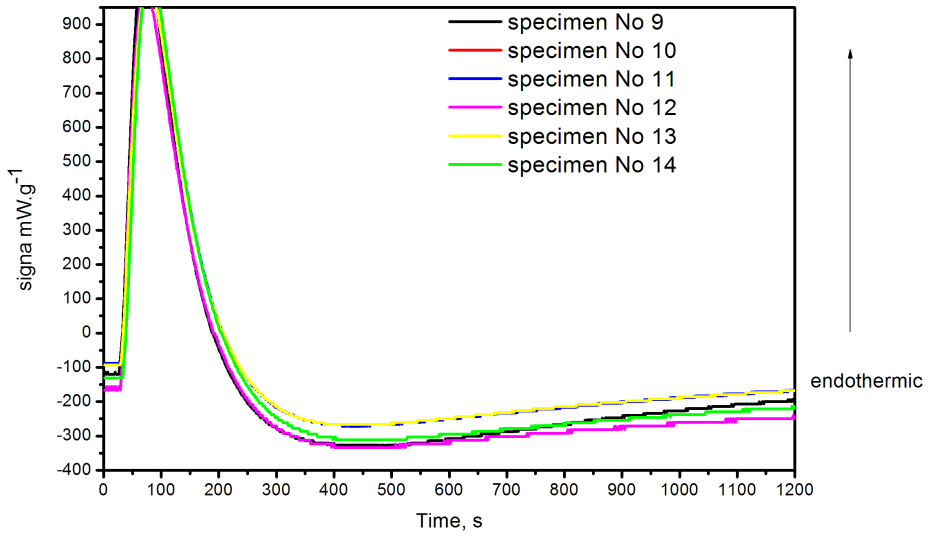

Fig. II.1.12 Calorimetric curves of specimens nos. 9 to 14 (Table II.1.7) (unpublished). The peaks are due to the reaction between Co and Sn to form the compound $CoSn_2$. The numbers

of the peaks correspond to the number of the specimen. The temperature of the reaction is 629 K. The time since the introducing of a sample into the calorimeter is plotted along the abscissa and the weight corrected DSC signal ($mW.g^{-1}$) is plotted along the ordinate. The signals' values are proportional to the enthalpy changes. The endothermic peaks show upward. This figure together with the next one II.1.13 shows that the reproducibility of the curves is not perfect but that the kinetics reaction is not different between the two temperatures 629 and 605 K.

According to X–ray diffraction and EMPA, the sample N10 is homogeneous

The enthalpy of formation of $CoSn_3$ compound has been measured by direct reaction (apparatus Calvet) at 605 K (thus the equilibrium form is $\beta CoSn_3$). Seven pellets with composition 25 at. % Co are prepared (Table II.1.7, nos. 15 – 21). The calorimetric curves are reproducible (Fig. II.1.13). The time of the isothermal heating is shown in Table II.1.7. The mean value of the enthalpies of formation of $\beta CoSn_3$ is -13 ± 0.4 $kJ.mol^{-1}$.

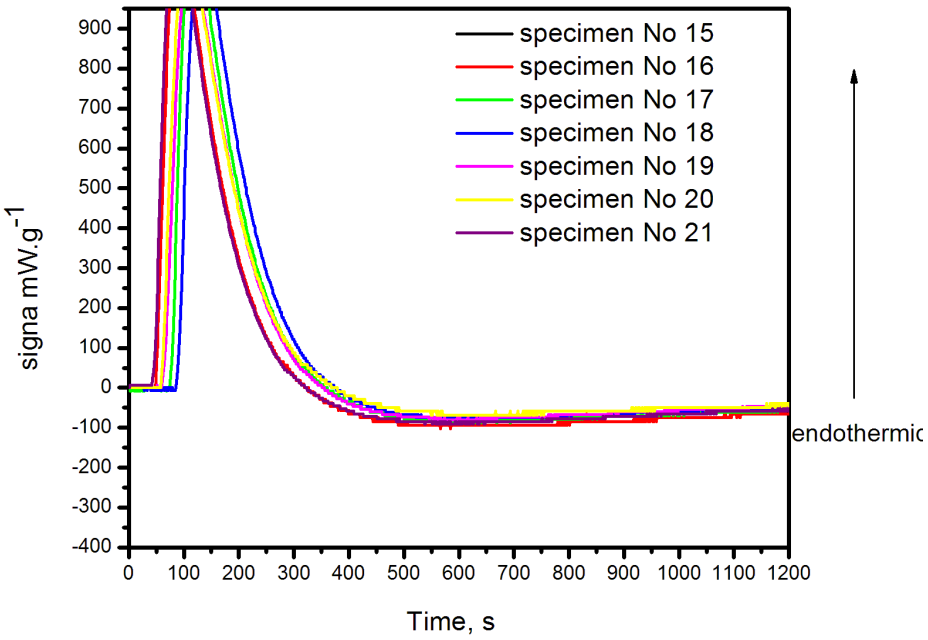

Fig. II.1.13 Calorimetric curves of specimens nos. 15 to 21 (Table II.1.7) (unpublished). The peaks are due to the reaction between Co and Sn to form the compound $\beta CoSn_3$. The numbers of the peaks correspond to the number of the specimen. The temperature of the reaction is 605 K. The time since the introducing of a sample into the calorimeter is plotted along the abscissa and the weight corrected DSC signal ($mW.g^{-1}$) is plotted along the ordinate. The signals' values are proportional to the enthalpy changes. The endothermic peaks show upward.

The EPMA and X–ray diffraction analyses have shown that the specimens synthesized at 605 K are homogeneous.

X–ray diffraction analyses of sample No. 15 (Table II.1.7, $CoSn_3$ compound) were performed under vacuum by means of high-temperature diffractometer X`Pert Philips with Cu $K_{\alpha 1}$ rays, heating rate of 5 K min^{-1} in the interval from room temperature to 653 K (Fig. II.1.14 – 16)

Crystal structure changes (modification of diffraction peaks) started at around 553 K and completed at 573 K (Fig. II.1.15). The specimen has been heated up to 653 K, but no more structure changes were observed. On cooling, peaks of $\alpha CoSn_3$ appear at around 353 K (Fig. II.1.16). Hence, a kind of hysteresis is observed. It is of worth noting that Lang and Jeitschko [33] reported that the transition temperature was observed by DSC on heating but not on cooling.

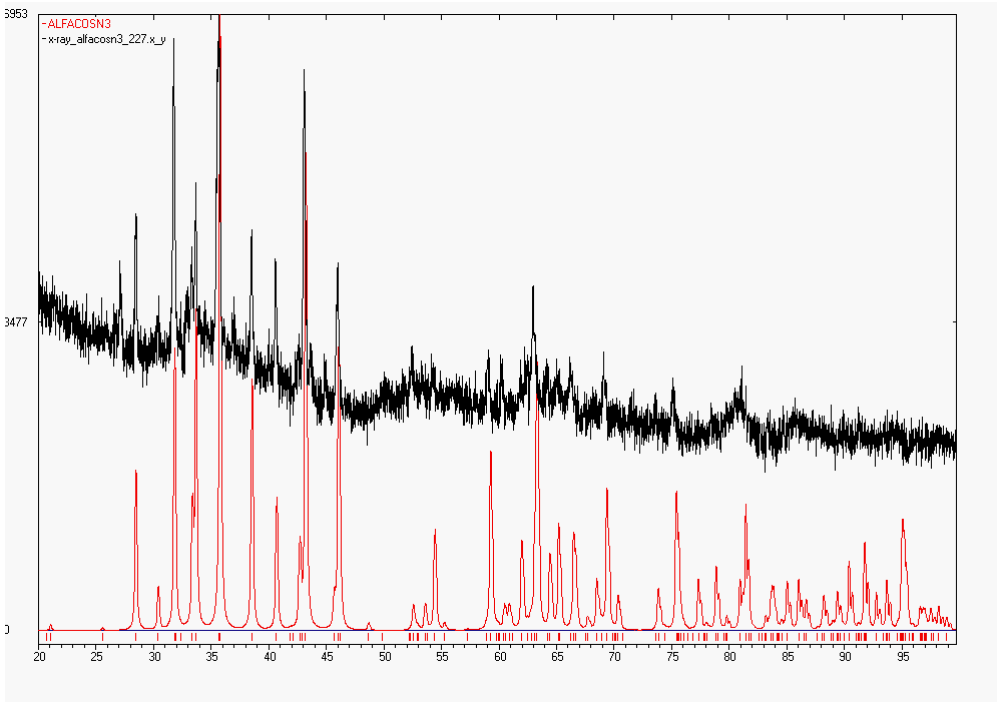

Fig. II.1.14 XRD spectrum of sample No 20 at 500 K (low-temperature form), superimposed with theoretical pattern of $\alpha CoSn_3$ (red curve), simulated by PowderCell 2.3, using room temperature data from [48], (unpublished).

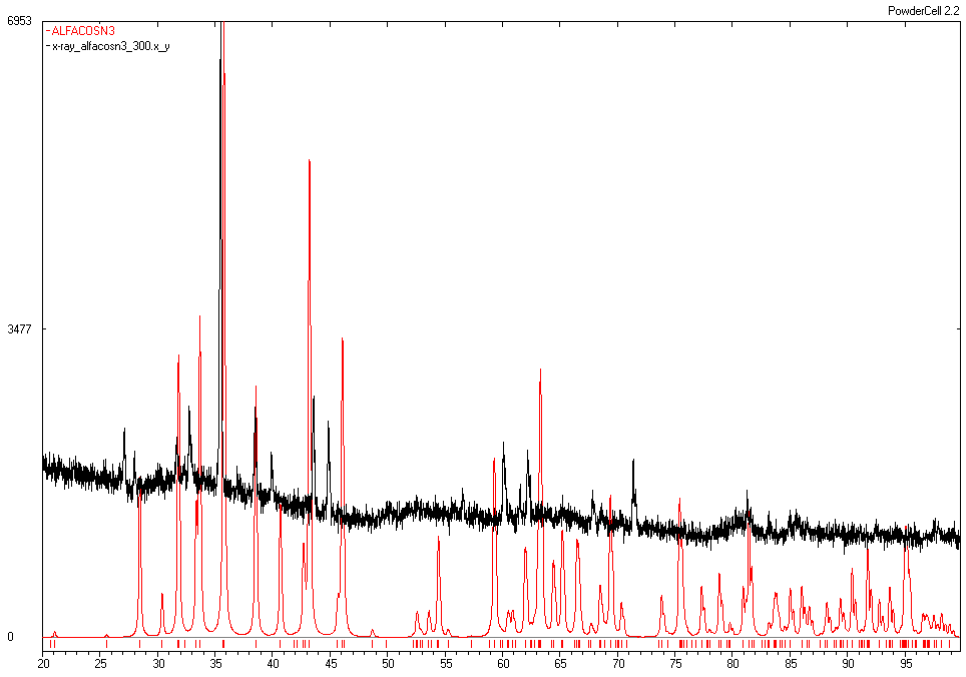

Fig. II.1.15 XRD spectrum of sample No 20 at 573 K (high-temperature form), superimposed with theoretical pattern of $\alpha CoSn_3$ (red curve, room temperature), simulated by PowderCell 2.3, using [48] (unpublished).

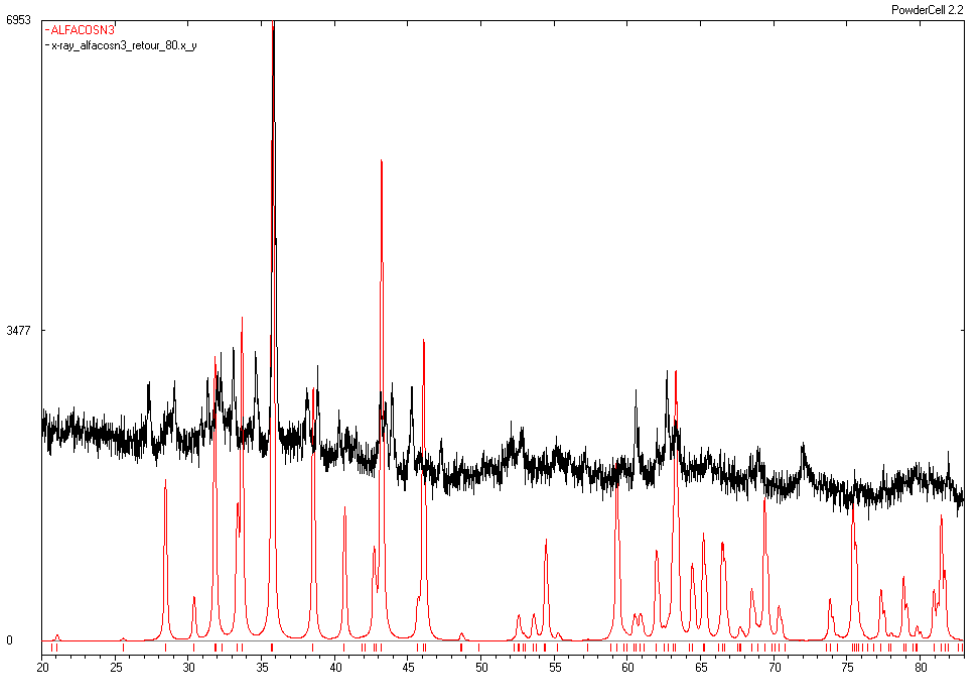

Fig. II.1.16 XRD spectrum of sample No 20 during cooling (around 353 K), superimposed with the theoretical pattern of $\alpha CoSn_3$ (red curve, room temperature), simulated by PowderCell 2.3, using [48] (unpublished).

➢ Phase diagram studies of the Co–Sn system

According to the Co–Sn phase diagram (Fig. II.1.22A), two phase transitions might be observed for a specimen with nominal composition of 75 at. % Sn within the specified temperature interval. They ought to correspond to the polymorphic transition PD2 ($\alpha CoSn_3 \rightarrow \beta CoSn_3$, at 548 K) and to the peritectic decomposition P3 of $\beta CoSn_3$ ($\beta CoSn_3 \rightarrow CoSn_2$+L, at 618 K). As one can see, the latter peak appears but the polymorphic transition PD2 could not be detected. The peak E2 (Fig. II.1.17A, curve 1) corresponds to the eutectic reaction ($\alpha CoSn_3$+βSn $\leftrightarrow$ L). Its appearance (although feeble) is due to the incomplete reaction No. II.1.7 as discussed above.

The anticipated transition $\alpha CoSn_3 \rightarrow \beta CoSn_3$ was not discovered in this specimen. A reason for not observing this peak is the supposed feeble enthalpy change of the considered solid-state transition. Another reason might be the difficult nucleation of the new phase. The hysteresis observed by X–ray studies could be evidence backing such a suggestion. In this case the P3 peak should correspond to the decomposition of the low-temperature phase at a lower temperature than the high-temperature form of the same phase. We could not study the kinetic behaviour of the transformations because of a lack of time and so this question is not yet completely solved.

One more series of alloys, situated in the two-phase region $CoSn_2$+$CoSn_3$, were synthesized in order to study the transition $\alpha CoSn_3 \rightarrow \beta CoSn_3$. For this purpose, three pellets having chemical composition 72.1 at. % Sn were prepared and annealed for two weeks at 565 K. One of them, referred further as sample 22 has been subjected to DSC analyses (two runs from 300 K to 700 K, Fig. II.1.17A and 17B (curves 2 and 3))**.**

One peak (P3, see Fig. II.1.17A) was detected on heating during each run – at 622 K (first cycle, curve 2) and at 619 K (second cycle, curve 3). The eutectic reaction ($\alpha CoSn_3$+βSn $\leftrightarrow$ L) has not appeared on heating, thus confirming the expected phase composition and the equilibrium Co–Sn phase diagram (Fig. II.1.22A). The expected transition PD2 was observed during the second cycle of specimen No. 22 only (Fig. II.1.17A, curve 3). This is an indication that the enthalpy change accompanying such a solid-state transition is rather small as expected.

On cooling, two partially overlapping heat effects were registered with both specimens 20 (Fig. II.1.17B, curve 1) and 22 (Fig. II.1.17B, curves 2 and 3). The peaks identified as P3 begin at about 532 K while these identified as E2 – at about 500 K. As one can see, the shift (i.e. the undercooling) of the peritectic reaction (P3: L+$CoSn_2 \leftrightarrow \beta CoSn_3$) from the equilibrium

invariant temperature (618 K) is significant while the eutectic reaction (E2: L ↔ $\alpha CoSn_3$+(βSn)) is practically not displaced. This might be explained by assuming nucleation problems for the $\beta CoSn_3$ phase.

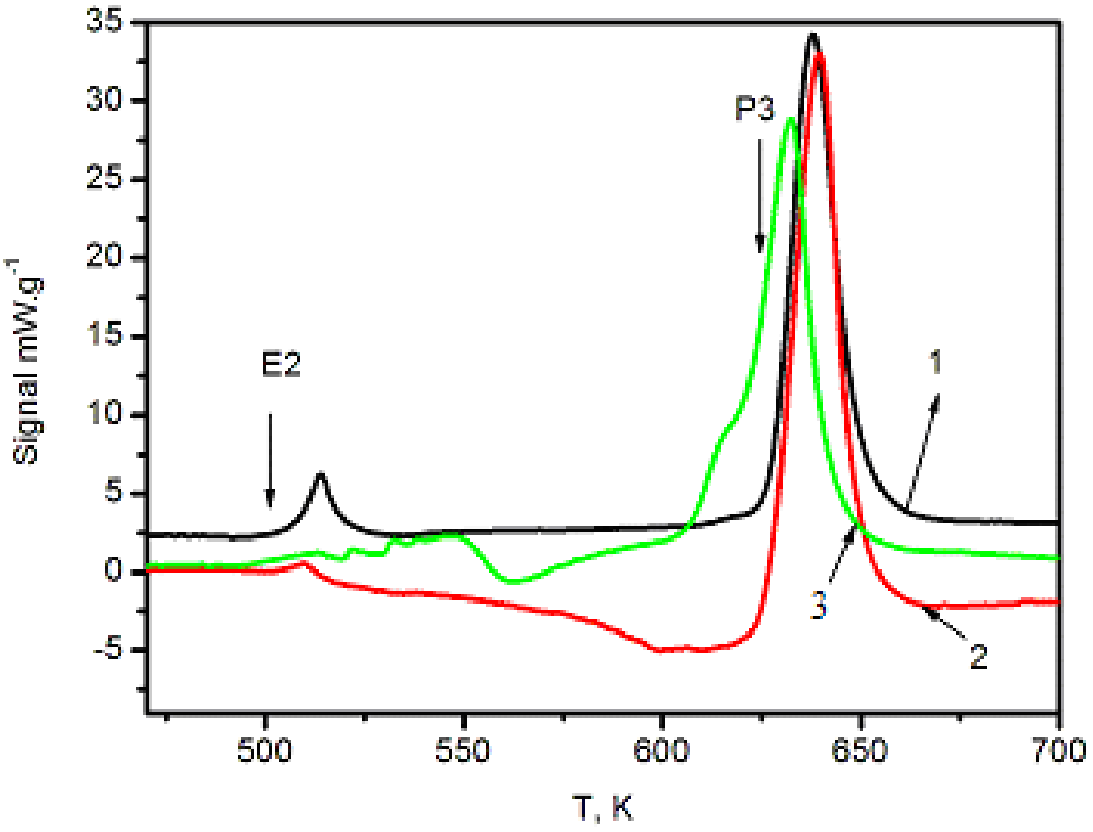

Fig. II.1.17A. Differential scanning calorimetry of specimens nos. 21 and 22 on heating [24]. Heating rate: 10 K min^{-1}. The curve 1 corresponds to sample No. 21, curve 2 and curve 3 – to sample 22, first and second cycle, respectively. The peaks E2 (at about 498 K) are due to the eutectic reaction, the peaks P3 (at about 621 K) – to the peritectic decomposition of $\beta CoSn_3$. The temperature (K) is plotted along the abscissa and the weight-corrected DSC signal ($mW.g^{-1}$) – along the ordinate.

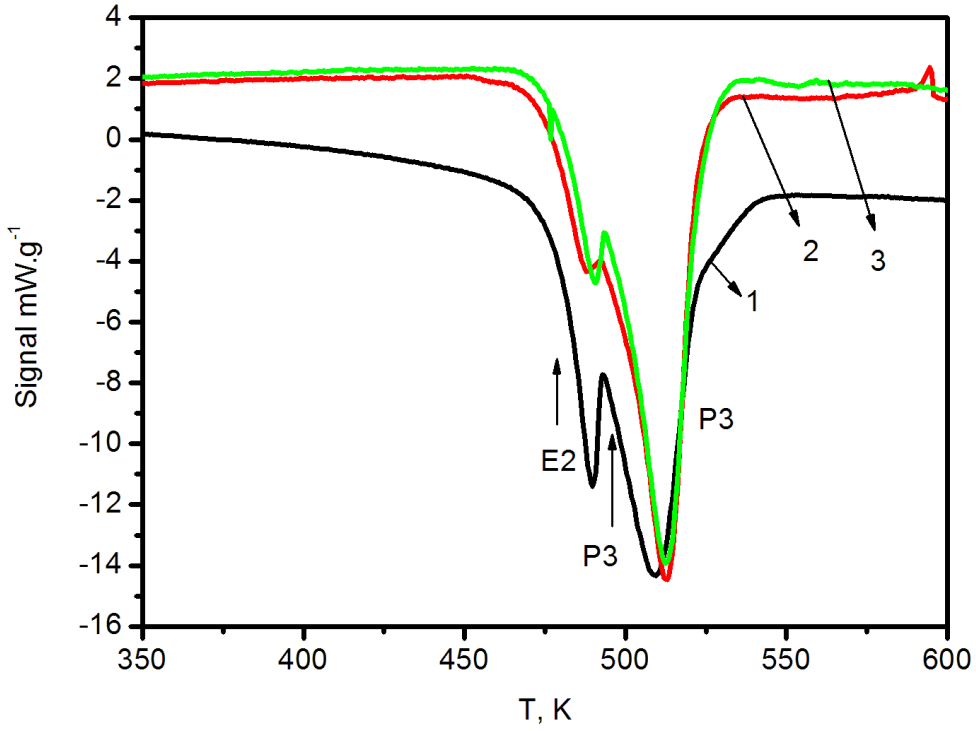

Fig. II.1.17B. Differential scanning calorimetry of specimens nos. 21 and 22 on cooling [24]. Cooling rate: 10 K min^{-1}. Curve 1 represents results of sample No 21, curves 2 and 3 – sample 22, first and second cycle, respectively. The temperature (T, K) is plotted along the abscissa and the weight corrected DSC signal (Signal, $mW.g^{-1}$) is plotted along the ordinate. Two overlapping peaks are observed at every cycle. For specimen No 20, the first one begins at about 492 K (P3) and the second about 485 K (E2); for specimen No. 22 – at about 492 K (first cycle), 493 K (second cycle) and the second about 457 K, and respectively at 465 K.

The order/disorder transformation in the phase Co_3Sn_2 (Fig. II.1.22A) was studied by differential scanning calorimetry. For this purpose, weighed quantities of pieces cut from a cobalt rod (5N) and Sn shots (4N) have been sealed under argon atmosphere in quartz tubes and annealed (Table II.1.9). In such a way, four specimens with compositions near to formula Co_3Sn_2 were prepared. After thermal treatment of specimen No 23 (Table II.1.9), the alloy has been studied by EMPA and some unreacted cobalt was observed. That is why supplementary heat treatment was done. To be precise, all specimens were re-melted twice in the same evacuated ampoules by means of induction furnace using power of 4 kW (i.e. at about 1473 K) and afterwards homogenized in a resistance furnace for 36 h at 1173 K (56 h at 1248 K for specimen No 23) (Table II.1.9).

Table II.1.9 Overall chemical composition and heat treatment conditions of specimens with composition near to the formula Co_3Sn_2. No – consecutive number of the specimen, X_{Sn} – tin mole fractions of the pertinent alloy, m – mass of the respective specimen (g).

No	x Sn	Annealing	mass
23	0.41	20 h at 953 K 56 h at 1248 K	2.8271
24	0.39	36 h at 1173 K	0.9882
25	0.40	36 h at 1173 K	1.6413
26	0.42	36 h at 1173 K	1.8447

DSC studies of all four Co_3Sn_2 specimens were performed in the interval from 300 to 1080 K with heating rates of 5 and 10 K min^{-1} (Fig. II.1.18). The thermal curves obtained with a rate of 5 K min^{-1} were not satisfactory, probably, due to the small enthalpy of transition.

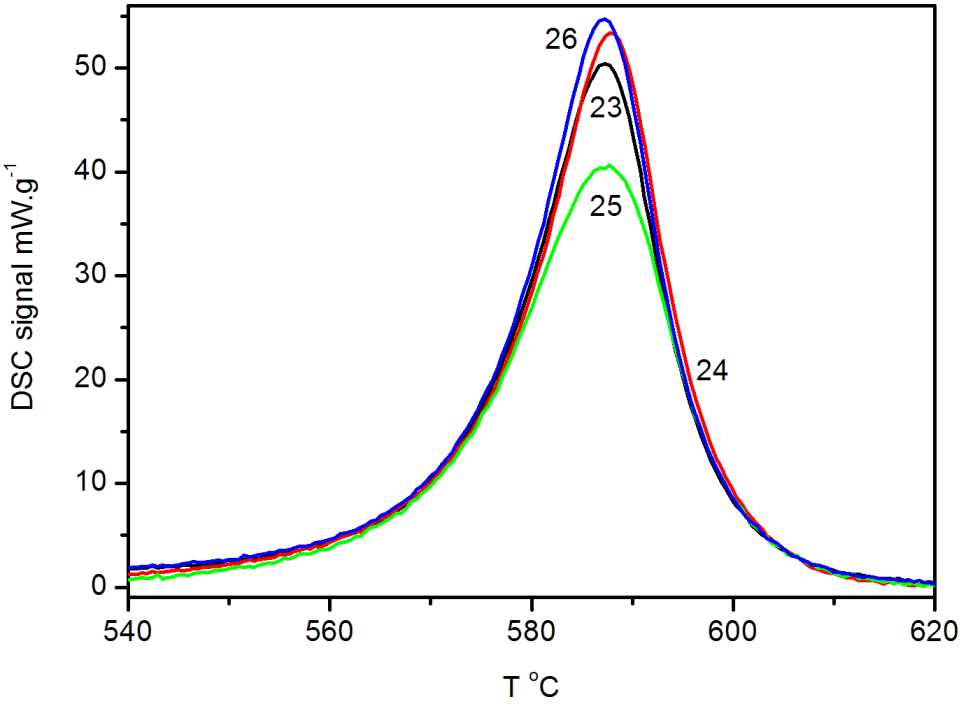

Fig. II.1.18 Differential scanning calorimetry of specimens nos. 23 to 26, on heating [24, 58]. The peaks (endothermic) are due to the transition $\alpha Co_3Sn_2 \rightarrow \beta Co_3Sn_2$. Heating rate: 10 K min^{-1}. The temperature (^0C) is plotted along the abscissa, and the weight-corrected DSC signal ($mW.g^{-1}$) – along the ordinate.

In Table II.1.10 temperatures and enthalpies of the transition $\alpha Co_3Sn_2 \rightarrow \beta Co_3Sn_2$ measured in this work are exhibited. The average temperature and enthalpy of transition is 833 ± 1.2 K and 0.750 ± 0.23 kJ.mol^{-1}, respectively. There is no literature enthalpy data for comparison, while the measured transition temperature is in good agreement with the value of 840 ± 11 K reported by Cömert and Pratt [16].

Table II.1.10 Results of the DSC studies of Co_3Sn_2 specimens [24, 58]. No – consecutive number of the specimen, m (g) – mass of the pertinent specimen, T (^{0}C) and $\Delta_f H$ (kJ.mol^{-1}) – temperature and enthalpy of the transition $\alpha Co_3Sn_2 \rightarrow \beta Co_3Sn_2$.

No	m g	T K	$\Delta_f H$ kJ·mol^{-1}
23	0.6124	834	0.733
24	0.7081	831	0.739
25	0.6959	830	0.745
26	0.7085	833	0.785

➢ Thermodynamic optimization of the Co–Sn system

A thermodynamic optimization of Co–Sn binary system has been done [22]. The results show a good agreement with the experimentally obtained (Table II.1.8). The experimental information used for the assessment of the Co–Sn system is presented in Table II.1.11.

Table II.1.11 Experimental information used for the assessment of the Co–Sn system [22]

Type of data	Reference
Topological data for the liquidus and the invariants (normalized temperatures)	[25]
Topological data for the liquidus and the invariants (normalized temperatures)	[26]
Topological data for the liquidus and the invariants	[27]
Topological data for the liquidus	[28]
Activities of tin in the solid phases (1273, 1073, 773 K) and extrapolated activities in the liquid phase (1273, 1073); Topological data about the phase boundaries.	[15]
Topological data about the phase boundaries and the invariants. Temperature of the Congruent melting point of Co_3Sn_2. Temperature of the order-disorder transformation in Co_3Sn_2.	[16]
Thermochemical data about the melting temperature of $CoSn_2$ and $CoSn_3$	[33]
Enthalpy of formation of liquid alloys (1823, 1780, 1759, 1675, 1671 K)	[20]
Enthalpy of formation of CoSn, Co_3Sn_2	[42]
Enthalpy of formation of CoSn	[23]

Waldner and Ipser [57] have developed an approach to the thermodynamic modelling of $B8_{2(1)}$-type compounds. In such a crystal lattice the tin atoms form a close-packed hexagonal sublattice, while the cobalt (1 and 2) atoms occupy the interstitial sites (e.g. Co(1) atoms fill all the octahedral interstitial sites, equal by number to the sites on the hexagonal sublattice; Co(2) atoms occupy part of the trigonal bipyramidal interstices of the Sn-atom array [39]). Due to the narrow βCo_3Sn_2 homogeneity range and in agreement with the chemical composition, the occupancy of the latter sites must be around 50 ± 6 %. Consequently, four-sublattice model is

needed in order to account for the order-disorder transformation, as discussed in details previously [24, 52]:

$$(Co)_1(Sn)_1(Co,Va)_{0.5}(Co,Va)_{0.5} \qquad \text{(II.1.8)}$$

Such an approach has been applied by Jiang et al. [38] while Liu et al. [1] have modelled this phase as stoichiometric compound. The input information used in the present work is different from that one of Jiang et al. [38], because corrections of the experimental liquidus temperatures have been introduced by us [22].

In support of the normalization we would like to notice that after temperature corrections, the high-temperature eutectic invariant (Table II.1.12) is estimated to lie at 1414 ± 7 K (by statistics of the normalized data of Lewkonja [25]). This is in good agreement with the recent measurements of Cömert and Pratt [16] giving a value of 1398 ± 2 K. Similarly, good accord between both authors is observed for the peritectic temperature P1 (1239 K) as well (Table II.1.12).

Table II.1.12 Temperatures, types and notations of the invariant equilibria in the Co–Sn system [22]. C.M. – congruent melting; PD1 – hypothetic peritectoid reaction; ED1 – hypothetic eutectoid reaction; P4 – degenerated peritectic reaction; ED2 – degenerated eutectoid reaction; PD2 and PD3 – degenerated peritectoid (eutectoid) reactions

Invariant reaction	Type	Temperature, K	Source
1	2	3	4
$L \leftrightarrow (\alpha Co)+\beta Co_3Sn_2$ $X_L=0.230$; $X_{FCC}=0.016$; $X_{\beta Co3Sn2}=0.393$	Eutectic (E1)	1414 [A] 1378 [A] 1381 1398±3 ~1385 1376 1381 1400	[25] [26] [27] [16] [17] [E] [38] [E] [1] [E] This work [22] [E]
$L \leftrightarrow \beta Co_3Sn_2$ $X_L=X_{\beta Co3Sn2}=0.399$	(C.M.)	1473 1443 1454 1472 1472	[16] [17] [E] [38] [E] [1] [E] This work [22] [E]

Table II.1.12 continuation

1	2	3	4
$L+\beta Co_3Sn_2 \leftrightarrow CoSn$ $X_L=0.729$; $X_{\beta Co3Sn2}=0.418$; $X_{CoSn}=0.500$	Peritectic (P1)	1239 [A] 1196 [A] 1239±3 1209 1238 1216 1240	[25] [26] [16] [17] [E] [38] [E] [1] [E] This work [22] [E]
$\beta Co_3Sn_2 \leftrightarrow \alpha Co_3Sn_2$ unidentified compositions	Order/disorder transformation and related invariants (PD1) [B]	840±17	[16]
$\alpha Co_3Sn_2 \leftrightarrow \beta Co_3Sn_2 + (\alpha Co)$ $X_{\alpha Co3Sn2}=0.397$; $X_{\beta Co3Sn2}=0.406$; $X_{FCC}=8.3E-4$		840 826	[1] [E] This work [22] [E]
$\beta Co_3Sn_2 \leftrightarrow \alpha Co_3Sn_2+CoSn$ $X_{\beta Co3Sn2}=0.411$; $X_{\alpha Co3Sn2}=0.399$; $X_{CoSn}=0.5$	(ED1) [B]	793	This work [22] [E]
$L+CoSn \leftrightarrow CoSn_2$ $X_L=0.959$; $X_{CoSn}=0.500$; $X_{CoSn2}=0.6667$	Peritectic (P2)	819 [A] 787 [A] 823 844±3 798 843 798 845	[25] [26] [16] [33] [17] [E] [38] [E] [1] [E] This work [22] [E]
$(\alpha Co) \leftrightarrow (\varepsilon Co)+\alpha Co_3Sn_2$ $X_{FCC}=2.8E-4$; $X_{HCP}=3.5E-5$; $X_{\alpha Co3Sn2}=0.397$	Eutectoid (ED2) [C]	694 ~693 695 696 693	[16] [17] [E] [38] [E] [1] [E] [22] [E]
$L+CoSn_2 \leftrightarrow \beta CoSn_3$ $X_L=0.996$; $X_{CoSn2}=0.6667$; $X_{\beta CoSn3}=0.75$	Peritectic (P3)	618±2 (DSC) 623±5 (DTA) 618	[33] [33] This work [22] [E]

Table II.1.12 continuation

1	2	3	4
$\beta CoSn_3 \leftrightarrow \alpha CoSn_3$ $X_{\beta CoSn3}=0.75$; $X_{\alpha CoSn3}=0.75$ $\beta CoSn_3 \leftrightarrow \alpha CoSn_3+L$ $X_{\beta CoSn3}=0.75$; $X_{\alpha CoSn3}=0.75$; $X_L=0.999$	Polimorphic transformation and related invariants	548±5	[33]
$\beta CoSn_3 \leftrightarrow \alpha CoSn_3+CoSn$ $X_{\beta CoSn3}=0.75$; $X_{\alpha CoSn3}=0.75$; $X_{CoSn}=0.5$	(P4) [C] (PD2) [C]	548 548	This work [22] [E] This work [22] [E]
$L \leftrightarrow \alpha CoSn_3+(\beta Sn)$ $X_L \approx 1$; $X_{\alpha CoSn3}=0.75$; $X_{(\beta Sn)}=1$	Eutectic (E2) [C, D]	~502 ~501 502 505 502 504	[25] [26] [17] [E] [38] [E] [1] [E] This work [22] [E]
$(\beta Sn) \leftrightarrow (\alpha Sn)$ $X_{\beta Sn}=1$; $X_{\alpha Sn}=1$ $(\beta Sn) \leftrightarrow (\alpha Sn)+ \alpha CoSn_3$ $X_{\alpha CoSn3}=0.75$; $X_{\beta Sn}=1$; $X_{\alpha Sn}=1$	Allotropic transformation and related invariant (PD3) [C]	286 286	[31,32] [E] This work [22] [E]

[A] – recalculated temperatures (normalized to the contemporary accepted value of the cobalt melting point); [B] – equilibrium related with order-disorder transformation and nearly degenerated; [C] – degenerated three-phase equilibrium (the compositions of two coexisting phases are very close one to another); [D] – the melting point of pure Sn is 505.08 K; [E] – assessed values

We have to note that Liu et al. [1] ignored the existence of the $CoSn_3$ phase and have modelled both Co_3Sn_2 modifications as stoichiometric phases. Moreover, these authors seemed to be unaware about the liquid phase enthalpy values obtained by Lück et al. [20]. That is why the assessment of Liu et al. [1] seems not suitable for further comparison with the results of the present work.

Another difference between the input data used in this study and those of Jiang et al. [38] is that tin activities (a_{Sn}) measured by Eremenko et al. [21] at 1573 K in liquid Co–Sn alloys, by the effusion method, have not been fully accepted here by reasons discussed below.

The technique used by Eremenko et al. [21] is related to the ratio between the evaporation rates of the pure liquid Sn (v_{Sn}^0) and that (v_{Sn}) of the alloyed liquid phase.

$$a_{Sn} = v_{Sn} / v_{Sn}^0 = p_{Sn}/p_{Sn}^0 \qquad \text{(II.1.9)},$$

where p_{Sn} and p_{Sn}^0 are tin partial pressures of the alloys and the pure tin liquid, in the same order.

Thus, the method implies the admission that only monoatomic species of Sn and of Co exist in the liquid phase. The appearance of more kinds of species in the binary melt (e.g. associates Co_nSn) and perhaps in the vapor phase would make invalid eqn. 1, because the dependence between v_{Sn} and p_{Sn} would be no more correct.

The existence of such species in Co–Sn [53] and Ni–Sn liquid phases [54] has already been discussed. The formation of a metastable Co_3Sn phase, by fast cooling of binary melt, observed by Schluckebier et al. [29] also illustrates the aptitude of cobalt–tin melts to form associates.

Associates corresponding to the formula Co_nSn (there is not such an equilibrium phase) have been observed by us during current drop calorimetry studies of the Co–Sn system. This is experimental indication about the existence of associates in liquid cobalt–tin alloys.

Partial molar dissolution enthalpies in infinitely dilute tin melts and CoSn formation enthalpy have been determined by Torgersen et al. [23] using drop solution calorimetry. These authors also suggest existence of Co_nSn_m clusters in order to explain their results.

Thus, due to what is mentioned above, the results reported by Eremenko et al. [21] seem to be subject of some systematic experimental uncertainties and have not been retained as input data.

Körber and Oelsen [19] were the first to study (at 1773 K only) the mixing enthalpy of the binary melts (Table II.1.1). They reported positive values for tin-rich alloys and negative – for cobalt-rich. Relatively recent experiments by Lück et al. [20] in the temperature interval from

1671 K to 1823 K have not confirmed this data. However, it has become clear from our work and other results, already published, that the sign of the enthalpy of mixing changes as function of the temperature (positive – above 1670 K and negative – below this temperature). The results of Lück et al. [20] have been selected for this work, while those of Körber and Oelsen [19] have not been used.

Tin activities in solid cobalt–tin phases have been measured at three temperatures by Cömert and Pratt [18] by means of the electromotive force method (Table II.1.11).

Experimental data for the enthalpies of formation of βCo_3Sn_2 and CoSn have been obtained by Predel and Vogelbein [42].

The lattice stabilities of the pure elements [55, 56] and the optimised coefficients obtained in this work are presented in Table II.1.13.

Table II.1.13 Thermodynamic database file for calculation of the Co–Sn phase diagram [22]

Functions describing the contributions of the various configurations of the phase Co_3Sn_2

Contribution of the configuration Co:Co (on the third and the fourth sublattices)
FUNCTION GREFCOCO = –20739.5

Contribution of the configuration Va:Va (on the third and the fourth sublattices)
FUNCTION GREFVAVA = –35292.4+11.5636*T

Interaction parameter of zero degree of the configuration Co:Va (on the third and the fourth sublattices) in disordered state
FUNCTION L0COVADI = –34491.7

Contribution of the configuration Co:Va (on the third and the fourth sublattices) in ordered state
FUNCTION G0COVAOR = –10100+7.6252*T

Interaction parameter of first degree of the configuration Co:Va (on the third and the fourth sublattices) in disordered state
FUNCTION L1COVADI = –9313.2

Interaction parameter of first degree of the configuration Co:Va (on the third and the fourth sublattices) in ordered state
FUNCTION L1COVACO = 3471

Description of the Gibbs energies of the binary Co–Sn phases

PHASE ACOSN3 ($\alpha COSN_3$)
2 SUBLATTICES, SITES .25: .75
CONSTITUENTS: CO : SN

G(ACOSN3,CO:SN;0)–0.25 H298(HCP_A3,CO;0)–0.75 H298(BCT_A5,SN;0) =
–11875+2.5*T+.25*GHSERCO+.75*GHSERSN

PHASE BCT_A5 (βSN)
CONSTITUENTS: SN

G(BCT_A5,SN;0)–H298(BCT_A5,SN;0) =
100.00<T<3000: +GHSERSN
Note: first arrangement is Co:Sn:Co,Va:Co,Va; second (ordered) is: Co:Sn:Co:Va;

PHASE CO3SN2
EXCESS MODEL IS REDLICH–KISTER_MUGGIANU
4 SUBLATTICES, SITES 1: 1: .5: .5
CONSTITUENTS: CO : SN : CO,VA : CO,VA

G(CO3SN2,CO:SN:CO:CO;0)– 2*H298(HCP_A3,CO;0)–H298(BCT_A5,SN;0) =
+GREFCOCO+2*GHSERCO+GHSERSN
G(CO3SN2,CO:SN:VA:CO;0)–1.5*H298(HCP_A3,CO;0)–H298(BCT_A5,SN;0) =
+G0COVAOR+.5*GREFCOCO+.5*GREFVAVA+.25*L0COVADI+1.5*GHSERCO
+GHSERSN
G(CO3SN2,CO:SN:CO:VA;0)–1.5*H298(HCP_A3,CO;0)–H298(BCT_A5,SN;0) =
+G0COVAOR+.5*GREFCOCO+.5*GREFVAVA+.25*L0COVADI+1.5*GHSERCO
+GHSERSN
G(CO3SN2,CO:SN:VA:VA;0)–H298(HCP_A3,CO;0)–H298(BCT_A5,SN;0) =
+GREFVAVA+GHSERCO+GHSERSN
L(CO3SN2,CO:SN:CO,VA:CO;0) = +.25*L0COVADI+.375*L1COVADI–G0COVAOR
–L1COVACO
L(CO3SN2,CO:SN:CO,VA:CO;1) = +.125*L1COVADI+L1COVACO
L(CO3SN2,CO:SN:CO:CO,VA;0) = +.25*L0COVADI+.375*L1COVADI–G0COVAOR
–L1COVACO
L(CO3SN2,CO:SN:CO:CO,VA;1) = +.125*L1COVADI+L1COVACO
L(CO3SN2,CO:SN:VA:CO,VA;0) = +.25*L0COVADI–.375*L1COVADI–G0COVAOR
+L1COVACO
L(CO3SN2,CO:SN:VA:CO,VA;1) = +.125*L1COVADI+L1COVACO
L(CO3SN2,CO:SN:CO,VA:VA;0) = +.25*L0COVADI–.375*L1COVADI–G0COVAOR
+L1COVACO
L(CO3SN2,CO:SN:CO,VA:VA;1) = +.125*L1COVADI+L1COVACO

PHASE COSN
2 SUBLATTICES, SITES .5: .5
CONSTITUENTS: CO : SN

```
    G(COSN,CO:SN;0)–0.5*H298(HCP_A3,CO;0)–0.5*H298(BCT_A5,SN;0) = –21200
       +5.223*T+.5*GHSERCO+.5*GHSERSN


PHASE  COSN2
 2 SUBLATTICES, SITES  .3333:  .6667
  CONSTITUENTS: CO : SN

    G(COSN2,CO:SN;0)–0.3333*H298(HCP_A3,CO;0)–0.6667*H298(BCT_A5,SN;0) =
       –15170+2.741*T+.3333*GHSERCO+.6667*GHSERSN

PHASE  COSN3                (βCOSN3)
 2 SUBLATTICES, SITES  .25:  .75
  CONSTITUENTS: CO : SN

    G(COSN3,CO:SN;0)–0.25 H298(HCP_A3,CO;0)–0.75 H298(BCT_A5,SN;0) =
       –10505+.25*GHSERCO+.75*GHSERSN


PHASE  DIAMOND_A4           (αSN)
  CONSTITUENTS: SN

    G(DIAMOND_A4,SN;0)–H298(BCT_A5,SN;0) =
         100.00<T<  298.14: –9579.608+113.992361*T–22.972*T*LN(T)
       –.00813975*T**2+2.7288E–06*T**3+25615*T**(–1)
         298.14<T<  800.00: –9063.001+104.831115*T–21.5750771*T*LN(T)
       –.008575282*T**2+1.784447E–06*T**3–2544*T**(–1)
         800.00<T< 3000.00: –10909.351+147.381111*T–28.4512*T*LN(T)


PHASE  FCC_A1
EXCESS MODEL IS REDLICH–KISTER_MUGGIANU
ADDITIONAL CONTRIBUTION FROM MAGNETIC ORDERING
    Magnetic function below Curie Temperature
    +1–.860338755*TAO**(–1)–.17449124*TAO**3–.00775516624*TAO**9
    –.0017449124*TAO**15 Magnetic function above Curie Temperature
    –.0426902268*TAO**(–5)–.0013552453*TAO**(–15)–2.84601512E–04*TAO**(–25)
 2 SUBLATTICES, SITES  1:  1
  CONSTITUENTS: CO,SN : VA

    G(FCC_A1,CO:VA;0)–H298(HCP_A3,CO;0) = +GCOFCC
    TC(FCC_A1,CO:VA;0) = 1396
    BMAGN(FCC_A1,CO:VA;0) = 1.35
    G(FCC_A1,SN:VA;0)–H298(BCT_A5,SN;0) =
         298.14<T< 3000.00: +5510–8.46*T+GHSERSN
    TC(FCC_A1,CO,SN:VA;0) = –1720
    L(FCC_A1,CO,SN:VA;0) = –19000+24.672*T

PHASE  HCP_A3
EXCESS MODEL IS REDLICH–KISTER_MUGGIANU
```

```
ADDITIONAL CONTRIBUTION FROM MAGNETIC ORDERING
    Magnetic function below Curie Temperature
    +1–.860338755*TAO**(–1)–.17449124*TAO**3–.00775516624*TAO**9
    –.0017449124*TAO**15 Magnetic function above Curie Temperature
    –.0426902268*TAO**(–5)–.0013552453*TAO**(–15)–2.84601512E–04*TAO**(–25)
 2 SUBLATTICES, SITES  1:  .5
  CONSTITUENTS: CO,SN : VA

    G(HCP_A3,CO:VA;0)–H298(HCP_A3,CO;0) = +GHSERCO
    TC(HCP_A3,CO:VA;0) = 1396
    BMAGN(HCP_A3,CO:VA;0) = 1.35
    G(HCP_A3,SN:VA;0)–H298(BCT_A5,SN;0) = +GSNHCP
    TC(HCP_A3,CO,SN:VA;0) = –1720
    L(HCP_A3,CO,SN:VA;0) = +9000

PHASE  LIQUID
EXCESS MODEL IS REDLICH–KISTER_MUGGIANU
  CONSTITUENTS: CO,SN

    G(LIQUID,CO;0)–H298(HCP_A3,CO;0) =
         298.14<T< 1768.00: +15085.037–8.931932*T–2.19801E–21*T**7
        +GHSERCO
         1768.00<T< 6000.00: +16351.056–9.683796*T–9.3488E+30*T**(–9)
        +GHSERCO
    G(LIQUID,SN;0)–H298(BCT_A5,SN;0) =    100.00<T< 3000.00: +GSNLIQ
    L(LIQUID,CO,SN;0) = –113890+568.4038*T–68.169*T*LN(T)
    L(LIQUID,CO,SN;1) = –56193.26+283.7657*T–33.6875*T*LN(T)
```

In Fig. II.1.19 experimental [23, 42] and calculated in this work integral molar enthalpies of formation ($\Delta_f H$) of the solid Co–Sn phases are represented, showing good agreement between both kinds of values. The $\Delta_f H$ values, estimated by Cömert and Pratt [16], on the basis of electromotive-force measurements, are plotted too.

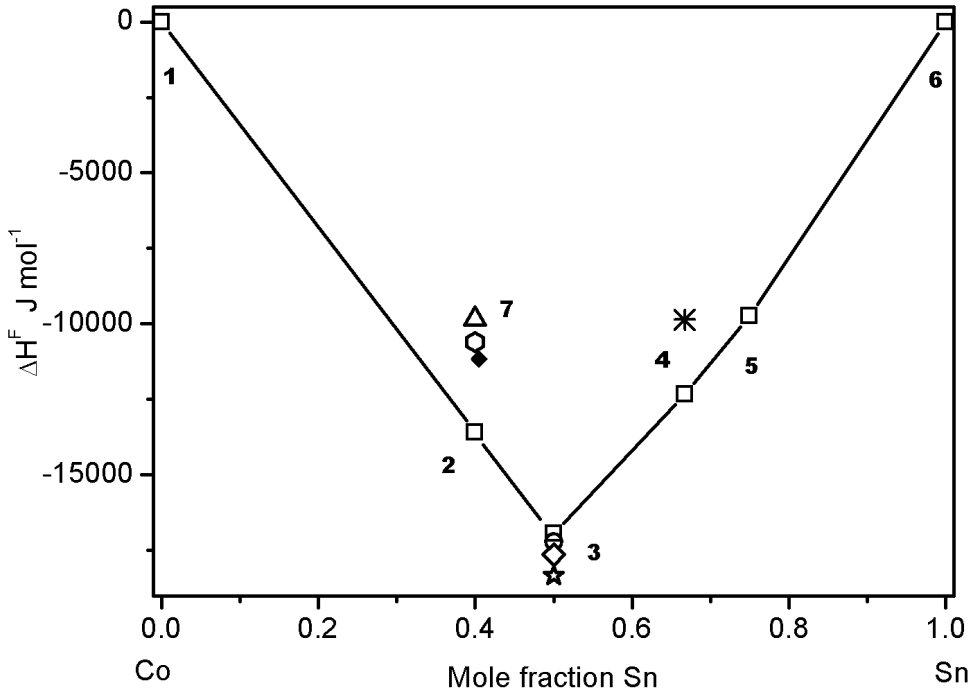

Fig. II.1.19. Integral molar enthalpies of formation at 298.15 K ($\Delta_f H$ kJ.mol^{-1}) of cobalt–tin alloys calculated in this work (1 – HCP Co; 2 – αCo_3Sn_2; 3 – CoSn; 4 – $CoSn_2$; 5 – $\alpha CoSn_3$; 6 – (βSn); 7 – βCo_3Sn_2) compared with experimental values of Predel and Vogelbein [42] (○) and of Torgersen et al. [23] (◇) [22]. Calculated and experimental [48] values for βCo_3Sn_2 at 1083 K are symbolised by △ and ⬠, respectively. The enthalpies of formation derived by Cömert and Pratt [16] are represented by ◆, ☆ and ✳. Mole fractions of tin are plotted along the abscissa. Reference states are HCP Co and (βSn) at 298.15 K

The latter authors have assessed the entropies of the Co–Sn compounds as well (Table 5 of ref. [16]), thus we were able to calculate the relevant molar Gibbs energies of formation at 298.15 K. We found that Co_3Sn_2 Gibbs energy of formation, estimated according to these data, is not large (negative) enough to keep it stable at 298.15 K. Thus, care has been taken during the optimization to assure the stability of this phase relatively to the adjacent (εCo) and CoSn. That is why, as one can see in Figs. II.1.20 A, B the optimised values of Sn partial chemical potentials in Co_3Sn_2 are larger (by absolute value) than these found by Cömert and Pratt [16], while calculated and measured chemical potentials of tin, in the other phases (including the liquid) are in good agreement.

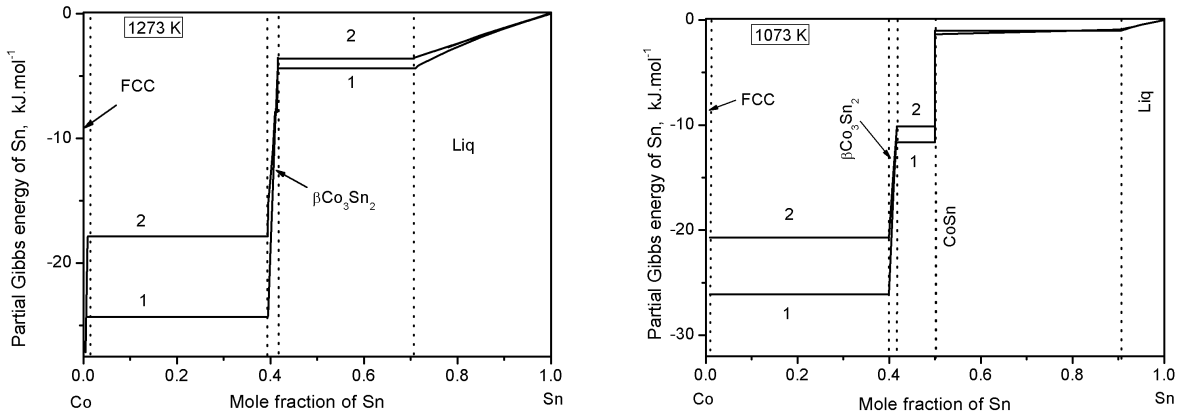

A. B.

Fig. II.1.20 Calculated (line 1) and measured (line 2) by Cömert and Pratt [16] partial Gibbs energies of tin at 1273 K (3A) and at 1073 K (3B) [22]. Reference state is liquid Sn at the corresponding temperatures.

In Fig. II.1.21 the calculated and experimental [20] integral molar enthalpies of formation (ΔH^F) of the liquid phase are juxtaposed. Sign-variable temperature dependence of the integral molar enthalpies of formation is observed (the $\Delta_f H$ values at 1573 K are added in order to illustrate the change of the sign). The calculated values are in good agreement with the experimental ones taking into account possible scattering of the calorimetric values.

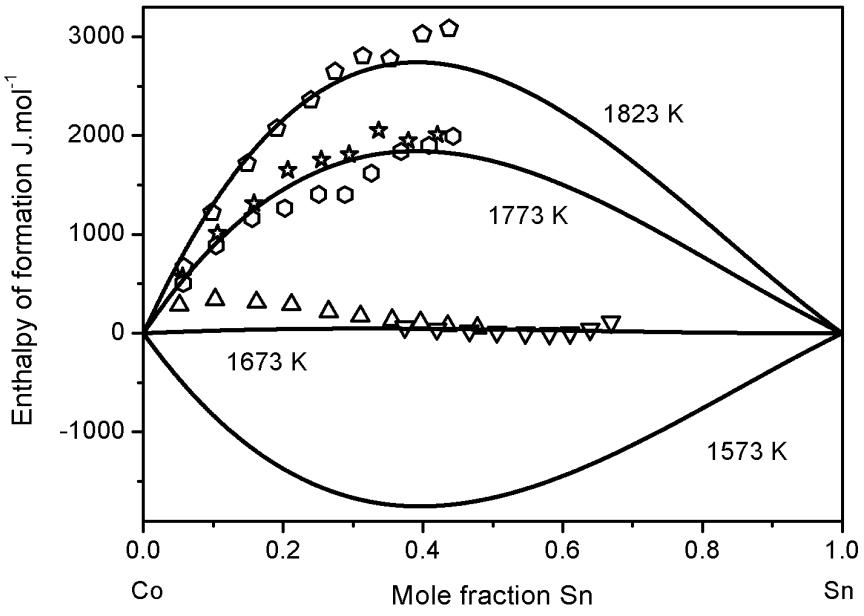

Fig. II.1.21 Integral molar enthalpies of formation ($\Delta_f H$ kJ.mol^{-1}) of the liquid cobalt–tin solutions at 1873 K, 1773 K, 1673 K and 1573 K (solid lines) compared with experimental data of Lück et al. [20]: ⬠ – 1873 K; ★ – 1780 K; ⬡ – 1759 K; △ – 1675; ▽ – 1671 K [22]. Reference states are liquid Co and Sn.

According to some liquid phase thermochemical data [19, 20] strong concentration dependence of the sign of deviation from ideal behaviour exist. Such deviations have not been reproduced, because priority has been given to the data of Lück et al. [20]. It is of worth noting that the extremum on the curve, representing the concentration dependence of the liquid solutions enthalpies of formation, coincides with the composition of the congruently melting phase βCo_3Sn_2 as expected from theoretical considerations.

Other experimental and assessed quantities that can be compared are the partial molar dissolution enthalpies of cobalt in infinitely dilute tin melts, determined by Torgersen et al. [23] at 874 K (12 kJ·mol^{-1}) and 1173 K (32 kJ·mol^{-1}). The corresponding values obtained in this work (12 and 32 kJ·mol^{-1}, respectively) are in excellent agreement with the experimental ones.

The calculated phase diagram (for temperatures above 250 K) is presented in Figs. II.1.22A and B. The calculated temperatures of the invariants are juxtaposed with experimental data in Table II.1.12. The most radical difference with some previously accepted variants of the Co–Sn phase diagram [26–28] consists in the admittance that the eutectic invariant E1 is situated at around 15 K higher temperature (i.e. at 1398±2 K). We must concede that some authors have already adopted the recent value [17, 18]. The experimental data of Lewkonia [25], as normalized in this work, indicate this temperature as well.

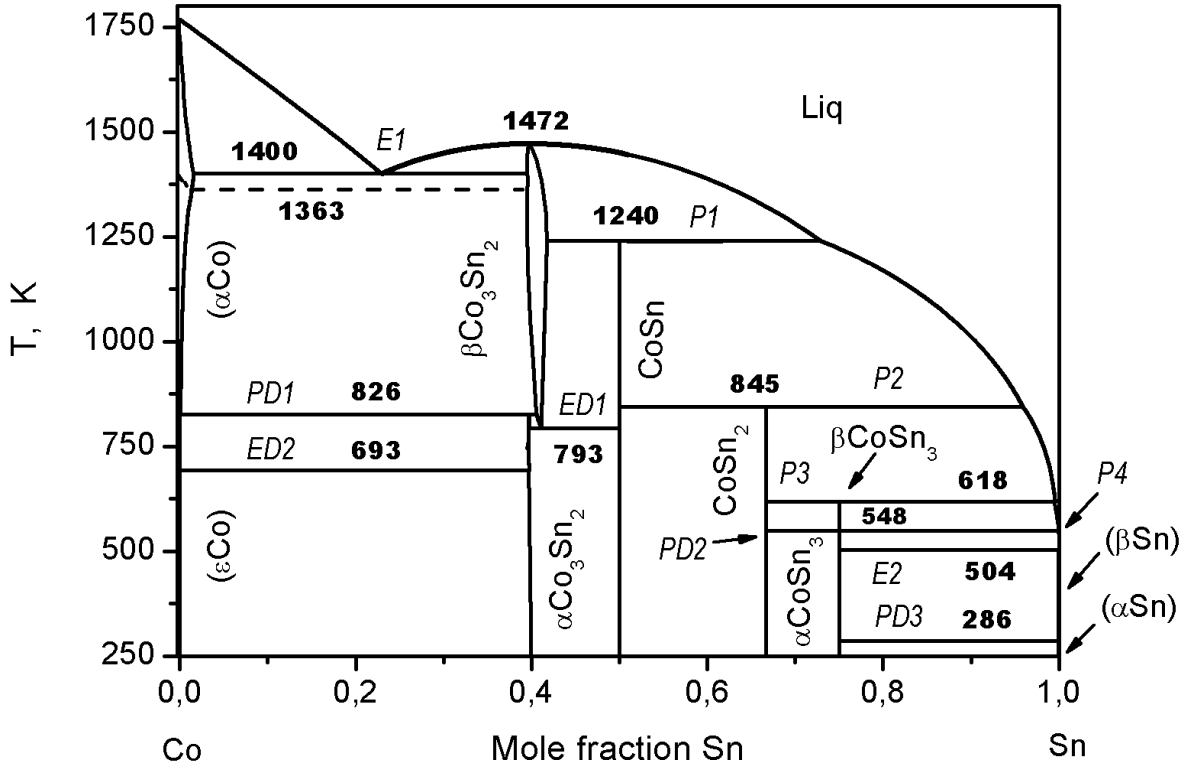

Fig. II.1.22A. The calculated Co–Sn phase diagram [22]. The dashed line represents the Curie temperature.

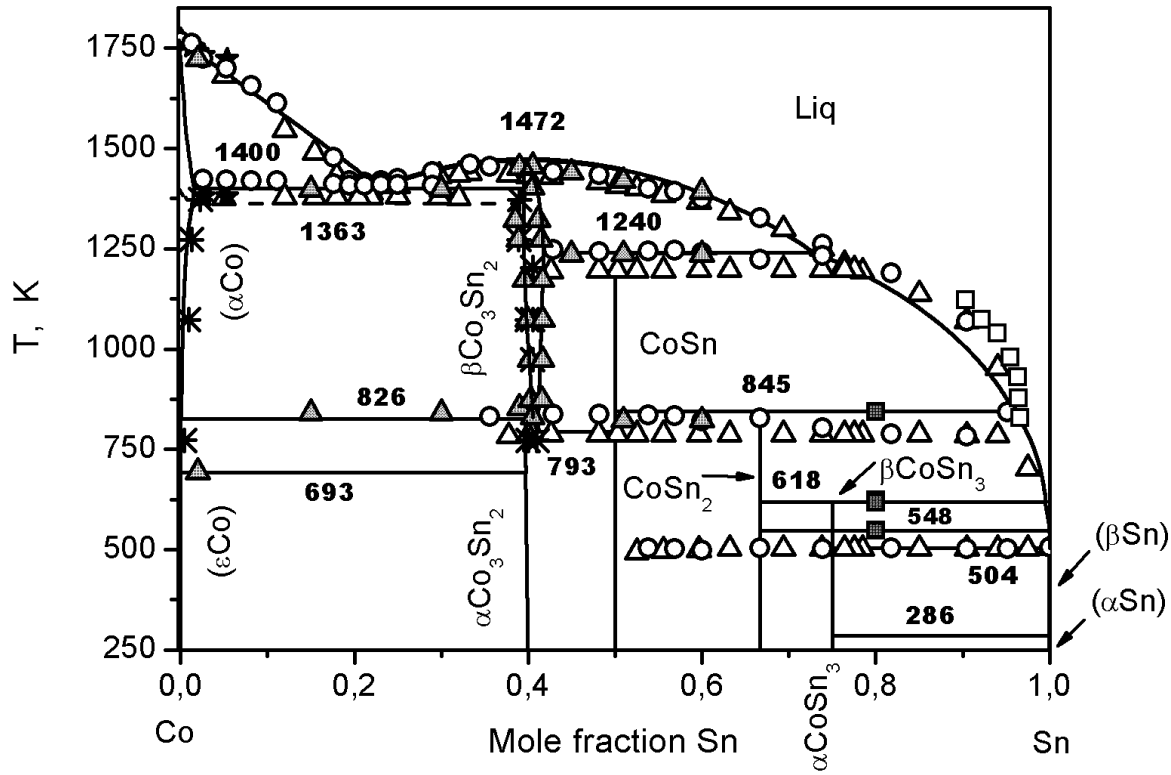

Fig. II.1.22B. The calculated Co–Sn equilibrium phase diagram with selected topological experimental data [22]: Lewkonja [25] – o; Zemczuzny and Belinsky [26] – Δ; Hashimoto [27] – ★; Darby and Jugle [28] – □; Cömert and Pratt [15] – ✳; Cömert and Pratt [16] – ▲; Lang and Jeitschko [33] – ■.

We would like to emphasize that, studies concerning the exact compositions of the eutectic and the peritectic points are lacking, and the literature data about them have merely been assessed. That is why, in Table. II.1.12 are shown calculated concentrations only.

The low-temperature equilibrium E2 could be considered as degenerated one, because the compositions of two coexisting phases (liquid solution and βSn) are practically equal.

The equilibrium (αCo) ↔ (εCo)+αCo_3Sn_2 (denoted as ED2 in Table II.1.12) is resolved in this work as (degenerated) eutectoid decomposition. Taking into account that the polymorphic transition of the pure cobalt is sluggish (see also [35]) it would be useful but not easy to get reliable experimental information about the characteristics of this equilibrium.

Another group of degenerated three-phase equilibria are these at 548 K (PD2 and P4, Fig. II.1.22A) and at 286.2 K (PD3, Fig. II.1.22A). They are due to the polymorphic transformation $\beta CoSn_3 \leftrightarrow \alpha CoSn_3$ and to the allotropic transformation (βSn) ↔ (αSn), respectively.

According to the calculations, the order-disorder transition of Co_3Sn_2 engenders two equilibria that are rather complicated for experimental investigations: $\alpha Co_3Sn_2 \leftrightarrow \beta Co_3Sn_2$+(αCo) (PD1 at 826 K) and $\beta Co_3Sn_2 \leftrightarrow \alpha Co_3Sn_2$+CoSn (ED1 at 793 K). The reason is that βCo_3Sn_2 exhibits some homogeneity range (around 0.4 to 0.42 mole fractions Sn) while the ordered form (αCo_3Sn_2) is nearly stoichiometric. Consequently, the equilibrium compositions of both coexisting modifications are very close one to another.

Experimental data about the temperature of the above mentioned order-disorder transition have been obtained [26] by differential thermal analyses. The appearance of thermal effects (i.e. discontinuity of the enthalpy) indicates that this phenomenon should be classified as first order phase transition. It is of worth noting that the experimentally found transition temperatures [16] are higher (up to 861 K) for alloys containing less than 40 at. % Sn than these for an alloy containing 40.5 at. % Sn (834 ±11 K). This is in conformity with the calculated phase diagram (see Fig. II.1.22A, invariants PD1 and ED1, respectively). In the works of Lewkonia [25], and Zemczuzny and Belinsky [26], thermal effects in the region 40 – 50 at. % Sn, have been reported at similar temperatures as well.

➢ Conclusion

- Thermodynamic optimization of Co–Sn binary system has been done. The results show a good agreement with the experimentally obtained.
- Enthalpies of formation of liquid phase have been measured by drop solution calorimetry at 991 K and 1020 K and by direct reaction calorimetry at 1010 and 1303 K. Feeble negative enthalpies of formation were found for the liquid phase at 991, 1010 and 1020 K, independently of the experimental technique, while positive values were registered at 1303 K.
- Enthalpies of formation of Co–Sn compounds have been measured by direct reaction calorimetry at 1287, 1033, 629 and 605 for Co_3Sn_2, CoSn and $CoSn_2$ and $CoSn_3$, respectively.
- The transition temperature between low and high-temperature forms of Co_3Sn_2 compound has been verified by differential thermal analyses and found around 833 ± 1.2 K. The enthalpy of transition was found to be: 0.750 ± 0.23 $kJ.mol^{-1}$.
- Differential thermal analyses of the transition between low and high-temperature forms of $CoSn_3$ have been done.

➢ Bibliography

[1] Liu L., C. Andersson, J. Liu, J. Electr. Mater. 33, 935 (2004).

[2] Sabitha R., M. Pushpavanam, M.M. Sujatha, T. Vasudevan, Trans. Metal Finishers Assoc. India 5 (1996) 267.

[3] Cho S.K., H.S. Han, C.K. Lee, C.I. Ahn, J.I. Park, Mater. Sci. Forum 439 (2003) 57.

[4] Tomachuk C.R., C.M. de A. Freire, M.Ballester, R. Fratesi, G. Roventi, 122 (1999) 6.

[5] Zaina Z., S. Nagalingam, A. Kassim, M. Hussein and W. Yunus, Solar Energy Materials and Solar Cells 81 (2004) 261.

[6] Shen J., R. Blachnik, Thermoch. Acta 399 (2003) 245.

[7] J. H. Zhan, X. G. Yang, S. D. Li, Y. Xie, W. C. Yu and Y. Qian, J. Sol. St. Chem. 152 (2000) 537.

[8] Cnobloch H., H. Nischik and F. von Sturm, J. Electroanal. Chem. 75 (1977) 747.

[9] Norén L., R. L. Withers, F. Javier García-García and Ann-Kristin Larsson, Solid St. Sciences 4 (2002) 27.

[10] Geny J.-F., G. Marchal, Ph. Mangin, Chr. Janot, M. Piecuch, Phys. Rev. B 25 (1982) 7449.

[11] Guilmin P., P. Guyot, G. Marchal, Phy. Lett. A 109 (1985) 174.

[12] Audouard A., J.-F. Geny, G. Marchal, M. Gerl, Philo. Mag. B 53 (1986) 1.

[13] Lopez Hirata V.M., F.M. Suarez, J.G. Cabanas-Moreno, Mater. Sci. Eng. A 181-182 (1994) 1258.

[14] Tamura N., M. Fujimoto, M. Kamino, S. Fujitani, Electrochim. Acta 49 (2004) 1949.

[15] Cömert H., J.N. Pratt, Thermochim. Acta 84 (1985) 273.

[16] Cömert H., J.N. Pratt, Metall. Trans. A 23 (1992) 2401.

[17] Ishida K., T. Nishizawa, J. Phase Equilibia 12 (1991) 88.

[18] Okamoto H., J. Phase Equilibria, 14 (1993) 3.

[19] Körber F., W. Oelsen, Mitt. Kaiser-Wilhelm-Inst. Eisenforsch. Dusseldorf 19 (1937) 209.

[20] Lück R., J. Tomiska, B. Predel, Z. Metallkde. 82 (1991) 944.

[21] Eremenko V., G. Lukashenko, V. Pritula, Izv. Akad. Nauk SSSR, Met. 3 (1971) 82.

[22] Vassilev G.P., K.I. Lilova, Contribution to the thermodynamics of the Co–Sn system, Archives of Metallurgy and Materials, Vol. 51 (3) (2006).

[23] Torgersen A., H. Bros, R. Castanet, A. Kjekshus, J. Alloys Comp. 307 (2000) 167

[24] Vassilev G.P., K.I. Lilova, J.C. Gachon, Calorimetric and phase diagram studies of the Co-Sn system, Intermetallics (2007), doi:10.1016/j.intermet.2007.02.006

[25] Lewkonja K., Z. Anorg. Allg. Chem. 59 (1908) 294.

[26] Zemczuzny S.F., S.W. Belinsky, Z. Anorg. Allg. Chem. 59 (1908) 364.

[27] Hashimoto U., J. Jpn. Inst. Met. 2 (1938) 67.

[28] Darby J.B., D.B. Jugle, Trans. Metall. Soc. AIME 245 (1969) 2515.

[29] Schluckebier G., E. Wachtel, and B. Predel, Z. Metallkd., 71 (1980) 456.

[30] Singh M., M. Barkei, G. Inden, S. Bhan, Phys. Stat. Sol. (a) 87 (1985) 165.

[31] Hansen M., K. Anderko, Constitution of Binary Alloys, 2nd edn., McGrow-Hill, NY, 1958.

[32] Massalski T., CD ROM: Binary Alloy Phase Diagrams, ASM International, OH, USA, 1996.

[33] Lang, A. W. Jeitschko, Z. Metallkde. 87 (1996) 759.

[34] Vassilev G. P., M. Jiang, J. Phase Equilibria and Diffusion, 25 (3) (2004) 259.

[35] Teatum E., K. Schneidner, J. Waber (1960) Compilation of calculated data useful in predicting metallurgical behaviour of the elements in binary alloy systems, LA-2345, Los Alamos Scientific Laboratory.

[36] Sokolovskaja E., L. Guzej, Metallochimia (in Russian), Ed. House of the Moscow University, Moskow, 1986 (see WEBELEMENTS.COM as well).

[37] Hillert M., M. Jarl, CALPHAD 2, 227 (1978).

[38] Jiang M., J. Sato, I. Ohnuma, R. Kainuma, K. Ishida, CALPHAD (Computer Coupling of Phase Diagrams and Thermochemistry) 28, 213 (2004).

[39] Lidin S., A-K. Larsson, J. Sol. State Chem. 118, 313 (1995).

[40] Larsson A-K., R. Withers, L. Steinberg, J. Sol. State Chem. 127, 222 (1996).

[41] Leineweber A., M. Ellner, E.J. Mittemeijer, J. Sol. State Chem. 159, 191 (2001).

[42] Predel B., W. Vogelbein, Thermochim. Acta 30, 201 (1979)

[43] Liu L.B., C. Andersson, J. Liu, Y.C. Chan, Interpack 2003-35126, Int. Electronic Packaging Technical Conf. Exhib. (NY: ASME, 2003) pp. 141-146.

[44] Nabil H., M. Piecuch, J. Durand, G. Marchall, J. de Physique 46 (C-8) (1985) 229.

[45] Mudry S., M. Komarnitsky, A. Korolyshyn, S. Prokhorenko,Proc. 14th Int. Scientific Conf. On Advanced Materials and Technologies, Glivice-Zakopane, Poland, 17 – 21 May 1995, pp. 333-336.

[46] Komarnitsky M., S. Mudry, V. Halchak, JALCOM 242 (1996) 157.

[47] Villars P. (Editor in Chief) Pauling File Binaries Edition, Inorganic Materials Database and Design System, CD-ROM, Germany, 2002, ISBN 3-00-009043-6.

[48] Villars P. (Editor), Pearson's Handbook Desk Edition, ASM International, 1997, ISBN 978-0-87170-603-4, OH, USA.

[49] Porter A. Trans Faraday Soc 1920;16:336.

[50] Vassilev GP. Thesis, University of Sofia, Bulgaria; 1977, 787

[51] Ray AE, Smith SR. J Phase Equilib 1991;12:644.

[52] Ansara I., N. Dupin in: COST 507, Definition of thermochemical and thermophyiscal properties to provide a database for the development of new light alloys, Vol. 2, 1998, European Commission, Belgium.

[53] Ivanov M., Z. Metallkd 82, 53 (1991)

[54] Hoch M., I. Arpshofen, B. Predel, Z. Metalkd 75, 30 (1984)

[55] Dinsdale A., A. Watson, A. Kroupa, J. Vrestal, A. Zemanova, J. Vizdal (Eds.), COST 531 Thermodynamic Database for Lead-free Solder Alloys, Version 1.2 (2005).

[56] Dinsdale A., CALPHAD 15, 317 (1991).

[57] Waldner P., H. Ipser, Intermetallics 10 485 (2002)

[58] K.I. Lilova, G.P. Vassilev, J.C. Gachon, *Enthalpies of formation of Co-Sn solid alloys*, VIII International Workshop of Associated Phase Diagram and Thermodynamic Committee (APDTC), Kosice, Slovakia, 19 November 2005, **Proceedings**, Editor W. Zakulski, ISBN 83-921845-5-6, Published by: Institute of Metallurgy and Materials Science, Polish Academy of Sciences, Krakow, Poland, p. 35 – 43

[59] McGlashan M.L. J.Chem Thermodynamics 1990, 22, 653-663

II. 2. Experimental Investigations of the Ni–Sn Binary System

The fabrication of a reliable solder joint in a microelectronics package depends, even partly, on the formation of intermetallic compound(s) at an interface between the solder and an Under–Bump–Metallurgy (UBM) layer. The kinetics of intermetallic compounds growth plays an important role in controlling the mechanical and electric properties. In modern microelectronic package, Ni coatings are often plated as a UBM layer on the substrate before the electronic components are soldered. Thus the investigations of the interface reactions between Ni and solder are becoming more and more attractive to materials scientists.

From the other side Sn–based alloys are most widely used in package. In order to simulate the interface reaction between Ni and Sn–based alloys (Sn–Bi alloy in our case) and to predict the microstructure evolution of the interface, the thermodynamic properties of the related systems should be well understood first.

The literature review shows that there are insufficiencies of topological and thermochemical data needed for the full thermodynamic description of the Ni–Sn system. Namely, enthalpies of formation of solid phases are not well known. Moreover, there is no data about the enthalpy of formation of Ni_3Sn high-temperature modification, while other experimental results show some scattering. Thus, the purpose of this work is to verify previous measurements and to obtain new data for the Ni–Sn solid alloys enthalpies of formation.

➢ Literature review

The Ni–Sn system has been the subject of a number of investigations, most of them dating back to the first half of the 20^{th} century. A detailed assessment of this phase diagram was published by Nash and Nash [1]. It was based on a rather arbitrary data selection of previous literature information. Their work also formed the basis of the Ni–Sn phase diagram published in the compilation by Massalski et al [2] (Fig. II.2.1).

The liquidus and solidus lines of the Ni–Sn system have been determined by a number of authors based on thermal analyses [3–5, 7–11] and metallographic examinations of as-cast and annealed alloys [4, 5, 8–10, 12–14]. The existence of two miscibility gaps in the liquid ~~as~~ suggested by Voss [7] and Mikula and Thomassen [9] was shown to be wrong by Heumann [10] and Nial [15].

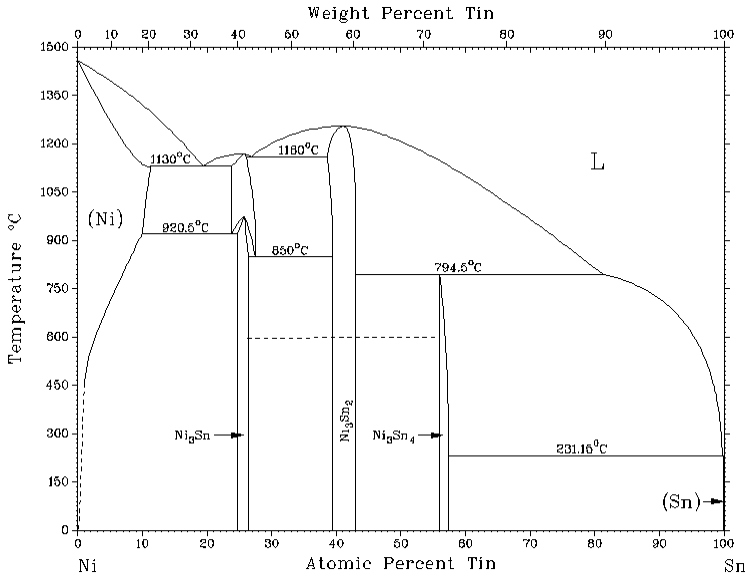

Fig. II.2. 1 The Ni–Sn phase diagram by T. Massalski [2]

The first intermediate phases found in the system were Ni_3Sn [3–7, 9, 10, 12–17, 19, 20–31], Ni_3Sn_2 [5–7, 9, 10, 12–17, 20–22, 26, 32] and NiSn [5, 6, 12–17, 33]. Voss [7] and Mikula and Thomasen [9] suggested the presence of Ni_4Sn that was later rejected by Heumann [10]. Mikula and Thomassen [9] also described the most Sn-rich phase Ni_3Sn_4, which was confirmed later by several authors [2, 10, 34]. Michel [26] reported the three phases Ni_3Sn, Ni_3Sn_2 and Ni_3Sn_4, whereas the existence of NiSn was not verified. Fetz and Jette [19, 35] and Lihl and Kirnbauer [21, 22] reported an additional phase between 50 and 60 at. % Sn, which was not included in the phase diagram compiled by Nash and Nash [1].

Nowadays it is approved that the most Ni-rich intermetallic compound is Ni_3Sn. It exists in two polymorphic forms: a high temperature (HT) form (stable between 850^0C and its congruent melting point at 1174^0C [10]) and in a low temperature form (LT) stable below 920^0C. The polymorphic transformation between these modifications belongs to the order-disorder type according to various sources [10, 20, 24].

Pak et al. [36] had reported a metastable phase with β–Cu_3Ti structure type, formed by martensitic transformation of the Ni_3Sn HT phase. Its existence was confirmed by Schmetterer and Flandorfer [37].

The Ni_3Sn_2 HT phase was investigated by Mikula and Thomassen [9]. Leineweber et al. [38–41] reinvestigated this part of the diagram recently. According to them, HT phase is hexagonal. They identified three different low temperature phases - two of them having incommensurate structures. The commensurate orthorhombic LT-phase is stable between 40 and 40.8 at. % Sn and is located between the two incommensurate phases. The LT' phase is

orthorhombic, too, and is stable between 40.8 and 42.5 at. % Sn, whereas the LT'' phase is stable at Sn contents lower than 39.2 at. % Sn. Fjellvag and Kjekshus [42] reported the transition Ni_3Sn_2 HT → Ni_3Sn_2 LT to be of first order. A suggestion for the phase transition comprising peritectoid and eutectoid reaction was included in the phase diagram calculation by Liu et al. [43]. The existence of three low-temperature phases was confirmed by Schmetterer and Flandorfer [37]. According to their results the phase transitions between Ni_3Sn_2 LT phases and the corresponding HT phase are at temperatures between 295 and 508^0C, that is much lower than the 600^0C estimated in [2].

The literature data about the crystal structures of the stable Ni-Sn phases are compiled in Table II.2.1.

Table II.2.1 Crystal structures of the stable binary Ni-Sn phases by literature data.

Phase	Homogeneity range at. %	Pearson symbol	Structurbericht designation	Space group	Prototype	Source
fcc Ni	≈0-10.6 at. % Sn	cF4	A1	$Fm\bar{3}m$	Cu	[43]
αSn	≈100 at. % Sn	cF8	A4	$Fd\bar{3}m$	C(diam.)	[43]
βSn	≈100 at. % Sn	tI_4	A5	$I4_1/amd$	βSn	[43]
Ni_3Sn_HT	25 at. % Sn	cF16	$D0_3$	$Fm\bar{3}m$	BiF_3	[37]
Ni_3Sn_LT	25 at. % Sn	hP8	$D0_{19}$	$P6_3/mmc$	Mg_3Cd	[37]
Ni_3Sn_2_HT	40 at. % Sn	hP6	$B8_1$	$P6_3/mmc$	Ni_2In	[37]
Ni_3Sn_2_LT	40 at. % Sn	oP20		$P6_3/mmc$	Ni_3Sn_2	[37]
Ni_3Sn_4	≈57 ат. % Sn	mC14	B20	C2/m	CoGe	[37]

Phase diagram calculations of the Ni–Sn–Pb, Ni–Sn–Cu and Ni–Sn systems based on the existing experimental data were published by Ghosh [44], Miettinen [45], Liu et al. [43] and COST2 database [46]

The Ni–Sn binary phase diagram was formerly assessed by Ghosh et al. [44] in order to extend for the sake of assessment of the Pb–Ni–Sn system. The final optimization was carried out, using data for the liquid phase [12, 47, 48], the enthalpies of formation of Ni–Sn compounds [16, 53] and the phase diagram data [9, 10, 13]. The excess parameters of liquid, fcc and bct phases were taken from SGTE database [48]. The intermediate phases having a finite solid solubility are described by the compound energy formalism.

More recently, based on the assessment by Ghosh [44], Miettinen [45] simplified models of some phases and reassessed this system in order to extend it to the Cu–Ni–Sn ternary system. Both versions of the assessments were in agreement with most of the experimental data.

The Ni–Sn binary system was reassessed by Liu [43] (Fig. II.2.2). For the final optimization, the liquidus determined by Heumann [10] and Mikula et al. [9], and the solidus of fcc_A1 (Ni) by [9], are used. The excess parameters of liquid, fcc and bct phases were taken from Dinsdale [54]. The invariants reactions are cited from those reviewed by P. Nash and A. Nash [1]. As for thermodynamic properties, mixing enthalpies of liquid Ni–Sn alloys measured through calorimetry at 1550 K by Haddad et al. [50], at 1775, 1702 and 1660 K by Luck et al. [49], and the enthalpy of formation of Ni_3Sn_LT at 298 K [6] are used in the optimization. Because Ni_3Sn_2 has a second-order transition, Ghosh [2] adopted the Bragg–Williams–Gorsky model to treat such a transition. However, when extended to high-order systems or to establish a thermodynamic database, such a model may cause trouble. In order to establish a Ni–Sn containing multi-component database, the transition between Ni_3Sn_2_HT and Ni_3Sn_2_LT was not treated as a second-order transition but as a first-order transition by [43].

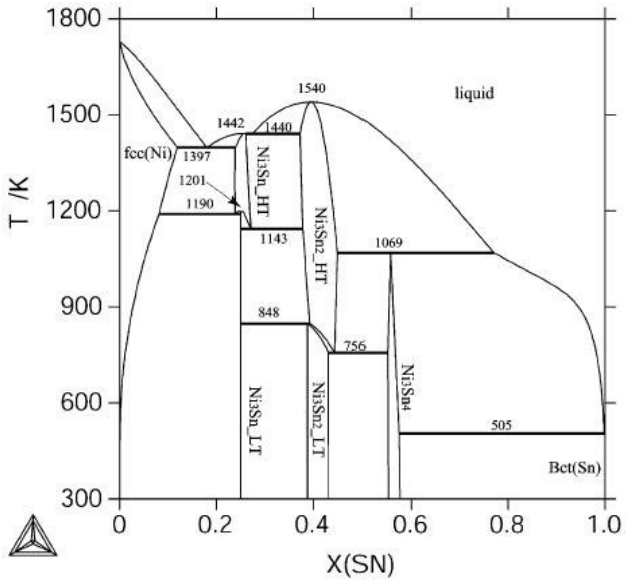

Fig. II.2.2 Phase diagram of the system Ni–Sn, calculated using the coefficients optimized by Liu et al. [43]

According to the COST database v.2.0 [46], the data for the Ni–Sn system was taken from Liu [43] and modified by Andy Watson for revised fcc Sn data. Bct data was retained from

original Ghosh assessment [442]. Fig. II.2.3 represents the phase diagram of Ni–Sn binary system, calculated, using COST database v.2.0 [46]. This is the most contemporary assessment of the Ni–Sn system.

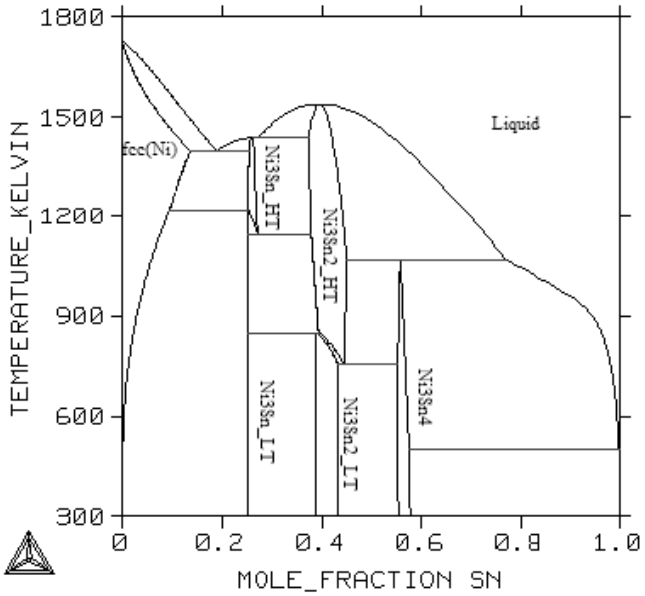

Fig. II.2.3 Phase diagram of the system Ni–Sn, calculated using the COST database v.2.0 [46].

The extrapolated phase equilibria between fcc_A1 and liquid calculated on [43] and [46] is shown at Fig. II.2.17 A, B.

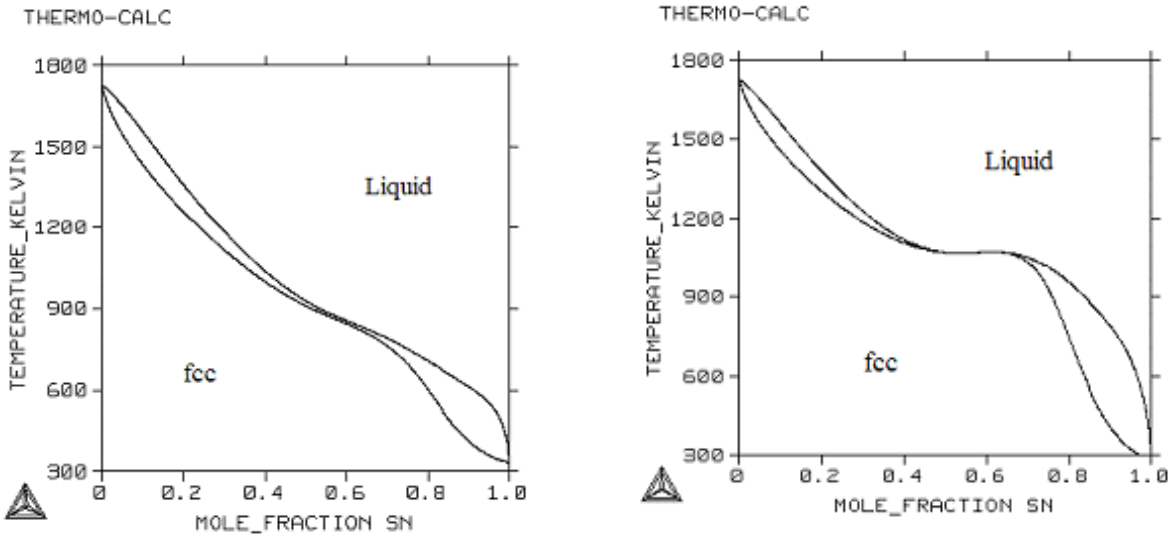

A B

Fig. II.2.3 extrapolated phase equilibria between fcc_A1 and liquid, calculated on Liu [43] (A) and COST database [46] (B).

Comparison between experimental and calculated data with optimized coefficients phase equilibria is shown in Table II.2.2. The temperatures of the invariant reaction $Ni_3Sn\_HT \Leftrightarrow Ni_3Sn\_LT + Ni_3Sn_2\_HT$ and $Ni_3Sn\_HT \Leftrightarrow Ni_3Sn\_LT$, assessed to be 1143 and 1201 K by Liu [43] deviate much from the experimental values, reported by [1, 23, 37, 51], but in a good agreement with [46]. Such deviations partially result from the simplification of the Ni_3Sn_LT to a stoichiometric compound. At the same time, the temperature [43] of the eutectoid reaction $Ni_3Sn\_HT \Leftrightarrow Ni(FCC) + Ni_3Sn\_LT$ is relatively low, in comparison with [46, 51], but is in a good agreement with the experimental and calculated values of [1, 23, 44]. The other invariants data show scattering in a certain composition and temperature range, which can be considered within the standard deviation. The transition temperature of $Ni_3Sn_2\_HT \Leftrightarrow Ni_3Sn_2\_LT$ reaction is not well-defined, which can due to the existence of three low-temperature Ni_3Sn_2 phases.

Table II.2.2. Experimental and estimated data about the invariants and the special points of the Ni – Sn phase diagram compared with the calculated values. X – mole fractions of Sn.

Reaction Type	T K	$X^{LEFT\ SIDE}$	X^{MIDDLE}	$X^{RIGHT\ SIDE}$	Reference
1	2	3	4	5	6
Eutectic			$L \Leftrightarrow Ni(FCC) + Ni_3Sn\_HT$		
	1403	$X_{Ni(FCC)} = 0.106$	$X_L = 0.187$	$X_{Ni3Sn} = 0.230$	[1]
	1404	$X_{Ni(FCC)} = 0.125$	$X_L = 0.176$	$X_{Ni3Sn} = 0.237$	[44]
	1403		$X_L = 0.191$	$X_{Ni3Sn} = 0.248$	[10]
	1397	$X_{Ni(FCC)} = 0.120$	$X_L = 0.181$	$X_{Ni3Sn} = 0.239$	[43]
	1412	$X_{Ni(FCC)} = 0.107$	$X_L = 0.187$	$X_{Ni3Sn} = 0.241$	[37]
	1398	$X_{Ni(FCC)} = 0.130$	$X_L = 0.190$	$X_{Ni3Sn} = 0.253$	[46]
Eutectic			$L \Leftrightarrow Ni_3Sn_2\_HT + Ni_3Sn\_HT$		
	1433	$X_L = 0.254$	$X_{Ni3Sn\_HT} = 0.260$	$X_{Ni3Sn2\_HT} = 0.379$	[1]
	1447	$X_L = 0.269$	$X_{Ni3Sn\_HT} = 0.291$	$X_{Ni3Sn2\_HT} = 0.392$	[44]
	1433	$X_L = 0.268$	$X_{Ni3Sn\_HT} = 0.273$	$X_{Ni3Sn2\_HT} = 0.357$	[10]
	1440	$X_L = 0.261$	$X_{Ni3Sn\_HT} = 0.274$	$X_{Ni3Sn2\_HT} = 0.373$	[43]

Table II.2.2. continuation

1	2	3	4	5	6
	1445	$X_L = 0.263$	$X_{xxx\_HT} = 0.280$	$X_{xxx2\_HT} = 0.367$	[37]
	1438	$X_L = 0.260$	$X_{Ni3Sn\_HT} = 0.270$	$X_{Ni3Sn2\_HT} = 0.370$	[46]
Eutectoid			$Ni_3Sn\_HT \Leftrightarrow Ni(FCC) + Ni_3Sn\_LT$		
	1194	$X_{Ni(FCC)} = 0.095$	$X_{Ni3Sn\_HT} = 0.232$	$X_{Ni3Sn\_LT} = 0.241$	[1]
	1195	$X_{Ni(FCC)} = 0.087$	$X_{Ni3Sn} = 0.246$	$X_{Ni3Sn\_LT} = 0.248$	[44]
	1193		$X_{Ni3Sn} = 0.233$	$X_{Ni3Sn\_LT} = 0.238$	[23]
	1273				[51]
	1190	$X_{Ni(FCC)} = 0.082$	$X_{Ni3Sn} = 0.239$	$X_{Ni3Sn\_LT} = 0.250$	[43]
	1221	$X_{Ni(FCC)} = 0.103$	$X_{Ni3Sn} = 0.250$	$X_{Ni3Sn\_LT} = 0.248$	[37]
	1217	$X_{Ni(FCC)} = 0.$	$X_{Ni3Sn} = 0.250$	$X_{Ni3Sn\_LT} = 0.252$	[46]
Eutectoid			$Ni_3Sn\_HT \Leftrightarrow Ni_3Sn\_LT + Ni_3Sn_2\_HT$		
	1123	$X_{Ni3Sn\_HT} = 0.260$	$X_{Ni3Sn\_LT} = 0.272$	$X_{Ni3Sn2\_HT} = 0.388$	[1]
	1123	$X_{Ni3Sn\_HT} = 0.255$	$X_{Ni3Sn\_LT} = 0.258$	$X_{Ni3Sn2\_HT} = 0.389$	[44]
	1123	$X_{Ni3Sn\_HT} = 0.261$	$X_{Ni3Sn\_LT} = 0.273$		[23]
	1185				[51]
	1143	$X_{Ni3Sn\_HT} = 0.250$	$X_{Ni3Sn\_LT} = 0.271$	$X_{Ni3Sn2\_HT} = 0.379$	[43]
	1184	$X_{Ni3Sn\_HT} = 0.255$	$X_{Ni3Sn\_LT} = 0.257$	$X_{Ni3Sn2\_HT} = 0.378$	[37]
	1144	$X_{Ni3Sn\_HT} = 0.250$	$X_{Ni3Sn\_LT} = 0.270$	$X_{Ni3Sn2\_HT} = 0.378$	[46]
Peritectic			$L + Ni_3Sn_2\_HT \Leftrightarrow Ni_3Sn_4$		
	1068	$X_{Ni3Sn2\_HT} = 0.425$	$X_{Ni3Sn4} = 0.555$	$X_L = 0.810$	[1]
	1066	$X_{Ni3Sn2\_HT} = 0.431$	$X_{Ni3Sn4} = 0.567$	$X_L = 0.793$	[44]
	1067	$X_{Ni3Sn2\_HT} = 0.420$	$X_{Ni3Sn4} = 0.543$	$X_L = 0.809$	[10]
	1066	$X_{Ni3Sn2\_HT} = 0.400$	$X_{Ni3Sn4} = 0.571$	$X_L = 0.904$	[9]
	1068				[51]
	1069	$X_{Ni3Sn2\_HT} = 0.450$	$X_{Ni3Sn4} = 0.557$	$X_L = 0.771$	[43]
	1071	$X_{Ni3Sn2\_HT} = 0.440$	$X_{Ni3Sn4} = 0.555$	$X_L = 0.810$	[37]
	1068	$X_{Ni3Sn2\_HT} = 0.45$	$X_{Ni3Sn4} = 0.556$	$X_L = 0.772$	[46]
Eutectic			$L \Leftrightarrow Ni_3Sn_4 + Sn(BCT)$		
	505	$X_{Ni3Sn4} = 0.570$	$X_L = 0.997$		[1]
	504	$X_{Ni3Sn4} = 0.571$	$X_L = 0.997$		[44]

Table II.2.2. continuation

1	2	3	4	5	6
	505		$X_L = 0.997$		[8]
	504		$X_L = 0.997$		[11]
	505	$X_{Ni3Sn4} = 0.575$	$X_L = 0.998$		[43]
	503	$X_{Ni3Sn4} = 0.575$	$X_L = 0.998$		[46]
Congruent Melting			$L \Leftrightarrow Ni_3Sn\_HT$		
	1447	$X_L = 0.250$			[1]
	1454	$X_L = 0.252$			[44]
	1447	$X_L = 0.252$			[10]
	1442	$X_L = 0.258$			[43]
	1462	$X_L = 0.258$			[37]
	1438	$X_L = 0.274$			[46]
Congruent Melting			$L \Leftrightarrow Ni_3Sn_2\_HT$		
	1537	$X_L = 0.400$			[1]
	1534	$X_L = 0.404$			[24]
	1567	$X_L = 0.400$			[10]
	1540	$X_L = 0.396$			[43]
	1553	$X_L = 0.400$			[37]
	1540	$X_L = 0.400$			[46]
Peritectoid			$Ni_3Sn_2\_HT + Ni_3Sn\_LT \Leftrightarrow Ni_3Sn_2\_LT$		
	700–800				[51]
	848	$X_{Ni3Sn\_LT} = 0.250$	$X_{Ni3Sn2\_HT} = 0.388$	$X_{Ni3Sn2\_LT} = 0.393$	[43]
	848	$X_{Ni3Sn\_LT} = 0.25$	$X_{Ni3Sn2\_HT} = 0.388$	$X_{Ni3Sn2\_LT} = 0.393$	[46]
Eutectoid			$Ni_3Sn_2\_HT \Leftrightarrow Ni_3Sn_2\_LT + Ni_3Sn_4$		
	700–800				[51]
	756	$X_{Ni3Sn2\_LT} = 0.432$	$X_{Ni3Sn2\_HT} = 0.444$	$X_{Ni3Sn4} = 0.552$	[43]
	682	$X_{Ni3Sn2\_LT} = 0.427$	$X_{Ni3Sn2\_HT} = 0.440$	$X_{Ni3Sn2} = 0.530$	[37]
	756	$X_{Ni3Sn2\_LT} = 0.430$	$X_{Ni3Sn2\_HT} = 0.440$	$X_{Ni3Sn4} = 0.550$	[46]

Table II.2.2. continuation

1	2	3	4	5	6
Phase Transition			$Ni_3Sn\_HT \Leftrightarrow Ni_3Sn\_LT$		
	1250	$X_{Ni3Sn} = 0.250$			[1]
	1246	$X_{Ni3Sn} = 0.250$			[44]
	1250	$X_{Ni3Sn} = 0.250$			[23]
	1223	$X_{Ni3Sn} = 0.250$			[33]
	1201	$X_{Ni3Sn} = 0.250$			[43]
	1217	$X_{Ni3Sn} = 0.250$			[46]
Congruent			$Ni_3Sn_2\_HT \Leftrightarrow Ni_3Sn_2\_LT$		
	778–784	$X_{Ni3Sn2} = 0.405$			[51]
	754	$X_{Ni3Sn2} = 0.405$			[37]
	753	$X_{Ni3Sn2} = 0.403$			[46]
	771	$X_{Ni3Sn2} = 0.400$			[18]

➢ Experimental calorimetric and phase diagram studies of the Ni–Sn system

The calorimetric experiments were made using direct calorimetry methods (Chapter I.1). The direct calorimetry method has not been applied previously to studies of this system. In this work experiments have been done at 728, 846, 943, 1332 and 1389 K [18].

The measured molar enthalpies of formation $\Delta_f H$ could be associated with three chemical reactions (eqs. II.1 - 3).

$$0.6Ni+0.4Sn = 1/5Ni_3Sn_2 \qquad \text{(II.1.1)}$$

$$0.75Ni+0.25Sn = 1/4Ni_3Sn \qquad \text{(II.1.2)}$$

$$0.57Ni+0.43Sn = 1/7Ni_3Sn_4 \qquad \text{(II.1.3)}$$

Table II.2.3 and Fig. II.2.4 represent a comparison between experimental and calculated enthalpies of formation of solid nickel–tin alloys. General agreement is observed, taking into account the possible experimental errors. The formation enthalpy of Ni_3Sn_2 _LT measured by Predel and Ruge [52] (–38.5 ± 0.8 kJ·mol^{-1}) is near to our results (–38.3 kJ.mol^{-1}, II.2.1) [18].

Table II.2.3 Comparison of experimental and calculated enthalpies of formation of solid nickel–tin alloys [56]. To conform to original papers, at 273 and 298 K reference states are fcc Ni and bct Sn; at 728, 846, 943, 1023, 1332, 1389 reference states are fcc Ni and liquid Sn

Phase	Temperature (K)	Enthalpy of formation (kJ·mol^{-1})	Reference
1	2	3	4
Ni_3Sn_LT	298	–26.31	[6]
		–26.66	[44] Calculated
		–25.51	[43] Calculated
	943	–24.4 ± 0.12	This work [18]
	1073	-24.90 ± 10	[37]

Table II.2.3 continuation

1	2	3	4
Ni_3Sn_HT	1332	–21.0 ± 2.4	This work [18]
Ni_3Sn_2_LT	273	–31.28	[53]
		–28.85	[43] Calculated
	298	–38.5 ± 0.8	[52]
		–31.79	[6]
		–30.32	[44] Calculated
		–28.87	[43] Calculated
	728	–38.00	This work [18]
Ni_3Sn_2_HT	1023	–38.64	[23]
		–35.68	[44] Calculated
		–35.53	[43] Calculated
	1323	-34.60 ± 10	[37]
	1389	–34.3 ± 1.7	This work [18]
Ni_3Sn_4	1023	–29.70	[23]
		–29.36	[44] Calculated
		–30.82	[43] Calculated
	846	–29.80 ± 0.10	This work [18]
	298	–25.33	[25]
	298	–24.00	[37]

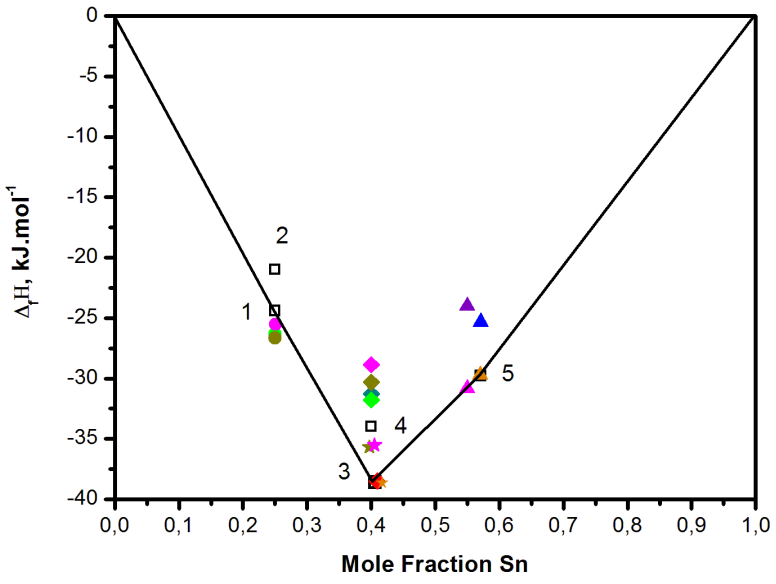

Fig. II.2.4 Integral molar enthalpies of formation at 728, 846, 943, 1332 and 1389 K ($\Delta_f H$ kJ.mol^{-1}) of solid nickel–tin alloys, obtained in this work (1 – Ni_3Sn_LT, 2 – Ni_3Sn_HT, 3 – Ni_3Sn_2_LT, 4 – Ni_3Sn_2_HT, 5 – Ni_3Sn_4), compared with experimental values of Predel and Vogelbein [6] (green), Predel and Ruge [52] (red), Korber and Oelsen [53] (dark cyan), Panteleimonov [23] (orange), Pearson [25] (blue), Schmettererr and Ipser [37] (violet) and calculated values of Ghosh [44] (dark yellow) and Liu [43] (magenta) (unpublished). Experimental and calculated values for Ni_3Sn_LT are symbolised by ○; for Ni_3Sn_2_LT – ◇; for Ni_3Sn_2_HT – ☆; and for Ni_3Sn_4 – △, respectively. Mole fractions of tin are plotted along the abscissa. At 273 and 298 K reference states are fcc Ni and bct Sn; at 728, 846, 943, 1023, 1332, 1389 reference states are fcc Ni and liquid Sn.

Measurements of enthalpy of Ni_3Sn high-temperature form (Ni_3Sn_HT) have been done by direct reaction calorimetry at 1332 K. Details about the working conditions and the experimental results are given in Table II.2.4.

Table II.2.4 Details about the working conditions and the experimental results [18, 56]: m – mass of the specimens (g); $\Delta_f H$ – enthalpy of formation (kJ·mol^{-1}) per mol of atoms; T – working temperature (^{0}C); X_{Sn} – composition of the specimen (mole fraction Sn); Phase – identification of the compound synthesized during the experiment. The values marked by asterisk are from unsuccessful experiments. Reference states are fcc Ni and liquid Sn at the respective working temperature.

No	X_{Sn}	Phase	T K	Time min	m g	$\Delta_f H$ kJ·mol^{-1}
1	2	3	4	5	6	7
1	0.400	Ni_3Sn_2_HT	1288	15	0.1558	–35.07
2					0.1392	–
3					0.1936	–
4					0.2178	–34.89
5					0.1507	–
6	0.406		1389	12	0.1221	–32.67
7					0.1005	–34.22

Table II.2.4 continuation

1	2	3	4	5	6	7
8					0.0883	–
9					0.1266	–36.10
10					0.1058	–
11	0.406	Ni_3Sn_2_LT	728	350	0.1487	–29.95
12					0.1221	–27.64
13					0.1239	–28.83
14					0.0988	–29.28
15					0.0879	–29.04
16	0.250	Ni_3Sn_HT	1332	15	0.1210	–22.74
17					0.1132	–19.89
18					0.1078	–18.39
19					0.1561	–23.41
20					0.1151	–
21	0.250	Ni_3Sn_LT	943	180 – 240	0.1114	–23.83
22					0.0841	–25.16
23					0.0946	–25.01
24					0.0748	–22.47
25					0.0964	–25.40
26	0.571	Ni_3Sn_4	846	240	0.0981	–29.52
27					0.1102	–31.37
28					0.1047	–29.39
29					0.0856	–29.02
30					0.1243	–29.84

Specimens with composition 25 at. % Sn were prepared in the same way, as described in Chapter II.1. Half of them (nos. 16 – 20, Table II.2.4) were used for determination of the Ni_3Sn_HT enthalpy of formation by direct reaction at 1332 K using Gachon calorimeter. The rest of them were used for determination of enthalpy of formation of Ni_3Sn_LT. Thus, the same composition for both phases was assured. The reaction times are shown in Table II.2.4.

As one can see from the thermal curves of specimens (Fig. II.2.5), there are exothermic parts for nos. 16, 17, 18, and 19. Nos. 20 was unsuccessful experiment and the result is not taken into account. The mean value of the enthalpy of formation of Ni_3Sn_HT phase is 21.0± 2.4 $kJ \cdot mol^{-1}$.

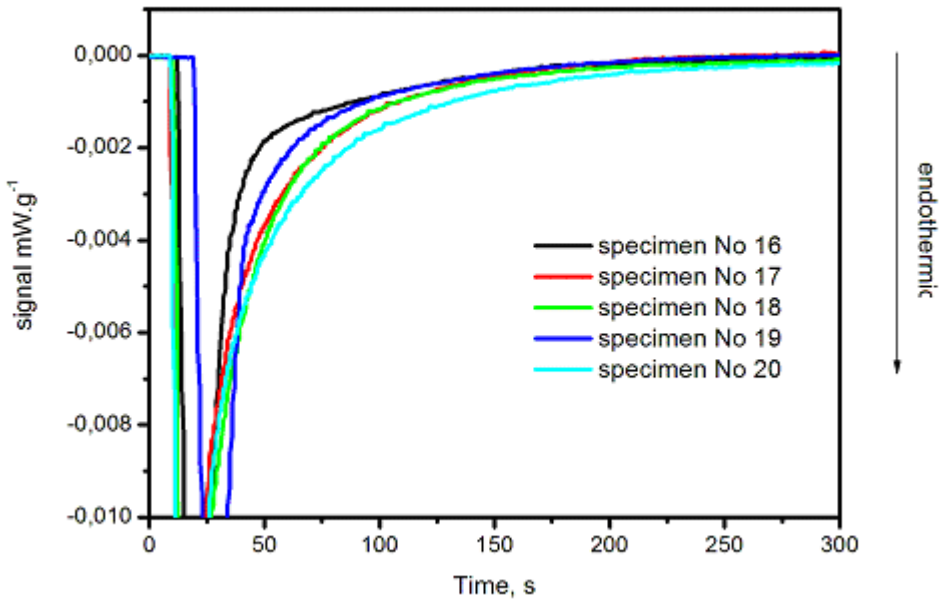

Fig. II.2.5 Calorimetric curves of specimens nos. 16 to 20 obtained during calorimetric experiments (formation of Ni_3Sn _HT) at 1332 K [56]. The endothermic peaks show downward.

EPMA analyses (specimen No. 17) performed after the calorimetric experimentation show the existence of two phases (Fig. II.2.6): Ni_3Sn (63 %) and Ni_3Sn_2 (37 %). These values are assessed by an empirical quantitative method. Thus, some complementary uncertainty for the enthalpy value should be anticipated. X–ray diffraction of specimen No 19 has been performed. The main phases are the high- and low-temperature forms of Ni_3Sn, respectively.

Diffraction lines, belonging to Ni_3Sn and a few peaks of Ni_3Sn_2_HT are registered with spec. No. 19. This finding is in agreement with the results of EPMA.

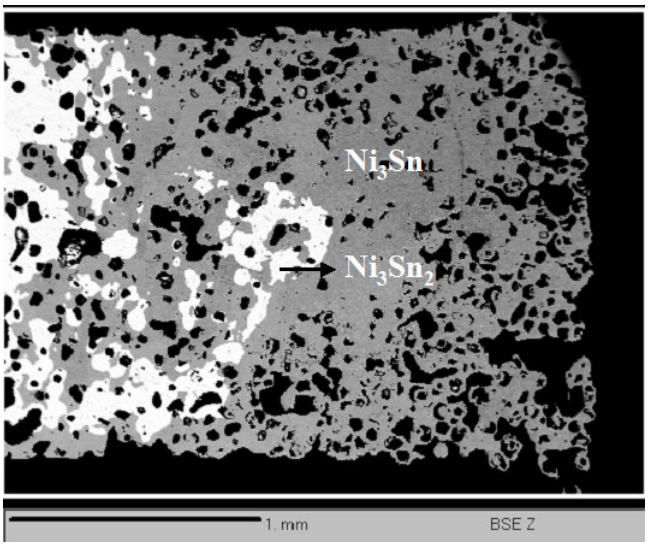

Fig. II.2.6 SEM image in BSE of specimen No 17, obtained by direct reaction between solid Ni and liquid Sn at 1332 K (unpublished). The matrix (grey areas) represents Ni_3Sn; the white phase is Ni_3Sn_2.

Measurements of Ni_3Sn low-temperature form (Ni_3Sn_LT) enthalpy have been done by direct reaction calorimetry at 943 K. Details about the working conditions and the experimental results are given in Table II.2.4 (nos. 21 to 25). Reproducible results are registered with all specimens (Fig. II.2.7). The reaction times are shown in Table II.2.4. The average Ni_3Sn_LT enthalpy of formation is -24.4 ± 0.12 kJ·mol^{-1}.

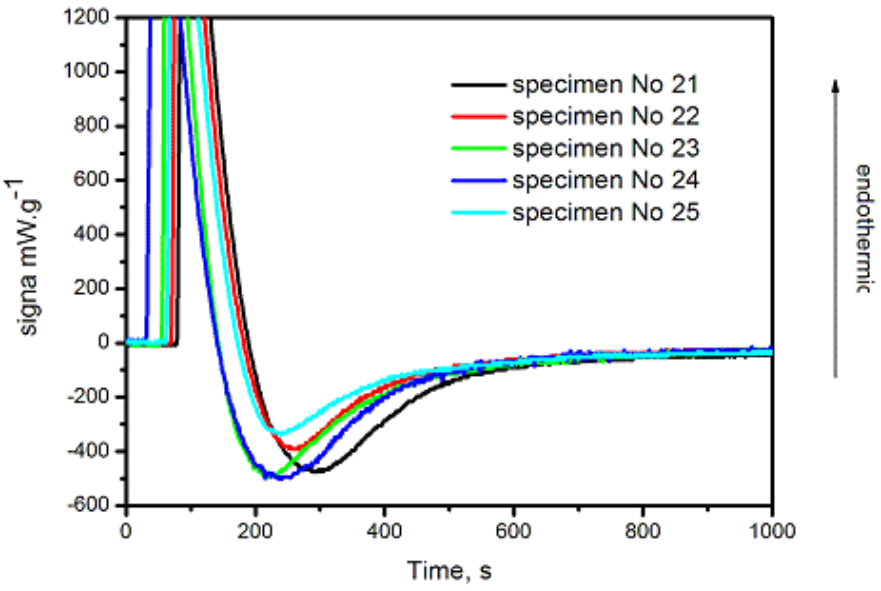

Fig. II.2.7 Calorimetric curves of specimens nos. 21 to 25 obtained during the synthesis of Ni_3Sn_LT at 943 K (unpublished). The time (duration) (t, s) is plotted along the abscissa, and the weight-normalized signals of the calorimeter ($mW \cdot g^{-1}$) – along the ordinate.

According to EPMA investigations (specimen No. 22) and X – ray diffraction of specimen No. 21 the alloys consist of homogeneous Ni_3Sn. (Fig II.2.8)

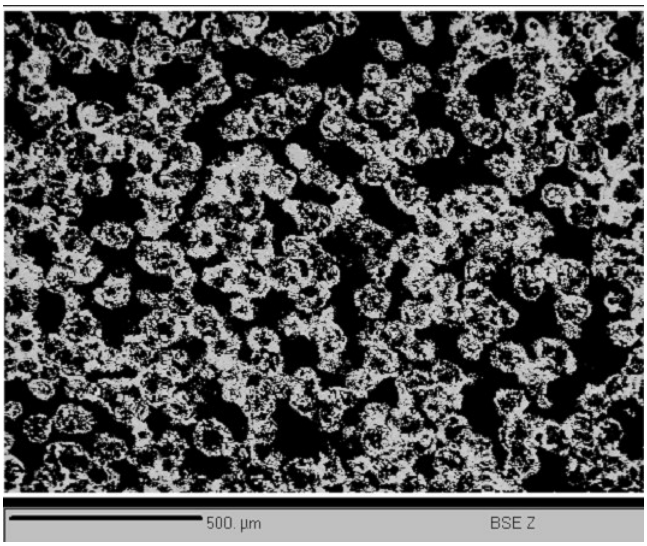

Fig II.2.8 SEM image in BSE of specimen No 22, obtained by direct reaction between solid Ni and liquid Sn at 943 K (unpublished). The alloys consist of homogeneous Ni_3Sn. The black areas are voids.

Two series of direct reaction calorimetric experiments (at 1288 and 1389 K) have been performed concerning Ni_3Sn_2_HT phase (Table II.2.4). In Fig. II.2.9 A and B experimental results of specimens nos. 1 to 10 are shown. The trials of specimens nos. 2, 3, 5, 8 and 10 have failed (they did not exhibit exothermic parts). This might be due to insufficient masses of the samples or to incomplete reactions (due to kinetic reasons). The reaction time is shown in Table II.2.3.

Thus, the "critical mass" of the specimen had to be determined empirically. The average enthalpy of formation of Ni_3Sn_2_HT at 1288 K, determined on samples 1 and 4, is -35.0 ± 0.13 $kJ \cdot mol^{-1}$, and at 1389 K with samples 6, 7 and 9, it is -34.3 ± 1.7 $kJ \cdot mol^{-1}$.

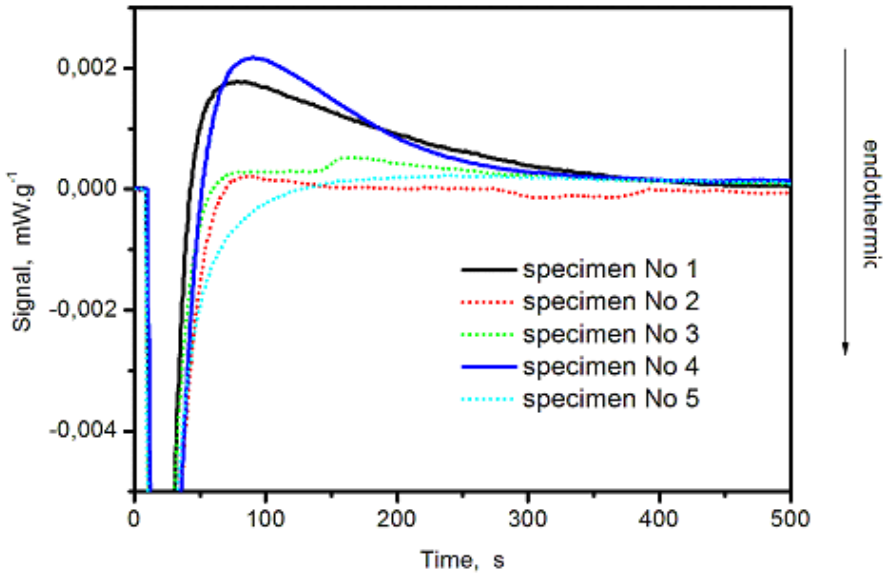

Fig. II.2.9 A Calorimetric curves of specimens nos. 1 to 5 obtained during the synthesis of Ni_3Sn_2_HT at 1288 K [56]. The numbers of the curves correspond to the numbers of the experiments. The dotted curves indicate the failed trials (2, 3 and 5) while the solid lines represent the successful ones. The durations of the experimentations (Time, s) are plotted along the abscissa, and the weight-normalized signals of the calorimeter ($mW \cdot g^{-1}$) - along the ordinate. The signals' values are proportional to the enthalpy changes. The endothermic peaks show downward.

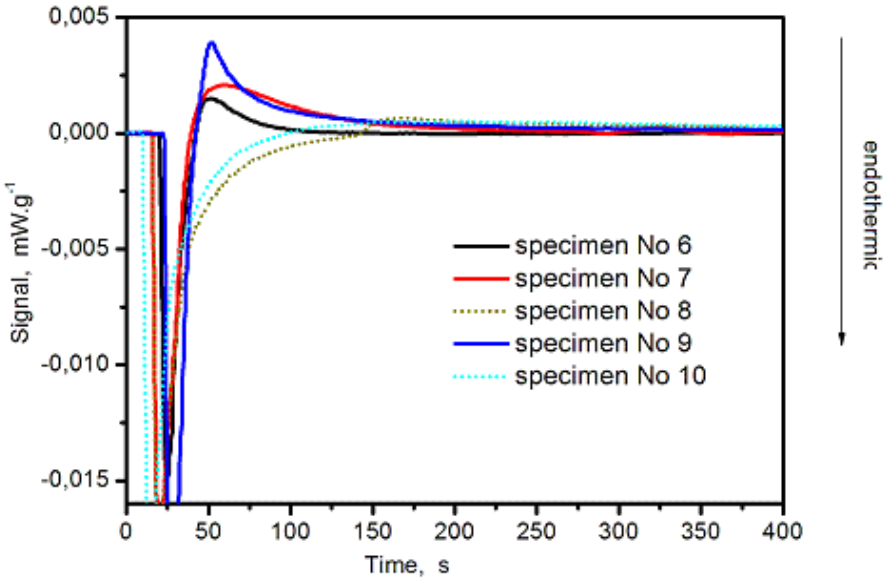

Fig. II.2.9 B Calorimetric curves of specimens nos. 6 to 10 obtained during the synthesis of Ni_3Sn_2_HT at 1389 K (unpublished). The numbers of the curves correspond to the numbers of

the experiments. The dotted curves indicate the failed trials (8 and 10) while the solid lines represent the successful ones. The durations of the experimentations (Time, s) are plotted along the abscissa, and the weight-normalized signals of the calorimeter ($mW \cdot g^{-1}$) - along the ordinate. The signals' values are proportional to the enthalpy changes. The endothermic peaks show downward.

The alloy No 6 has been investigated after the reaction, by electron probe microanalyses (EPMA) using apparatus Cameca SX 100. While the predominant phase is Ni_3Sn_2, about 10 % of Ni_3Sn_4 have been found in the specimen (Fig. II.2.10). These values are assessed by an empirical quantitative method. In such a way, the incompleteness of the chemical reaction has been confirmed, thus explaining the failure of the calorimetric experiment.
According to the phase diagram (Fig. II.2.2) two Ni_3Sn_2 forms (low- and high-temperature) exist.

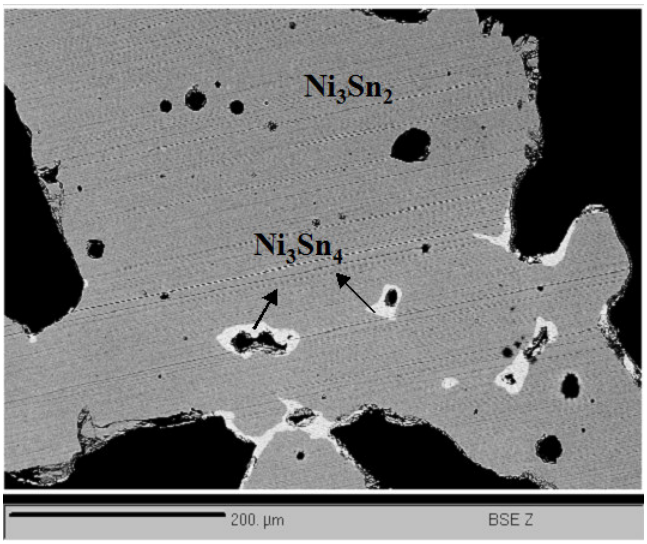

Fig. II.2.10 SEM image in BSE of specimen No 6, obtained by direct reaction between solid Ni and liquid Sn at 1389 K (unpublished). The matrix represents Ni_3Sn_2; the white phase is Ni_3Sn_4.

Details about the measurement of enthalpy of formation of the low-temperature form of Ni_3Sn_2 (Ni_3Sn_2_LT) are also presented in Table II.2.4 (nos. 11 – 15). They have been performed at 728 K in a Calvet type calorimeter, by direct reaction. The reaction time, shown in Table II.2.4 is longer, compared to those applied in the previous case. That is why fluctuations of the signal and the base line have been observed, but reproducible results are obtained for all specimens (Fig. II.2.11). The average Ni_3Sn_2_LT enthalpy of formation is -29.00 ± 0.85 $kJ \cdot mol^{-1}$.

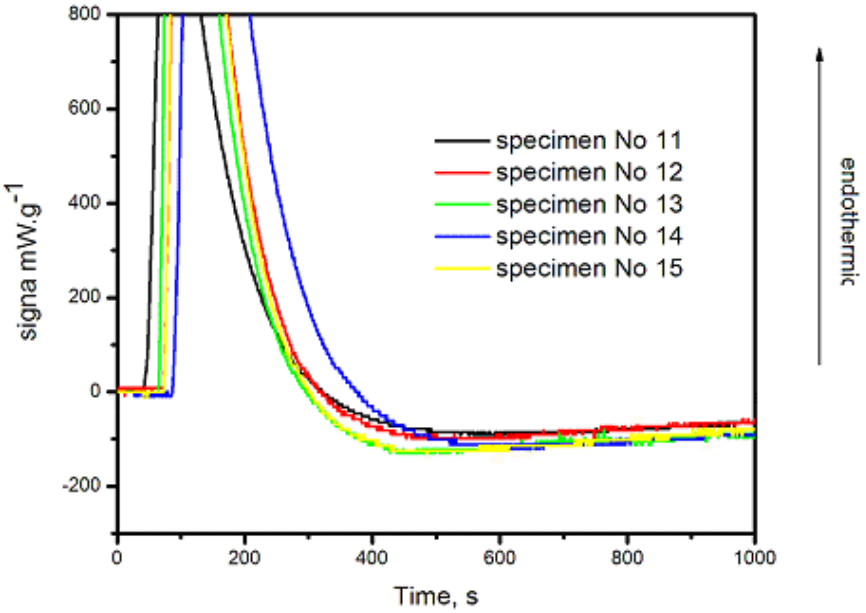

Fig. II.2.11 Calorimetric curves of specimens nos. 11 to 15 obtained during the synthesis of Ni_3Sn_2_LT at 728 K (unpublished). The numbers of the curves correspond to the numbers of the experiments. The durations of the experimentations (Time, s) are plotted along the abscissa, and the weight-normalized signals of the calorimeter ($mW \cdot g^{-1}$) – along the ordinate. The signals' values are proportional to the enthalpy changes. The endothermic peaks show upward.

High-temperature X-ray diffraction of specimen No 4 was performed using a heating rate of 5 $K.min^{-1}$. Diffractograms were obtained at five temperatures: room temperature, 298, 513, 643, 763 and 823 K. The apparatus used for the measurements is X`Pert Philips with Cu $K_{\alpha 1}$ rays. It was found that the main phase at room temperature is Ni_3Sn_2_LT. The experimental diffraction lines are compared with those, calculated by the program PowderCell2.3, spectra. Literature data about the pertinent space groups are used for the calculations [55]. Slight differences between calculated and experimental lines are observed, but they are due to the variation of the cell parameters as a result of the high temperature. Change of the crystal structure at 513 K (displacement of the diffraction peaks) has been observed. In general a thermal perturbation is observed in the interval between room temperature to 823 K (Fig. II.2.12 A, B, C). This data indicates that the transition between low- and high-temperature modifications might occur at temperatures lower than expected.

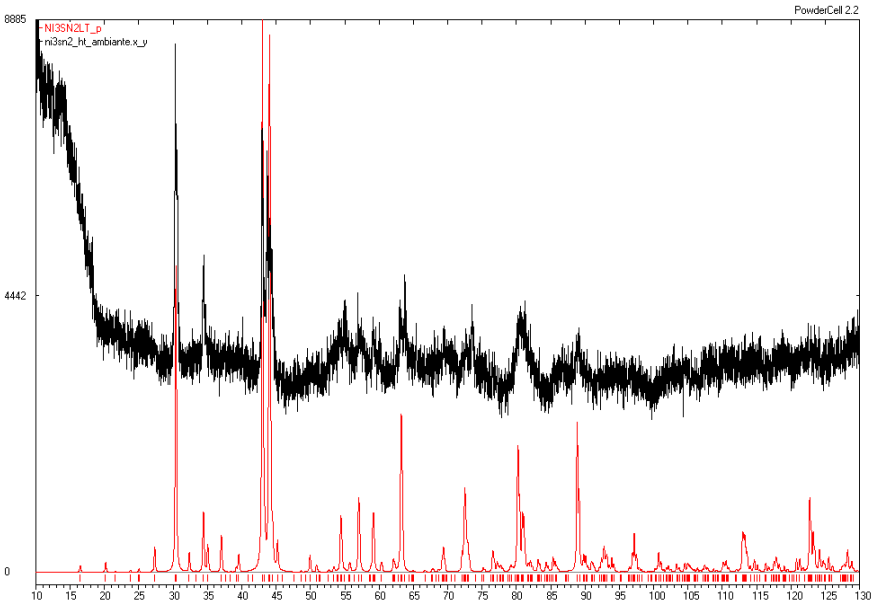

Fig. II.2.12 A XRD spectrum of sample No 4 at room temperature (unpublished), superimposed with theoretical pattern of Ni_3Sn_2 (red curve), simulated by PowderCell 2.3, using [55].

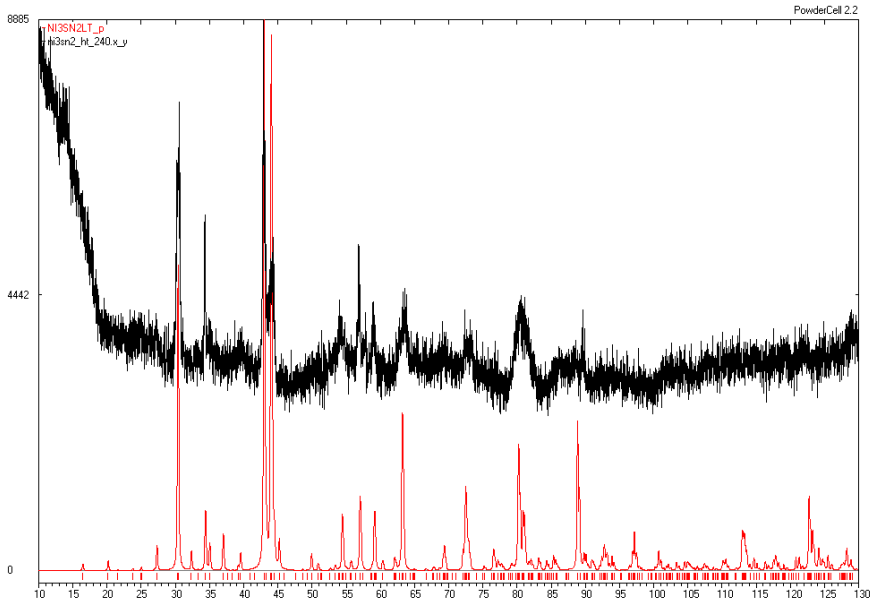

Fig. II.2.12 B XRD spectrum of sample No 4 at 513 K (unpublished), superimposed with theoretical pattern of Ni_3Sn_2 (red curve), simulated by PowderCell 2.3, using [55].

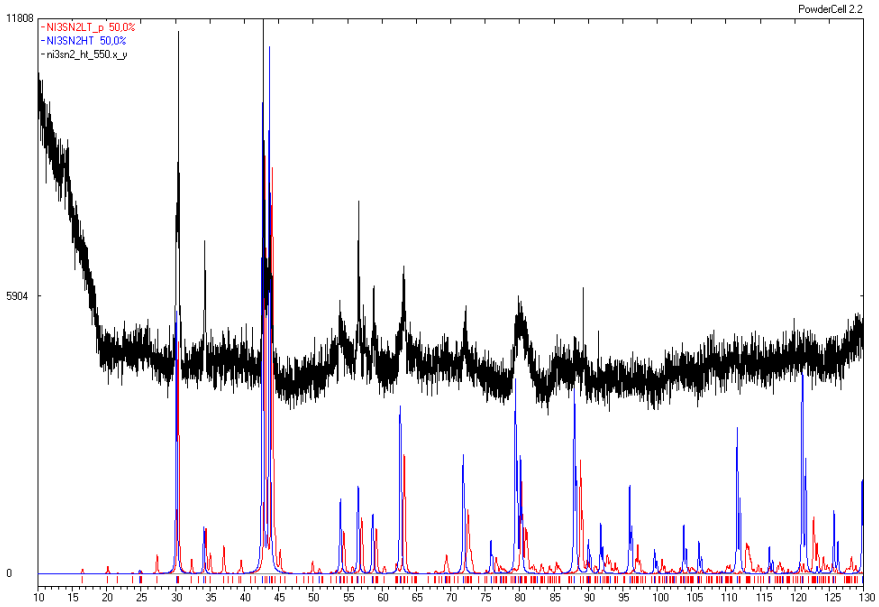

Fig. II.2.12 C XRD spectrum of sample No 4 at 846 K [56], superimposed with theoretical patterns of Ni_3Sn_2_LT (red curve) and Ni_3Sn_2_HT (blue curve), simulated by PowderCell 2.3, using [55].

X-ray diffraction of specimen No. 11 has indicated that the main phase is Ni_3Sn_2_LT. A few diffraction lines belonging to other compounds – Ni_3Sn_4 and Ni_3Sn_LT are observed. According to EPMA (Fig. II.2.13) the main phase is Ni_3Sn_2 (59 %) as well. There are three more phases: Ni_3Sn_4 (26 %), Ni_3Sn (3 %) and almost pure Ni (12 %). These values are assessed by an empirical quantitative method.

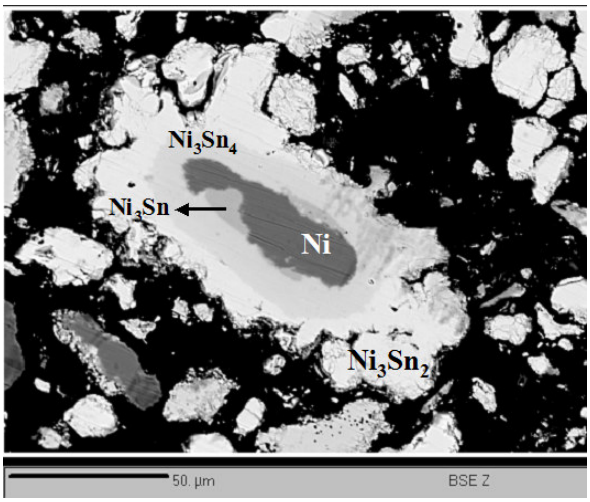

Fig. II.2.13 SEM image in BSE of specimen No 11, obtained by direct reaction between

solid Ni and liquid Sn at 728 K (unpublished). The matrix represents Ni_3Sn_2. The other three phases are Ni_3Sn_4, Ni_3Sn and almost pure Ni.

The results demonstrate that the reaction between Ni and Sn is incomplete at the conditions applied to study the low-temperature form. That is why the experimentally obtained enthalpy of formation of Ni_3Sn_2_LT is less (negative) in comparison with that one of Ni_3Sn_2_HT (-29.0 ± 0.85 kJ·mol^{-1} and -34.0 ± 0.17 kJ·mol^{-1}).

Similar results (concerning the peculiar enthalpies of formation values of the high- and low-temperature forms (Ni_3Sn_2_HT and Ni_3Sn_2_LT), respectively are obtained by other authors [23, 43, 52, 53]. We suppose that incomplete reactions are the causes for such discrepancies.

To obtain more reasonable value of enthalpy of formation, new experiment was performed. Five pellets with a composition of 40 at. % Sn, named S1–5 were prepared under argon atmosphere and annealed in evacuated and sealed quartz tubes at 1273 K for one week. Afterwards the specimens were cooled slowly in air in order to obtain the low temperature form of Ni_3Sn_2.

Differential thermal analyses (2 runs in the interval 300 to 1080 K with 3 K/min) were performed with sample No S2. According to the phase diagram calculated by the authors using the coefficients optimised by Liu et al. [43] the expected transition temperature has to be around 750 and 850 K. The peak P1, at around 771 K, is in agreement with the expected transition temperature between low- and high-temperature Ni_3Sn_2 forms (Fig. II.2.14). The enthalpy of transition is 3.97 kJ.mol^{-1}. Using the enthalpy of formation of Ni_3Sn_2_HT (-34.0 ± 0.17 kJ.mol^{-1}), we recalculated that the enthalpy of formation of Ni_3Sn_2_LT is -38.6 kJ.mol^{-1}.

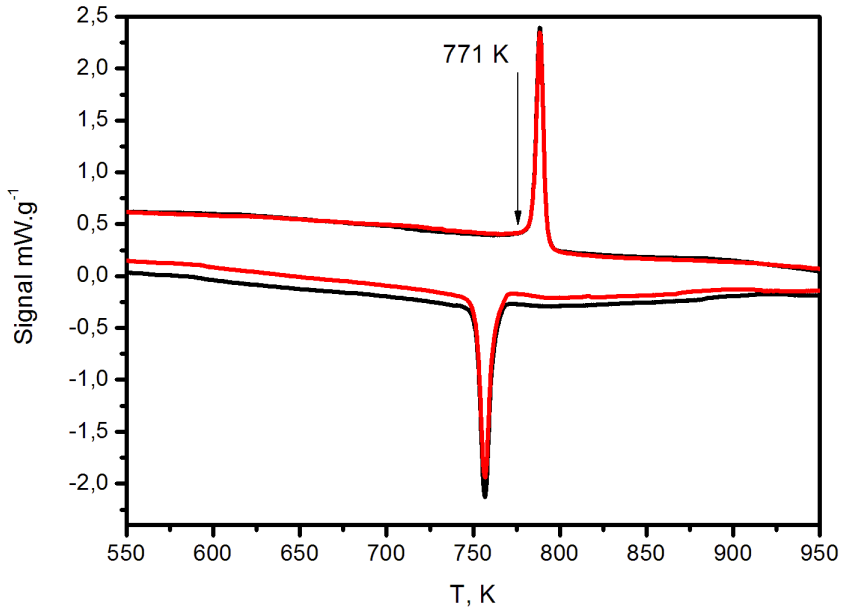

Fig. II.2.14 Differential scanning calorimetry curves of specimens, obtained at 1273 K (first run – black curve, second run – red curve) (unpublished). The working interval is 300 – 1080 K and the heating rate is 3 K.min^{-1}. The peak at around 771 K is in agreement with the expected transition temperature between low- and high-temperature Ni_3Sn_2 forms. The signal of differential scanning calorimeter (mW/g) is plotted along the ordinate and temperature (T, K) – along the abscissa.

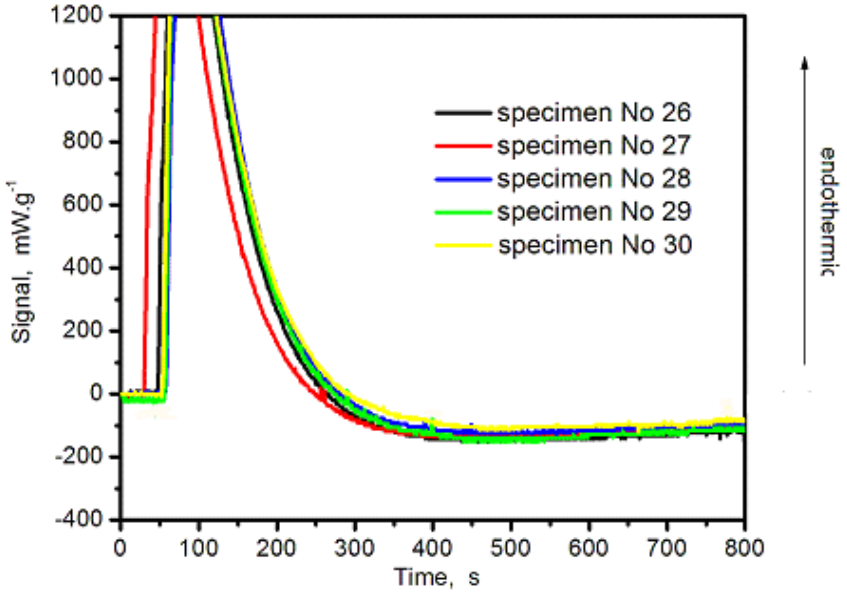

Fig. II.2.15 Calorimetric curves of specimens nos. 26 to 30 obtained during the synthesis of Ni_3Sn_4 at 846 K (unpublished). The endothermic peaks show upward. The time (duration) (t,

s) is plotted along the abscissa, and weight-normalized signals of the calorimeter ($mW \cdot g^{-1}$) - along the ordinate.

Measurements of Ni_3Sn_4 enthalpy of formation are performed at 846 K by Calvet calorimeter (Table II.2.4, nos. 26 – 30). The reaction time, shown in Table II.2.4 is relatively long because of the low temperature, and some fluctuations of the baseline are registered (Fig. II.2.15). The average enthalpy of formation of Ni_3Sn_4 is -29.8 ± 0.1 $kJ \cdot mol^{-1}$.

The alloy No 27 has been investigated after the reaction, by electron probe microanalyses (EPMA) using apparatus Cameca SX 100 (Fig. II.2.16). The main phase is Ni_3Sn_4, as expected. There are two more phases: Ni_3Sn_2 (11%) and Ni_3Sn (9%). These values are assessed by an empirical quantitative method.

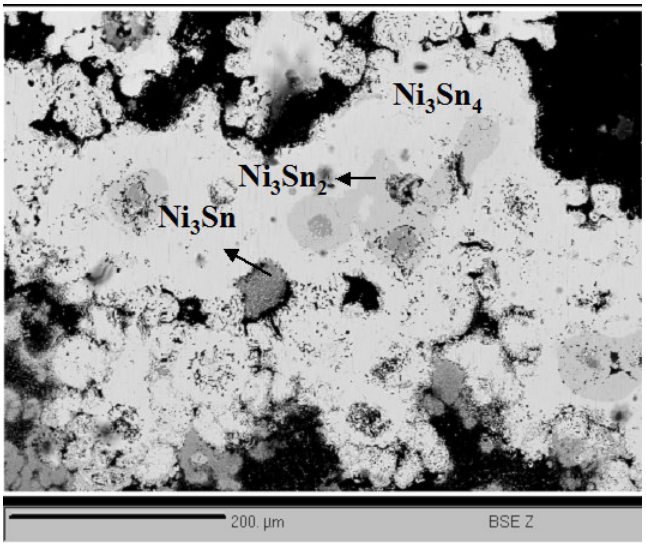

Fig. II.2.16 SEM image in BSE of specimen No 27, obtained by direct reaction between solid Ni and liquid Sn at 846 K (unpublished). The matrix represents Ni_3Sn_4. The light gray phase is Ni_3Sn_2 and the dark gray – Ni_3Sn.

➢ Conclusion

- Enthalpies of formation of Ni–Sn compounds have been measured by direct reaction calorimetry at 1332, 943, 1288, 728 and 846 K for Ni_3Sn_HT, Ni_3Sn_LT, Ni_3Sn_2_HT, Ni_3Sn_2_LT and Ni_3Sn_4, respectively. The experimentally obtained values are –21.0, –24.4, –38.3, –34.3, –29.8 kJ.mol^{-1}, reference states are fcc Ni and liquid Sn.
- For the first time data about the enthalpy of formation $\Delta_f H$ of Ni_3Sn_HT has been obtained.
- The transition temperature and enthalpy between low and high-temperature forms of Ni_3Sn_2 compound have been verified by differential thermal analyses and found to be around 771 K and 0.4 kJ.mol^{-1}.

➢ Bibliography

[1] Nash A, Nash P. Bull. Alloy Phase Diag 1985;6:350.

[2] Massalski TB, Okamoto H, Subramanian PR, Kacprzak L. 'Binary Alloy Phase Diagrams', ASM International 1996.

[3] Gautier H. Bull. Soc Encour Ind Natl 1896;1:1313.

[4] Charpy MG. Bull Soc Encour Ind Natl 1897;2:384.

[5] Guillet ML. Rev Met 1907;4:535.

[6] Predel B., W. Vogelbein, Thermochim. Acta, 30 (1979) 205.

[7] Voss G. Z Anorg Chem 1908 ;57 :35.

[8] Hanson D, Sandford ES, Stevens H. J Inst Met 1934;55:117.

[9] Mikula W, Thomassen L. Trans AIME, Inst Metal Div 1937;124:111.

[10] Heumann T. Z Metallkd 1943;35:206.

[11] Heycock CT, Neville FH. J Chem Soc 1890;57:378.

[12] Viguroux E. Compt Rend Inst Fr-Acad Sci 1907;144:639.

[13] Viguroux E. Compt Rend Inst Fr-Acad Sci 1907;144:712.

[14] Viguroux E. Compt Rend Inst Fr-Acad Sci 1907;144:1351.

[15] Oftedal I., Z. Phys. Chem. 1928;132:208

[16] Viguroux E. Compt Rend Inst Fr-Acad Sci 1907;145:246.

[17] Viguroux E. Compt Rend Inst Fr-Acad Sci 1907;145:429.

[18] Vassilev G.P., K.I. Lilova, J.C. Gachon, Enthalpies of formation of Ni–Sn compounds, Thermochimica Acta, 447 (1) (2006) 106 – 108

[19] Fetz E, Jette ER. J Chem Phys 1936;4:537.

[20] Nial O. Svensk Kemisk Tidskrift 1947-1948; 59-60:172.

[21] Lihl F, Kirnbauer H. Monatsh Chem 1955;86:745.

[22] Lihl F, Kirnbauer H. Z Metallkd 1955;46:438.

[23] Panteleimonov LA, Khanna AY, Sokolova IG, Bagdasaryan AK. Vestn Mosk Univ Ser II: Khim 1964;19:45.

[24] Rahlfs P. Metallwirtschaft 1937;16:343.

[25] Pearson WB, Thomson LT. Can J Phys 1957;35(4):349.

[26] Michel W. Ann Phys 1963;11:321.

[27] Bandyopadhyay J, Gupta KP. Metall Trans 1970;1:327.

[28] Woo OT, Rezek J, Schlesinger M. Mater Sci Eng 1975;18:163.

[29] Schubert K, Burkhardt W, Esslinger P, Günzel E, Meissner HG, Schütt W, Wegst J, Wilkens
M. Naturwissenschaften 1956;43:248.
[30] Shadangi SK, Singh M, Panda SC, Bhan S. Indian Journal of Technology 1986;24:105.
[31] Shadangi SK, Singh M, Panda SC, Bhan S. Crystal Research and Technology 1986;21:867.
[32] Brand P. Z Anorg Allg Chem 1967;353:270.
[33] Bhargava MK, Schubert K. J Less-Common Met 1973;33
[34] Jeitschko W, Baberg B. Acta Crystallographica B 1982;38:598.
[35] Fetz E, Jette ER. Trans AIME 1937;124:133.
[36] Pak HR, Saburi T, Nenno S. Bull Jpn Inst Met 1973;37:1128.
[37] Schmettererr C., H. Flandorfer, U. Saeed, C. Luef, H. Ipser, Intermetallics, in preparation
[38] Leineweber A, Ellner M, Mittermeijer EJ. J Solid State Chem 2001;159:191.
[39] Leineweber A, Oeckler O, Zachwieja U. J Solid State Chem 2004;177:936.
[40] Leineweber A., J Solid State Chem 2004;177:1197-1212.
[41] Leineweber A, Mittermeijer EJ, Knapp M, Baehtz C. Materials Science Forum 2004;443-444:247-250
[42] Fjellvag H, Kjekshus A. Acta Chem Scand A 1986;40A:23.
[43] Liu HS, Wang J, Jin ZP. CALPHAD 2005;28(4):363.
[44] Ghosh G. Metallurgical and Materials Transactions A 1999;30:1481
[45] Miettinen, J. CALPHAD 27 (2003) 309.
[46] Dinsdale A., A. Watson, A. Kroupa, J. Vrestal, A. Zemanova, J. Vizdal COST 531 Thermodynamic Database for Lead-free Solder Alloys, Version 2.0 (2006)
[47] Eremenko V., G. Lukashenko, V. Pritula, Izv. Akad. Nauk SSSR, Met. 3 (1971) 82
[48] Dinsdale A., Report DMA (A), 195, National Physical Laboratory, 1989
[49] Luck R., J. Tomiska, B. Predel, Z. Met.kd. 79 (1988) 345.
[50] Haddad R., M. Gaune-Escard, J.P. Bros, A. Havlicek, E. Hayer, K.L. Komarek, J. Alloys Compounds 247 (1997) 82.
[51] Havlicek A., Thesis, University of Vienna, 1991
[52] Predel B., H. Ruge, Thermochim. Acta, 3 (1972) 411.
[53] Korber F., W. Oelsen, Mitt Kaiser Wilhelm Inst. F. Eiseforsch. 19 (1937) 209
[54] Dinsdale A., CALPHAD **15,** 317 (1991).
[55] Villars P. (Editor), Pearson's Handbook Desk Edition, ASM International, 1997, ISBN 978-0-87170-603-4, OH, USA

[56] Vassilev G.P., K.I. Lilova, J.C. Gachon, Calorimetric studies of the Ni-Sn system, VIII International Workshop of Associated Phase Diagram and Thermodynamic Committee (APDTC), Kosice, Slovakia, 19 November 2005, Proceedings, Editor W. Zakulski, ISBN 83-921845-5-6, Published by: Institute of Metallurgy and Materials Science, Polish Academy of Sciences, Krakow, Poland, p. 27 – 34.

II. 3. Thermodynamic Investigations of the Ni–Sn–Bi Ternary System

The Pb–Sn eutectic solder is widely used by the electronic industry for packaging applications. This solder has been used for years and meets the performance requirements very well, but lead has negative impacts on the environment. Because of this environmental concern, it is anticipated that lead-bearing solders will be phased out either voluntarily by industry or through legislation in a few years. Many lead-free solders have been proposed as possible replacements, and some of them have been used in industry for quite some time. For example**,** the eutectic Bi–Sn solder (58 wt.% Bi–42 wt.% Sn, Bi42Sn) is an important candidate for replacing the Pb–Sn eutectic solder in many applications [1].

In printed circuit boards (PCB) manufacturing, a solderable surface finish is coated over the Cu traces to maintain solderability over a period of shelf time. Nickel layers, both electrolytic and electroless, are used in several important lead-free finishes, such as the Au/Ni and Pd/Ni, which have the additional advantage of being very flat, making them ideal for fine lead-pitch and area-array surface mount components. The Au and Pd over-layers are used to protect the Ni layers from oxidizing. They are thin (0.02–0.2 mm) and disappear very quickly into the solder during the reflow operation, exposing the Ni layer to the solder [2]. Therefore, in lead-free PCB soldering, the interactions between Ni and Bi–Sn solder have to be considered.

Since the properties of the Ni–Sn–Bi ternary system at higher temperature and different compositions are not well known, experiments for assessment of isothermal sections and some calorimetric studies of solid and liquid phases have been performed. The main purpose was to obtain new thermochemical data and to investigate the phase equilibria in this ternary system.

➢ Literature review

A detailed description of Ni–Sn binary system and the three intermetallic compounds Ni_3Sn, Ni_3Sn_2, Ni_3Sn_4 (Fig. II.2.1) has been made in Chapter II.2.

Sn and Bi form a eutectic point at 43 at. % Bi and 140 °C, with 12.4 at. % Bi soluble in (ßSn) at the eutectic temperature [3] (Fig. II.3.1).

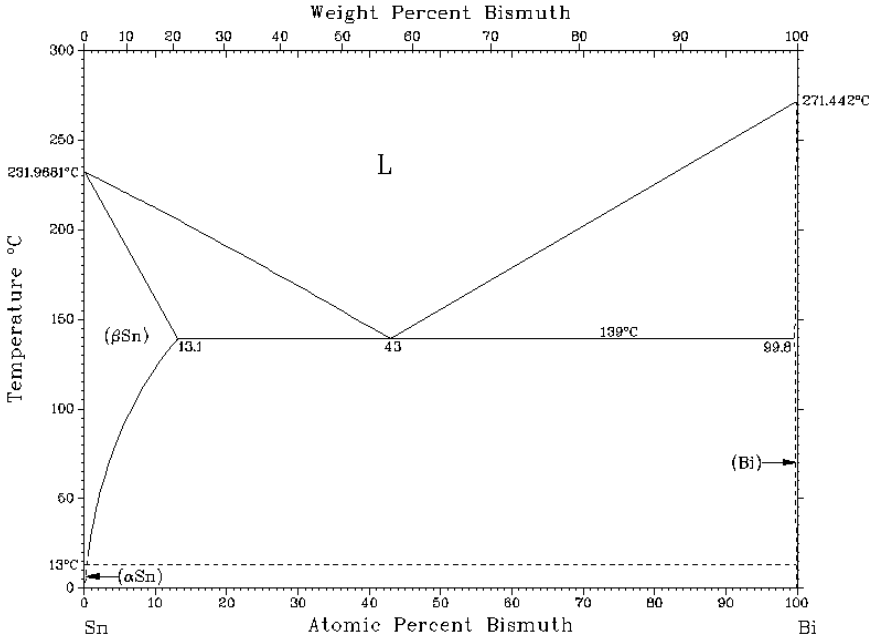

Fig. II.3.1 The Sn–Bi phase diagram by T. Massalski [4]

That binary system is relatively familiar [4 – 14]. The thermodynamic properties of liquid Bi-Sn alloys were measured at 723 K over the whole composition range by an electromotive force (EMF) method using a liquid electrolyte by Asryan and Mikula [15]. These data are in very good agreement with earlier calorimetric measurements by Wittig and Huber [16] at 743 K, Yazawa et al. [17] at 690 K, and finally by Sharkey and Pool [18] at 725 K as well as with EMF data reported by Seltz and Dunkerley [19] for 608 K. The binary interaction parameters of Bi–Sn were established by Flandorfer et al. [20]. The enthalpy of mixing was found to be independent of temperature. According to the COST database v.2.0 [21], the data for the Sn–Bi system was taken from H. Ohtani, K. Ishida [22] and D Malakhov, X J Liu [23]. In version 2.1b the data for the liquid and rhombohedral phases was modified by Vizdal [24].

The literature data about the crystal structures of the stable Bi-Sn phases are compiled in Table II.3.1.

Table II.3.1 Crystal structures of the stable binary Bi-Sn phases by literature data.

Phase	Homogeneity range at. %	Pearson symbol	Structurbericht designation	Space group	Prototype	Source
Bi	≈100 at. % Bi	hR2	A7	$R\bar{3}m$	αAs	[4]
αSn	≈100 at. % Sn	cF8	*A4*	$Fd\bar{3}m$	C(diam.)	[4]
βSn	≈100 at. % Sn	tI_4	A5	$I4_1/amd$	βSn	[4]

Two stable compounds exist in the Ni–Bi system: $NiBi_3$ and NiBi. All authors agree that the first is stoichiometric while the second exhibits a small homogeneity region. In any case, the phase diagram compiled by Predel [25] differs from the one of Nash [26] and Massalski [4] (Fig. II.3.2), concerning the NiBi-phase homogeneity range and the liquidus topology at more than about 50 at. %.

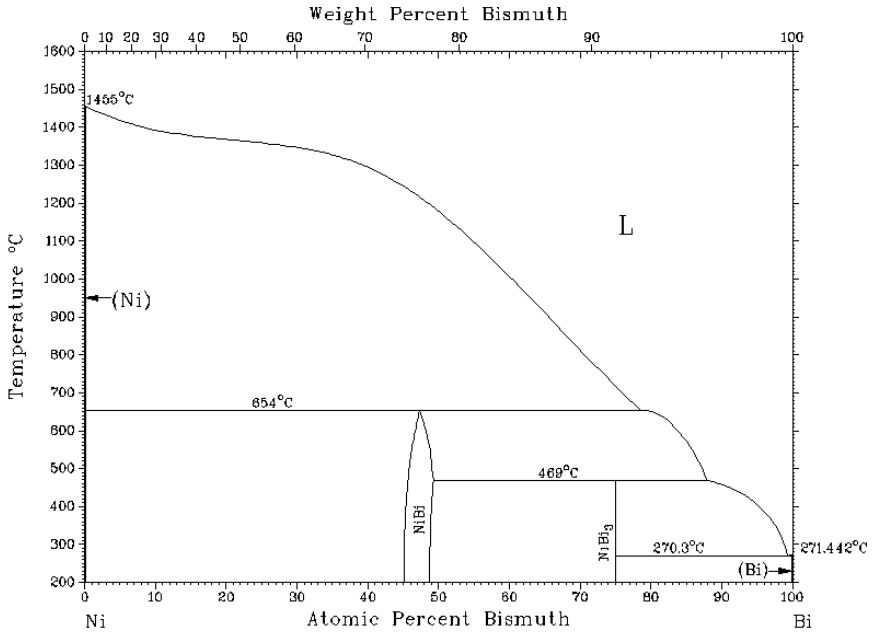

Fig. II.3.2 The Ni–Bi phase diagram by T. Massalski [4]

Portvein [27] and Voss [28] constructed the liquidus in the central and Ni-rich side of the system by thermal analysis method. The Bi melting point has been acknowledged as 542 K, about 2 K below the presently accepted value. A possible source of error is connected with the relatively high Bi vapor pressure (boiling point 1837 K). Ni-activity values in the Bi-rich liquid phase and the enthalpy of formation of the NiBi were measured, respectively, by Iwase and

McLean [29] using an EMF technique and by Predel and Ruge [30] by means of calorimetric experiments. Heat capacity and magnetic measurements of the compound NiBi are known as well [31, 32]. Assessment of the NiBi heat capacity has been done by Barin [33] based on the data of Predel and Ruge [30]. Vassilev et al. [34, 35] have recently done experimental studies and thermodynamic optimization of this system (Fig. II.3.3).

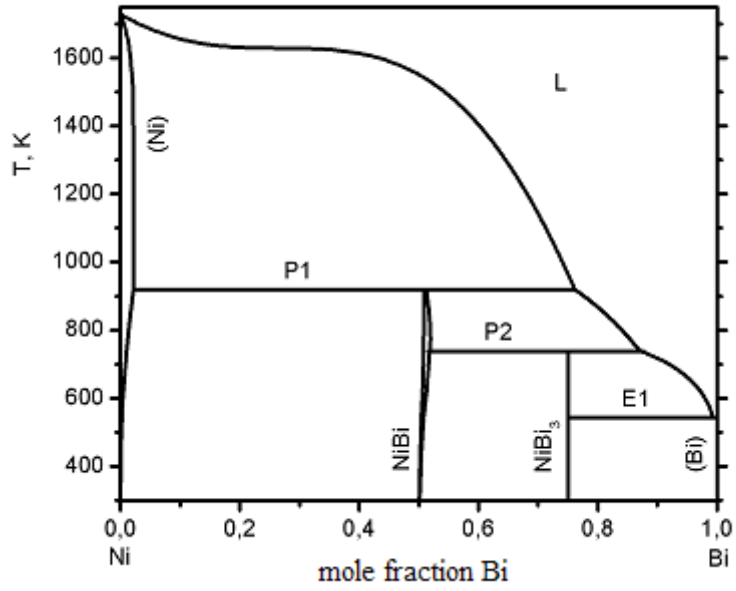

Fig. II.3.3 The Ni–Bi phase diagram, calculated by Vassilev et al. [34]

The literature data about the crystal structures of the stable Ni-Bi phases are compiled in Table II.3.2.

Table II.3.2 Crystal structures of the stable binary Ni-Bi phases by literature data.

Phase	Homogeneity range at. %	Pearson symbol	Structurbericht designation	Space group	Prototype	Source
Bi	≈100 at. % Bi	hR2	A7	$R\bar{3}m$	αAs	[4]
Ni	≈0 at. % Bi	cF4	A1	$Fm\bar{3}m$	Cu	[4]
NiBi	47-51 at. % Bi	hP4	$B8_1$	$P6_3mmc$	NiAs	[49]
$NiBi_3$	75 at. % Bi	oP16	$F5_6$	Pnma	$CaLiSi_2$	[49]

Some experimental studies on the Ni–Sn–Bi ternary system have been done, regarding the reactions between Ni and the eutectic SnBi solder in the solid state. Kang et al. [36] studied the reaction at 443 K for up to 20 minutes, and found that only Ni_3Sn_4 formed. Chen et al. [2] verified that interaction at 358, 373, 393, and 408 K. Only Ni_3Sn_4 was detected as a result of the reaction. None of the other Ni–Sn intermetallic compounds and none of the Ni–Bi intermetallic compounds were observed. In addition, fine Bi-rich particles within the Sn-rich phase of the solder were found. Their amount increased with the aging temperature. The formation of these fine Bi-rich particles is due to the fact that the Sn-rich phase can dissolve substantial amounts of Bi. It was also found that, as aging time increased, the region immediately adjacent to the Ni_3Sn_4 layer was preferentially occupied by the Bi-rich phase. This is because Sn in that region had reacted with Ni to form Ni_3Sn_4, leaving a nearly continuous Bi-rich phase above the Ni_3Sn_4.The experiments of Tao et al. [37] at 453, 513, 573, 633, and 693 K confirmed the Ni_3Sn_4 formation. At lower temperatures (453, 513, 573, 633 K), Ni_3Sn_4 formed at the interface as a thin continuous layer, which was protective and resulted in the parabolic growth kinetics. However, reaction at a higher temperature (693 K) produced at the interface a thick reaction zone, which was a two-phase mixture of Ni_3Sn_4 + solder. Wetting properties of Sn–Bi alloys on the Ni substrate and their interfacial reactions were examined and an isothermal section at 573 K for the ternary Sn–Bi–Ni system was proposed by Lee et al. [38].

➢ Experimental phase diagram studies of Ni–Sn–Bi system

Powders (325 mesh) of pure metals (Ni (4N), Sn (5N), Bi (4N)) (production of Goodfellow) were used to prepare pellets (5 mm of diameter and 3 to 4 mm thick) with predetermined compositions (Table II.3.3) in the same way as described in Chapter II.1. The synthesis of the alloys for phase diagram studies was performed in evacuated and sealed quartz tubes at 733, 773, 903 and 1273 K [39]. The samples were annealed for three (those at 733 and 773 K) or two (those at 903 and 1273 K) weeks. Such relatively short times were chosen because the samples were done by intimately mixed powders that facilities the diffusion and mutual dissolution and reaction of the specimens. Moreover the annealing temperatures were above the melting points of the pure constituents Bi and Sn (544.6 K and 505.1 K, respectively [4]). This circumstance allows the diffusion in liquid state that is much faster than the solid-state diffusion.

Table II.3.3. Nominal compositions of the specimens used for studies of the phase equilibria of the system Ni–Sn–Bi alloys at 733 K (nos. 1 – 18), 773 K (nos. 19 – 33), 903 K (nos. 34 – 45) and 1273 K (nos. 46 – 58) [39].

No	Nominal composition			No	Nominal composition		
	X_{Ni}	X_{Sn}	X_{Bi}		X_{Ni}	X_{Sn}	X_{Bi}
1	2	3	4	1	2	3	4
1	0.800	0.114	0.086	30	0.200	0.370	0.430
2	0.630	0.060	0.310	31	0.200	0.500	0.300
3	0.600	0.229	0.171	32	0.500	0.360	0.140
4	0.620	0.340	0.040	33 [A]	0.713	0.237	0.050
5	0.500	0.400	0.100	34	0.440	0.020	0.540
6	0.480	0.320	0.200	35	0.350	0.200	0.450
7	0.420	0.280	0.300	36	0.400	0.560	0.040
8	0.400	0.200	0.400	37	0.700	0.120	0.180
9	0.400	0.343	0.257	38	0.590	0.180	0.230
10	0.360	0.240	0.400	39	0.500	0.220	0.280
11	0.300	0.400	0.300	40	0.500	0.080	0.420
12	0.250	0.500	0.250	41	0.460	0.050	0.490

Table II.3.3. continuation

1	2	3	4	1	2	3	4
13	0.240	0.160	0.600	42	0.520	0.370	0.110
14	0.200	0.457	0.343	43	0.230	0.660	0.110
15	0.200	0.600	0.200	44	0.620	0.050	0.330
16	0.160	0.200	0.640	45	0.800	0.114	0.086
17	0.120	0.080	0.800	46	0.200	0.300	0.500
18	0.100	0.800	0.100	47 [A]	0.200	0.350	0.450
19	0.400	0.200	0.400	48 [A]	0.200	0.430	0.370
20	0.300	0.400	0.300	49 [A]	0.160	0.680	0.160
21	0.250	0.500	0.250	50 [A]	0.150	0.650	0.200
22	0.400	0.343	0.257	51	0.300	0.280	0.420
23[A]	0.600	0.229	0.171	52	0.400	0.200	0.400
24	0.480	0.320	0.200	53	0.400	0.343	0.257
25	0.240	0.160	0.600	54	0.600	0.229	0.171
26	0.120	0.080	0.800	55	0.800	0.114	0.086
27 [A]	0.675	0.225	0.100	56	0.713	0.238	0.050
28	0.200	0.250	0.550	57	0.675	0.225	0.100
29	0.200	0.320	0.480	58	0.250	0.500	0.250

[A] – specimens where separation of a pure bismuth phase was observed.

Thereafter the tubes were quenched in cold water. The mass loss of these regular specimens was about 1 % or less.

Some of samples were "defective**",** i.e. the bulk alloys have lost about 15 to 20 % of the initial weights of the respective mechanical mixtures. It is supposed to be mainly due to evaporation and subsequent condensation of bismuth in the top interior of the ampoules. This phenomenon is due to the relatively high bismuth vapor pressure [39] and temperature variation in the furnace. Unfortunately, we were unable to use a proper furnace for all samples.

Hence, the results obtained with these specimens (nos. 23, 27, 33, 47–50, see Table II.3.3) were considered qualitatively only and were not included in the isothermal sections constructed in this work.

The triangulations of the system (i.e. the selections of the initial compositions) and the choice of the working temperatures were done, taking into consideration the particularities of the binary Ni–Sn [4, 20, 40–43] and Ni–Bi [4, 34, 35] phase diagrams.

The equilibrated specimens were analyzed by Electron Probe Micro Analysis (EPMA), carried on by Cameca SX 100 apparatus and using pure Ni, Sn and Bi as standards.

Attempts to use X–rays analyses were not successful because the specimens turned out to be multiphase in most cases and the identifications of the diffraction peaks were rather ambiguous.

The phase equilibria liquid – solid phase (e.g. NiBi, Ni_3Sn_2, Ni_3Sn_4) appeared to be inclined towards the Bi-corner at all temperatures. The work temperatures were higher than the melting points of the elements Bi and Sn (544.6 K and 505.1 K, respectively). Hence, they have been mixing completely in liquid state. Thus, the phases (Bi) and (Sn) observed in samples nos. 14 and 15 (these samples have chemical compositions positioned in the vicinity of to the binary Bi–Sn eutectic, Table II.3.3) are results of the solidification during the fast cooling after the annealing. In both samples eutectic microstructures including Ni_3Sn_4 crystals were recorded (Fig. II.3.4 A, B).

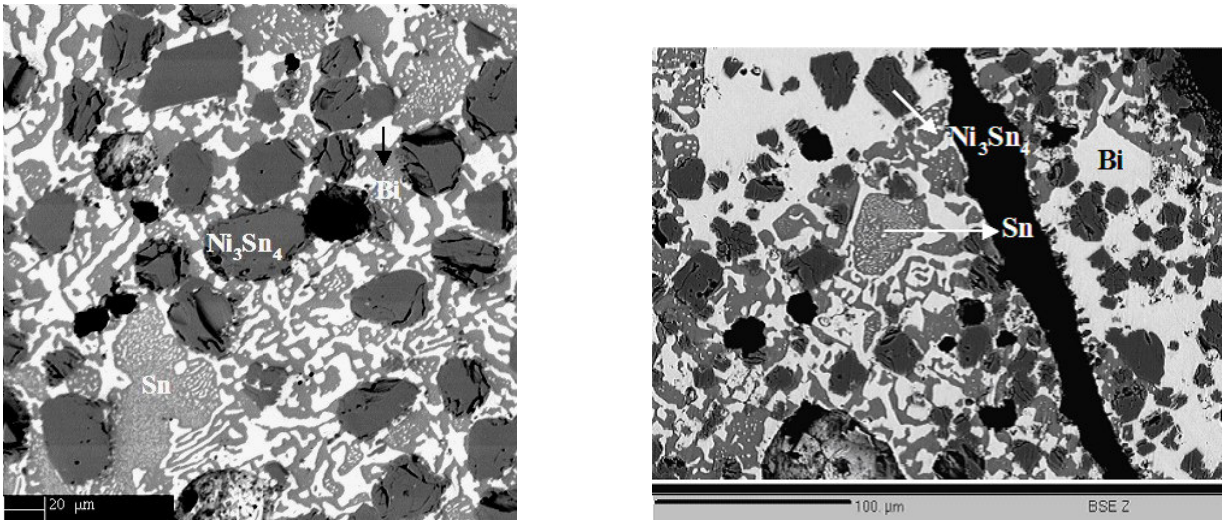

A B

Fig. II.3.4A B Scanning electron microscope micrographs of specimens nos. 14 and 15 [39]. White areas are of (Bi), grey – (Sn) and the dark grey crystals – Ni_3Sn_4.

Consequently it could be suggested that the following ternary eutectic reaction subsists in the Ni–Bi–Sn system:

$$L \rightarrow (Bi) + (Sn) + Ni_3Sn_4$$

Differential thermal analyses (DTA) of specimens nos. 14 and 15 were performed by DSC Setaram 111 and Perkin Elmer DSC 7, respectively. In order to avoid oxidation specimen

No. 14 was placed in an evacuated and sealed Pyrex tube while the DTA analyses of specimen No 15 were done in open alumina crucible under argon flow.

In Fig. II.3.5A the DTA curves obtained with sample No. 14 three runs of heating and cooling are presented. DTA curves registered with specimen No. 15 have similar shape too (Fig. II.3.5B). The peak E is associated with the eutectic reactions in the binary Bi–Sn and probably in the ternary Ni–Bi–Sn systems. In both cases (i.e. with No. 14 and with No. 15) a melting point of 412 K was deduced from the crossing point of the base–line and the extension of the peak E. The peak L (at around 470 K) is related with the crossing of the liquidus line at heating. The corresponding heat effect is at 450 K for sample No. 15.

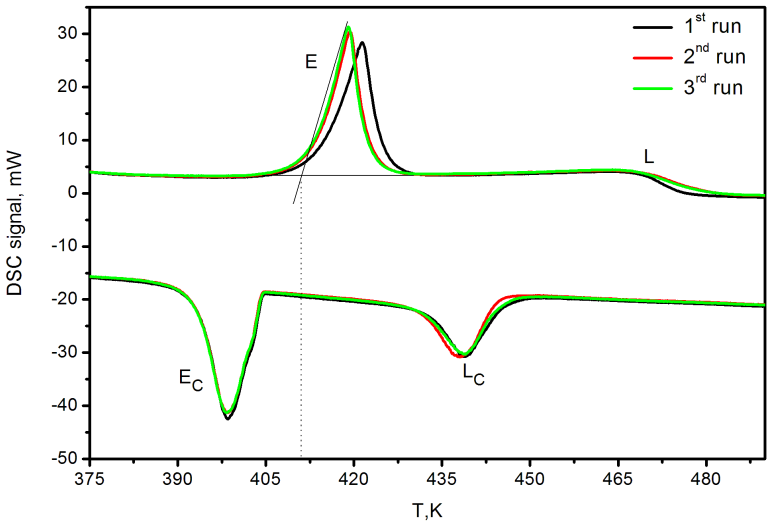

Fig. II.3.5A Differential thermal analyses of specimens No. 14 [39]. The peak E corresponds to the eutectic, and L corresponds to the liquidus. The black solid line represents one conventional baseline. The signal of differential scanning calorimeter (mW) is plotted along the ordinate and temperature T (K) – along the abscissa. The working interval for specimen No. 14 is from 300 to 623 K and the heating and cooling rates are of 3 $K.min^{-1}$. The dashed vertical line is situated at 411.6 K.

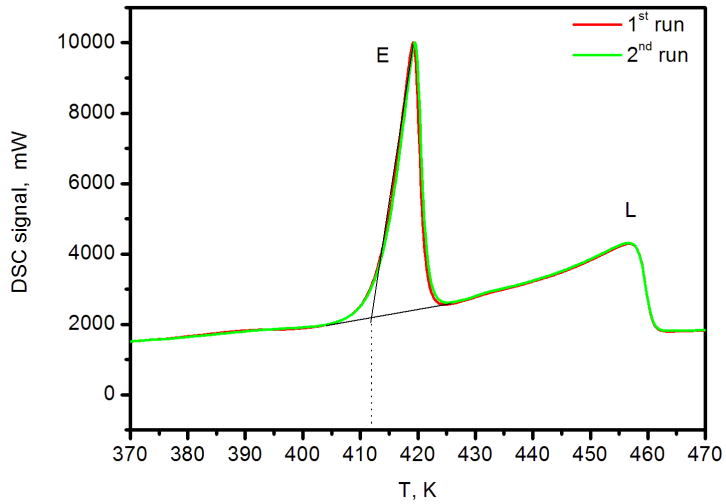

Fig. II.3.5B Differential thermal analyses of specimens No. 15 (unpublished). The peak E corresponds to the eutectic, and L corresponds to the liquidus. The black solid line represents one conventional baseline. The signal of differential scanning calorimeter (mW) is plotted along the ordinate and temperature T (K) – along the abscissa. The working interval for specimen No. 15 is from 330 to 480 K and the heating rate is of 20 K.min^{-1} . The dashed vertical line is situated at 412.1 K.

The thermal perturbations L_c and E_c (Fig. II.3.5) correspond, respectively, to the crossing of the liquidus line and the eutectic invariant at cooling. On the bases of these results it could be concluded that the melting point of the ternary eutectic does not differ notably from that one of the binary eutectic.

It has been found in various cases that the cooling curves are very helpful when overlapping heat effects had to be distinguished [44, 45]. Thus, the cooling curves in Fig. II.3.5 can be used for seeking supplementary evidence for the existence of the ternary eutectic. Indeed, the exothermic heat effect E_c is constituted apparently by two overlapping peeks. Its shape is quite reproducible in all the three runs. As one of the effects ought to be due to the crystallization of the binary eutectic, the second (at lower temperature) should be related with the solidification of the hypothetical ternary eutectic liquid phase.

The ternary extensions of the binary compounds known in the end-systems Ni–Bi (i.e. NiBi and $NiBi_3$) and Ni–Sn (i.e. Ni_3Sn, Ni_3Sn_2 and Ni_3Sn_4) were regularly observed in the annealed samples. Actually, the compounds Ni_3Sn_2 and Ni_3Sn have high- and low-temperature modifications denoted, respectively, as Ni_3Sn_2_HT and Ni_3Sn_HT, and Ni_3Sn_2_LT and Ni_3Sn_LT. These notations are used furthermore (Tables II.3.4 and II.3.6) taking into account the annealing and the transition temperatures as indicated in the literature [4, 20, 40–43].

The results of the EPMA analyses of specimens nos. 1–58 are exhibited in Table II.3.4. The annealing temperatures were 733, 773, 903 and 1273 K. One should be aware that the liquid phase (L) decomposes at cooling to bismuth– and tin–rich crystals, thus the location of the liquidus at the working temperatures could not be established accurately. Bismuth–nickel dendrites are occasionally observed as well. The relative amounts (%) of the phases, determined by an empirical quantitative method are shown in Table II.3.4 as well.

Table II.3.4. Results of the phase equilibria studies of the Ni–Bi–Sn system with specimens annealed at 733 K (nos. 1 – 18), 773 K (nos. 19 – 33), 903 K (nos. 34 – 45) and 1273 K (nos. 46 – 58) [39]. No – consecutive number of the specimen; Phases – phases, observed in the quenched specimen; Am. – relative amounts (%) of the phases, determined by quantitative metallography; Composition – chemical composition of the pertinent phase (X_{ij} – mole fractions of Ni, Sn and Bi) obtained by EPMA.

No	Phases	Am. %	Composition		
			X_{Ni}	X_{Sn}	X_{Bi}
1	2	3	4	5	6
1	(Ni) Ni_6Sn_2Bi NiBi	20 50 30	0.999 0.68±0.02 0.527	0.001 0.19±0.01 0.020	0.000 0.12±0.02 0.453
2	NiBi Ni_3Sn_LT	50 50	0.507 0.738	0.003 0.258	0.490 0.004
3	NiBi $NiBi_3$ Ni_3Sn_2_LT	45 40 15	0.483 0.289 0.611	0.061 0.004 0.379	0.456 0.707 0.010

Table II.3.4 continuation

1	2	3	4	5	6
4	Ni_6Sn_2Bi	40	0.66±0.02	0.22±0.01	0.12±0.02
	Ni_3Sn_2_LT	50	0.604	0.388	0.008
	NiBi	10	0.411	0.085	0.504
5	Ni_3Sn_2 _LT	90	0.564	0.436	0.000
	L^A	10	0.007	0.009	0.984
6	Ni_3Sn_2_LT	40			
	$NiBi_3$	60	0.602	0.393	0.005
	L^A		0.006	0.988	0.006
	L^A		0.031	0.002	0.967
7	Ni_3Sn_2_LT	30	0.565	0.433	0.002
	L^A	70	0.020	0.000	0.980
8	Ni_3Sn_2_LT	10	0.612	0.387	0.000
	$NiBi_3$	15	0.248	0.000	0.752
	L^A	75	0.018	0.000	0.982
9	Ni_3Sn_2	30	0.557	0.443	0.000
	L^A	70	0.015	0.008	0.977
10	Ni_3Sn_2_LT	25	0.577	0.422	0.001
	dendrite	75	0.136	0.034	0.830
11	Ni_3Sn_4	50	0.460	0.532	0.008
	L^A	50	0.002	0.973	0.025
	L^A		0.000	0.022	0.978
12	Ni_3Sn_4	40	0.428	0.568	0.004
	L^A	60	0.011	0.02	0.969
	L^A		0.006	0.971	0.023
13	Ni_3Sn_2_LT	30	0.563	0.422	0.015
	$NiBi_3$	20	0.244	0.000	0.756
	L^A	60	0.003	0.000	0.997
14	Ni_3Sn_4	30	0.447	0.553	0.000
	L^A	70	0.005	0.02	0.975
	L^A		0.002	0.976	0.232
15	Ni_3Sn_4	30	0.433	0.567	0.000
	L^A	70	0.005	0.025	0.970
	L^A		0.000	0.982	0.018
16	Ni_3Sn_2_LT	30	0.562	0.438	0.000
	L^A	70	0.002	0.973	0.025
	L^A		0.000	0.012	0.988
17	Ni_3Sn_2_LT	10	0.581	0.405	0.014
	$NiBi_3$	5	0.252	0.002	0.746
	L^A	85	0.003	0.000	0.997
18	Ni_3Sn_4	20	0.420	0.578	0.002
	L^A	80	0.001	0.981	0.018
	L^A		0.000	0.033	0.967

Table II.3.4 continuation

1	2	3	4	5	6
19	Ni_3Sn_2_HT	15	0.605	0.387	0.008
	L [A]	85	0.017	0.983	0.000
	L [A]		0.000	0.978	0.022
20	Ni_3Sn_4	50	0.479	0.519	0.002
	L [A]	50	0.008	0.021	0.971
	L [A]		0.007	0.965	0.028
21	Ni_3Sn_4	50	0.453	0.547	0.000
	L [A]	50	0.003	0.981	0.016
	L [A]		0.000	0.015	0.985
22	Ni_3Sn_2_HT	70	0.567	0.433	0.000
	L [A]	30	0.000	0.011	0.989
23 [B]	Ni_3Sn_LT	30	0.755	0.245	0.000
	dendrite	70	0.191	0.000	0.809
24	Ni_3Sn_2_HT	60	0.600	0.392	0.008
	L [A]	40	0.000	0.000	1.000
	L [A]		0.000	0.98	0.02
25	Ni_3Sn_2_HT	20	0.598	0.399	0.003
	L [A]	80	0.000	0.002	0.998
	L [A]		0.000	0.996	0.004
26	Ni_3Sn_2_HT	10	0.604	0.390	0.006
	L [A]	90	0.000	0.000	1.000
	L [A]		0.000	0.989	0.011
27 [B]	Ni_3Sn	45	0.749	0.249	0.002
	Ni_3Sn_2_HT	35	0.612	0.374	0.014
	NiBi	20	0.460	0.000	0.540
28	Ni_3Sn_2_HT	25	0.560	0.440	0.000
	L [A]	80	0.000	0.974	0.026
	L [A]		0.000	0.016	0.984
29	Ni_3Sn_4	35	0.447	0.553	0.000
	L [A]	65	0.000	0.968	0.032
	L [A]		0.000	0.017	0.983
30	Ni_3Sn_4	40	0.474	0.526	0.000
	L [A]	60	0.000	0.973	0.027
	L [A]		0.000	0.015	0.985
31	Ni_3Sn_2_HT	20	0.612	0.385	0.003
	L [A]	80	0.000	0.000	1.000
	L [A]		0.000	1.000	0.000
32	Ni_3Sn_2_HT	50	0.575	0.424	0.003
	L [A]	50	0.000	0.009	0.991
33 [B]	Ni_3Sn_LT	85	0.753	0.247	0.000
	Ni_3Sn_2_HT	5	0.562	0.438	0.000
	NiBi	10	0.497	0.025	0.478

Table II.3.4 continuation

1	2	3	4	5	6
34	NiBi	5	0.740	0.260	0.000
	L [A]	60	0.497	0.016	0.487
	L [A]	35	0.250	0.000	0.750
35	Ni_3Sn_2_HT	30	0.607	0.383	0.010
	L [A]	60	0.000	0.000	1.000
	L [A]		0.000	1.000	0.000
36	Ni_3Sn_4	80	0.450	0.550	0.000
	L [A]	20	0.060	0.099	0.841
	L [A]		0.004	0.968	0.028
37	(Ni)	30	0.980	0.020	0.000
	Ni_3Sn_LT	20	0.731	0.252	0.017
	NiBi	50	0.541	0.000	0.449
38	Ni_3Sn_LT	10	0.748	0.252	0.000
	Ni_6Sn_2Bi	45	0.62±0.02	0.22±0.01	0.16±0.02
	NiBi	45	0.501	0.000	0.499
39	Ni_3Sn_2_HT	15	0.584	0.366	0.050
	L [A]	85	0.000	0.995	0.005
	L [A]		0.000	0.002	0.998
40	Ni_3Sn_2_HT	5	0.610	0.390	0.000
	NiBi	40	0.480	0.011	0.509
	L [A]	55	0.000	0.026	0.974
41	Ni_3Sn_2_HT	80	0.733	0.264	0.003
	NiBi	20	0.501	0.016	0.483
42	Ni_3Sn_2_HT	80	0.571	0.426	0.002
	L [A]	20	0.030	0.005	0.965
43	Ni_3Sn_4	80	0.444	0.556	0.000
	L [A]	20	0.003	0.970	0.027
	L [A]		0.003	0.02	0.977
44	(Ni)	10	0.984	0.016	0.000
	NiBi	90	0.506	0.008	0.486
45	(Ni)	10	0.992	0.008	0.000
	Ni_6Sn_2Bi	40	0.69±0.02	0.20±0.01	0.12±0.02
	NiBi	60	0.527	0.02	0.453
46	Ni_3Sn_2_HT	10	0.560	0.440	0.000
	L [A]	90	0.000	0.970	0.023
	L [A]		0.000	0.020	0.980
47 [*]	(Ni)	25	0.599	0.401	0.000
	Ni_3Sn_HT	75	0.000	0.961	0.039
			0.000	0.029	0.971
48 [B]	Ni_3Sn_2_HT	55	0.580	0.420	0.000
	L [A]	45	0.000	0.970	0.030
	L [A]		0.000	0.030	0.970

Table II.3.4 continuation

1	2	3	4	5	6
49 [B]	Ni_3Sn_2_HT	40	0.562	0.438	0.000
	L [A]	60	0.005	0.022	0.973
	L [A]		0.002	0.971	0.026
50 [B]	Ni_3Sn_2_HT	80	0.590	0.410	0.000
	L [A]	20	0.000	0.030	0.970
	L [A]		0.000	0.960	0.040
51	Ni_3Sn_HT	20	0.580	0.420	0.000
	L [A]	80	0.000	0.970	0.030
	L [A]		0.000	0.030	0.970
52	Ni_3Sn_2_HT	50	0.626	0.364	0.010
	L [A]	50	0.000	0.000	1.000
53	Ni_3Sn_2_HT	65	0.590	0.410	0.000
	L [A]	35	0.000	0.970	0.030
	L [A]		0.000	0.010	0.990
54	Ni_3Sn_HT	75	0.750	0.250	0.000
	L [A]	35	0.010	0.000	0.990
55	(Ni)	60	0.900	0.100	0.000
	Ni_3Sn_HT	20	0.760	0.240	0.000
	L [A]	20	0.000	0.0000	1.000
56	Ni_3Sn_HT	85	0.743	0.257	0.000
	L [A]	15	0.000	0.002	0.998
57	Ni_3Sn_HT	80	0.730	0.270	0.000
	L [A]	20	0.000	0.990	0.010
58	Ni_3Sn_2_HT	20	0.569	0.431	0.000
	L [A]	80	0.000	0.031	0.969

[A] – The liquid phase (L) decomposes at cooling to bismuth- and tin-rich crystals, thus its composition at the working temperatures could not be established accurately.

[B] – specimens where separation of a pure bismuth phase was observed during the synthesis.

An important finding of the phase equilibria studies is the detection of a formerly unknown Ni–Sn–Bi compound in numerous samples annealed at 733 and 903 K [39]. The formula of this phase is approximately Ni_6Sn_2Bi (for details see Table II.3.7). Pertinent scanning electron microscope micrographs of samples nos. 1, 4 and 38 annealed at 733 K and at 903 K are shown in Fig. II.3.6A,B and II.3.7, respectively.

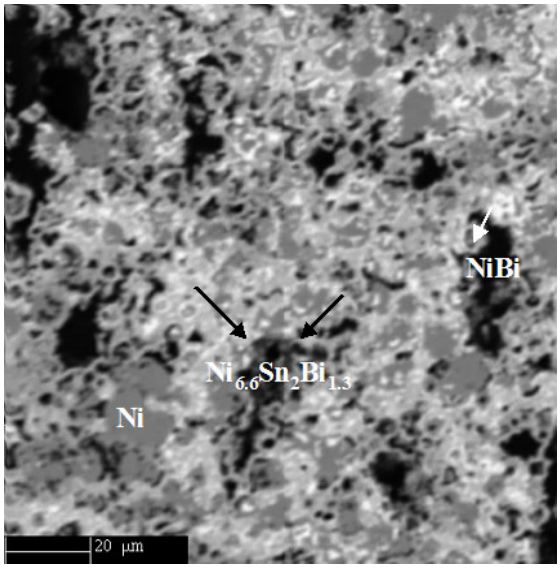

A

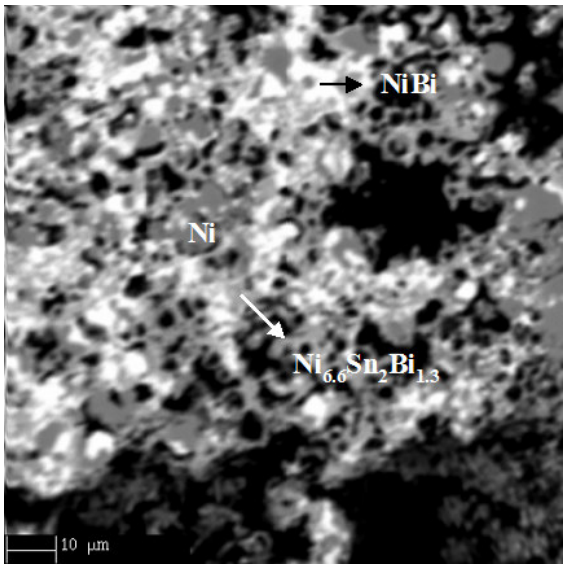

B

Fig. II.3.6A and B. Micrographs of specimens nos. 1 and 45, respectively (unpublished). The dark gray phase is of pure Ni, the white phase represents NiBi and the light-gray phase has the composition $Ni_{6.6}Sn_2Bi_{1.3}$. The black areas are voids.

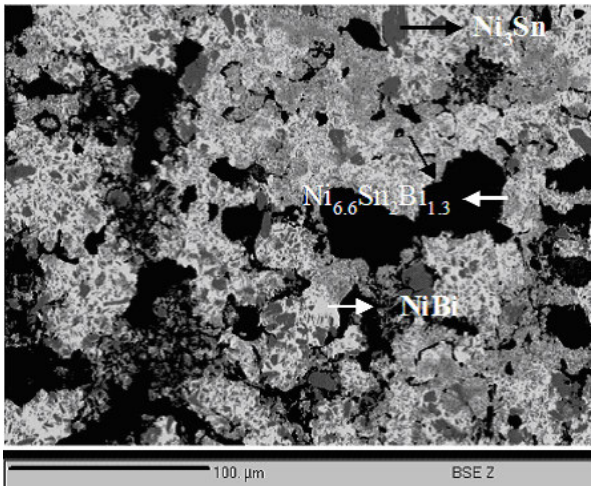

Fig. II.3.7. Micrographs of specimen No 38 (unpublished). The dark phase is of Ni_3Sn; small light phase represents NiBi and the light gray phase – Ni_6Sn_2Bi.

After obtaining the above mentioned indications about the existence of a formerly unknown Ni–Sn–Bi phase we performed a special series of experiments to check up this finding. Specimen S1 and S2 with nominal composition 68% Ni, 20% Sn and 12% Bi have been prepared and put in an alumina crucible placed into iron container. This arrangement was designed for

avoiding the kind of side reactions, which occurred in sealed silica tubes. This container was heated at 873 K in a furnace for two weeks, under flowing argon atmosphere and quenched in cold water. According to the EPMA analysis of specimen S1 three phases were obtained: (Ni)+NiBi+Ni_6Sn_2Bi. The specimen S2, already annealed at 873 K for two weeks, was processed for 3 months to verify the phase equilibria and analysed. Only two phases were obtained – NiBi and $Ni_6Sn_2Bi_1$. No remarkable change in the composition of the ternary phase has been observed, which means that the compound is probably stoichiometric**.**

In addition, mechanical alloying method was applied to synthesize the ternary phase. For that purpose ribbons of Ni, Sn and Bi powder were produced (325 mesh) using manual mill (68% Ni, 19% Sn and 13% Bi). This way of preparation should provide more homogeneous samples. The specimen (S3) was annealed at 903 K in evacuated and sealed quartz tubes for 3 months. Three phases have been obtained: NiBi, Ni_3Sn and Ni_6Sn_2Bi.

The statistical interpretation of all 13 EPMA point analyses of this phase lead to the following results about its chemical composition (in mole fractions of the corresponding element): X_{Ni} = 0.66±0.03, X_{Sn} = 0.21±0.02, X_{Bi} = 0.13±0.02. It could be suggested that the ternary compound is either stoichiometric, either it has a tiny homogeneity range.

The ternary phase was not observed in the samples annealed at 733 K neither in those annealed at 1273 K. In the latter case the reason might be that this compound has a melting point lower than 1273 K, while its absence at 733 K is merely due to the circumstance that the ampoules containing the samples with chemical compositions pertinent for the formation of the ternary phase (nos. 23, 27, 33, Table II.3.4) happened to be defective as discussed above.

In Fig. II.3.8 is represented X–ray diffractogram (Cu K_α) of the powdered sample S3 (curve 1) compared to simulated pattern of NiBi (curve 2). For the simulation the space group and number (*$P6_3mmc$*, No 194, Pearson symbol hP4), suggested by Hägg and Funke [46] and by Zhuravlev et al. [47] using the software package PowderCell2. The diffractograms was checked up for the presence of other phases (the most probable were Ni_3Sn_LT and (Ni)) [48]. A system of diffraction peaks belonging to NiBi and another system of 7 peaks that probably can be associated with the formerly unknown ternary phase Ni_6Sn_2Bi were found only.

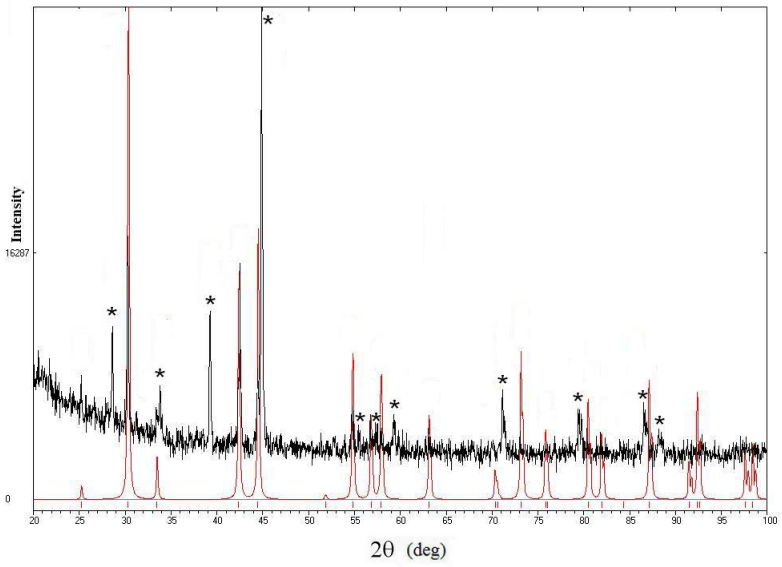

Fig. II.3.8. X–ray diffractograms (Cu K_α) of the powdered sample S3 (curve 1) compared to simulated pattern of NiBi (curve 2) [39]. The intensity of the diffraction peaks (counts per second) is plotted along the ordinate, and the diffraction angles (2θ, deg) are plotted along the abscissa. The peaks probably belonging to the ternary compound Ni_6Sn_2Bi are marked by asterisk.

In Table II.3.5 are shown details of the X–ray studies. Although we found seven probable diffraction peaks of the phase Ni_6Sn_2Bi a detailed study of its crystal structure would be out of the scope of this work.

Table II.3.5 Diffraction peaks (298 K, Cu $K\alpha_1$) of the specimen S3 (chemical composition 68 at.% Ni, 19 at.% Sn and 13 at.% Bi) [39]. No – number of the diffraction peak; 2Θ – diffraction angles, deg, d – interlattice distances, nm; Intensity – relative intensity (%) of the diffraction peaks.

No	Intensity %	d nm	2Θ deg	Phase
1	25	0.3525	25.2	NiBi
2	35	0.3118	28.6	Ni_6Sn_2Bi
3	53	0.2943	30.3	NiBi
4	19	0.2675	33.5	NiBi

5	23	0.2650	33.8	Ni_6Sn_2Bi
6	38	0.2292	39.4	Ni_6Sn_2Bi
7	48	0.2131	42.5	NiBi
8	27	0.2035	44.5	NiBi
9	100	0.2018	44.9	Ni_6Sn_2Bi
10	19	0.1674	54.8	NiBi
11	16	0.1657	55.4	Ni_6Sn_2Bi
12	18	0.1620	56.7	NiBi
13	17	0.1607	57.3	Ni_6Sn_2Bi
14	15	0.1591	57.9	NiBi
15	18	0.1559	59.2	Ni_6Sn_2Bi
16	15	0.1472	63.1	NiBi
17	12	0.1337	70.3	NiBi
18	22	0.1325	71.1	Ni_6Sn_2Bi
19	14	0.1294	73.0	NiBi
20	11	0.1254	75.8	NiBi
21	18	0.1206	79.4	Ni_6Sn_2Bi
22	14	0.1193	80.5	NiBi
23	14	0.1175	81.9	NiBi
24	20	0.1124	86.5	Ni_6Sn_2Bi
25	16	0.1120	86.9	NiBi
26	15	0.1063	92.9	NiBi

In Figs. II.3.9–11 are represented isothermal sections of the Ni–Sn–Bi at 733, 903 and 1273 K, respectively. The phase boundaries are drawn taking into account the chemical compositions obtained by EPMA as shown in Table II.3.4. The positions of the original samples are plotted and various symbols are used to represent the number of the phases identified at the respective temperatures.

Fig. II.3.9 represents the isothermal section constructed at 733 K. The two-phase region Ni_3Sn_4 + L contains the specimens nos. 12, 14, 15, 18. Specimens nos. 5, 9 and 16 belong to Ni_3Sn_2 + L. The three-phase region Ni_3Sn_2 + $NiBi_3$ + L was well defined by nos. 7, 10, 13, 17 and both 6 and 8 alloys. Metastable phase equilibria are observed in the specimens nos. 2 – 4 (Table II.3.3). For example the ternary phase was not observed in samples No. 2 and 3 while NiBi should not exist in specimen No. 4.

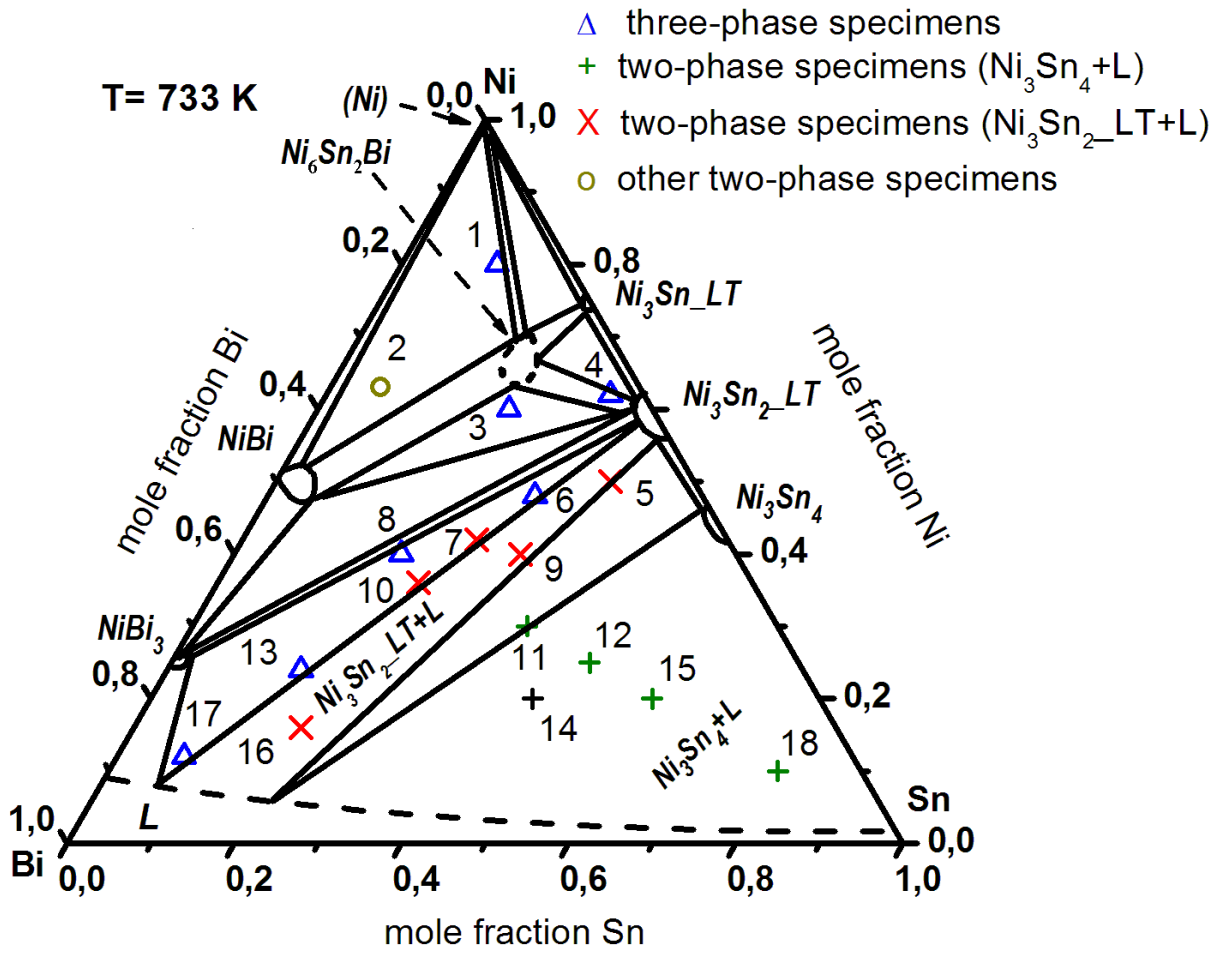

Fig. II.3.9 Isothermal section of the Ni–Bi–Sn diagram at 733 K constructed using the data obtained in this work [39]. The original chemical compositions of the samples are plotted. The hypothetical homogeneity region of the ternary compound with approximate formula Ni_6Sn_2Bi is shown with dashes.

Similar problems are observed in the section constructed at 903 K (Fig. II.3.10) with samples nos. 37 (no ternary phase) and 38 (the phase Ni_3Sn_LT should not appear). No 44

belongs to two-phase field (Ni) + NiBi, although its nominal composition presumes (Ni) + NiBi + Ni_6Sn_2Bi.

In all these cases solid-state equilibria only are involved and these exceptions might be explained with diffusion or nucleation problems.

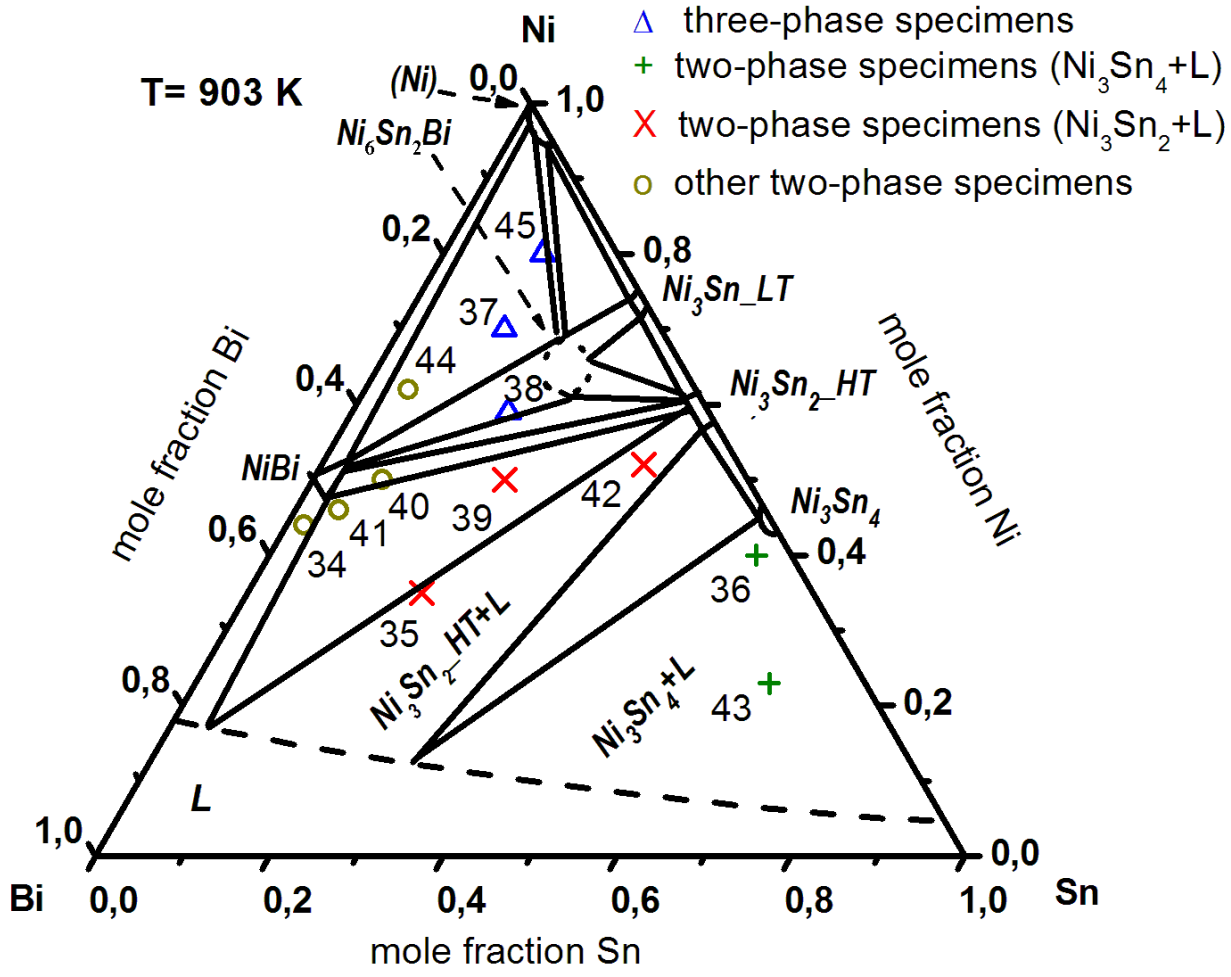

Fig. II.3.10. Isothermal section of the Ni–Bi–Sn diagram at 903 K constructed using the data obtained in this work [39]. The original chemical compositions of the samples are plotted. The hypothetical homogeneity region of the ternary compound with approximate formula Ni_6Sn_2Bi is shown with dashes.

The two-phase region Ni_3Sn_4 + L was determined by specimens nos. 36 and 43. Specimens nos. 35 and 49 are in Ni_3Sn_2 + L two-phase field. No 39 belong to that field to, although its nominal composition presumes three-phase region Ni_3Sn_2 + NiBi + L. No 41 is in three-phase region Ni_3Sn_2 + NiBi + L, No 34 in NiBi + L and No 40 in NiBi + Ni_3Sn_2.

Regarding the appearance of the phase Ni_3Sn_2_HT in samples Nos. 46 and 58 (isothermal section at 1273 K, Fig. Fig. II.3.11) it could be accepted that it was formed during the cooling of the alloys rather then to suppose a much narrower liquid phase region. The two-phase region Ni_3Sn_2 + L is determined by specimens nos. 52 and 53. Three-phase region Ni_3Sn + L is defined by nos. 54, 56 and 57. Sample No 55 belongs to three-phase field (Ni) + Ni_3Sn + L. Specimens nos. 46, 47, 48, 49, 50, 51 and 58 are in liquid phase.

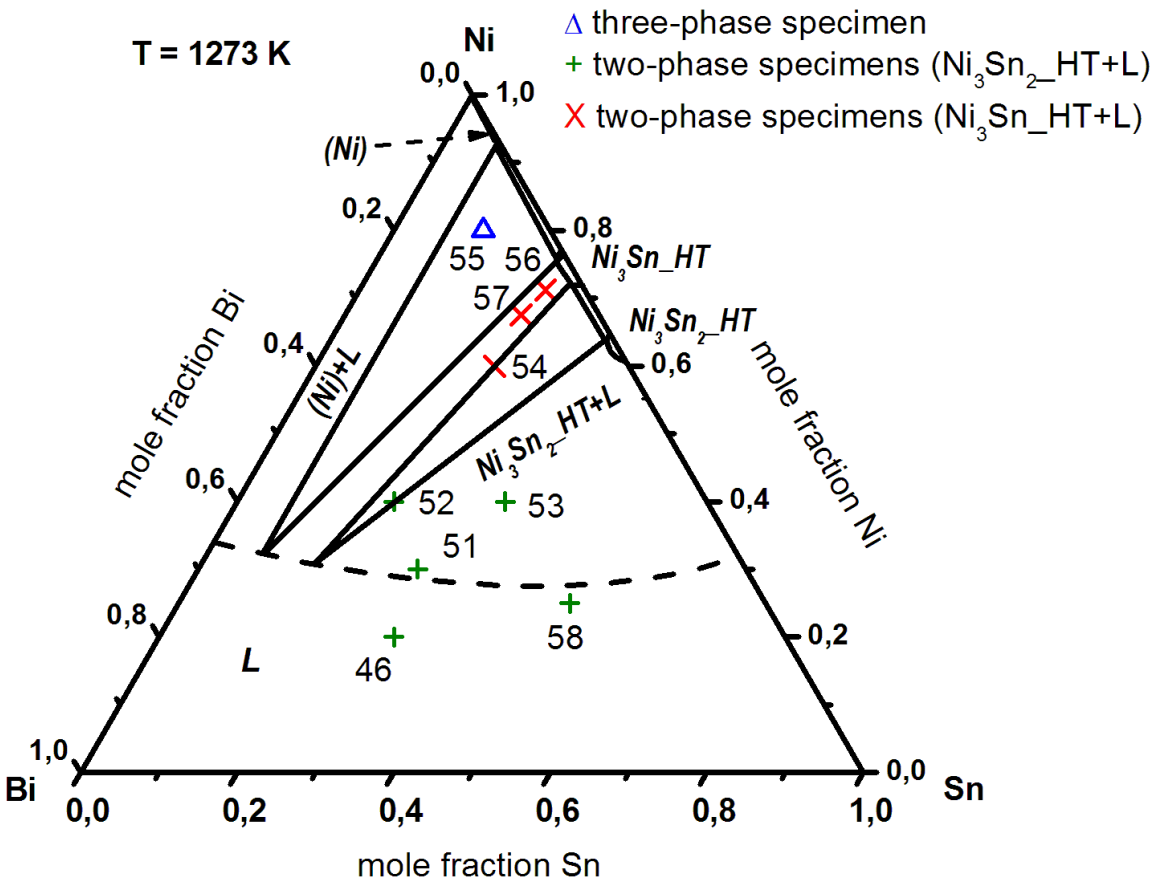

Fig. II.3.11. Isothermal section of the Ni–Bi–Sn diagram at 1273 K constructed using the data obtained in this work [39]. The original chemical compositions of the samples are plotted.

The mutual solubility of Bi and Sn in their binary phases with Ni is also of interest. As one can see, the solubility of the bismuth and tin in the Ni–Sn and the Ni–Bi compounds is small (usually no more than 2–3 at.%). The liquidus could not be constructed in neither of isothermal sections (Fig. II.3.9–11) because of the spontaneous separation of bismuth and tin at solidification

➢ Calorimetric studies of solid and liquid phases of Ni–Sn–Bi system

Calorimetric studies of solid phases have been performed by direct reaction calorimetry at 733 K: nos. 59–72 and at 1273 K: nos. 73 and 74 (Table II.3.6), using Setaram–Calvet 800 C and Gachon calorimeters, respectively [39]. The masses of the specimens vary in the interval 0.14–0.30 g. The enthalpy values are average from five separate trials. The total annealing time (in the calorimeter) was around 1 week for nos. 59–72. In the case with samples nos. 73 and 74 it was not convenient to withdraw the specimens in air while hot. Thus they were left within the calorimeter crucible until reaching the room temperature and thereafter directly analysed.

These specimens were investigated by EPMA in order to check up their chemical compositions and to identify the phases.

Specimens nos. 59–72 have identical chemical compositions with most of these used for phase equilibria studies only (i.e. with nos. 6, 7, 10, 13, 17, 8, 11, 12, 15, 18, 14, 9, 3 and 1, respectively, Table II.3.3). This was done in order to compare directly, phase diagram data obtained with specimens suffered different heat treatments.

Table II.3.6. Nominal compositions of the specimens used for calorimetric and phase equilibria studies of the system Ni–Sn–Bi: at 733 K (nos. 59 – 72), and at 1273 K (nos. 73 and 74) [39]. No – consecutive number of the specimen; Nominal composition – chemical composition of the pertinent samples (X_{ij} – mole fractions of Ni, Sn and Bi); $\Delta_f H$ – enthalpy effects obtained by direct calorimetry, ($J \cdot g^{-1}$) and the corresponding standard deviations of the results. Reference state: fcc–Ni, liquid Bi and liquid Sn at the respective temperature.

No	Nominal composition			$\Delta_f H$
	X_{Ni}	X_{Sn}	X_{Bi}	$J \cdot g^{-1}$
1	2	3	4	5
59	0.480	0.320	0.200	–320±20
60	0.420	0.280	0.300	–227±5
61	0.360	0.240	0.400	–163±4
62	0.240	0.160	0.600	–102±5

Table II.3.6 continuation

1	2	3	4	5
63	0.120	0.080	0.800	–62±4
64	0.400	0.200	0.400	–170±5
65	0.300	0.400	0.300	–195±7
66	0.250	0.500	0.250	–300±5
67	0.200	0.600	0.200	–102±7
68	0.100	0.800	0.100	–63±3
69	0.200	0.457	0.343	–120±2
70	0.400	0.343	0.257	–384±4
71	0.600	0.229	0.171	–382±8
72	0.800	0.114	0.086	–254±4
73	0.712	0.238	0.050	–272±18
74	0.675	0.225	0.100	–222±17

The final compositions of the phases were verified by EPMA (Table II.3.7).

Table II.3.7. Results of the EPMA analyses of specimens obtained by direct reaction calorimetry experiments (at 733 K: nos. 59 – 72 and at 1273 K: nos. 73 and 74) [39]. No – consecutive number of the specimen; Phases – phases, observed in the corresponding specimen; Amount – relative amounts (%) of the phases, determined by quantitative metallography; Composition – chemical composition of the pertinent phase (X_{ij} – mole fractions of Ni, Sn and Bi) obtained by EPMA.

No	Phases	Amount %	Composition		
			X_{Ni}	X_{Sn}	X_{Bi}
1	2	3	4	5	6
59	Ni_3Sn_2_LT	40	0.602	0.393	0.005
	L^A	60	0.006	0.988	0.006
	L^A		0.031	0.002	0.967
60	Ni_3Sn_2_LT	30	0.565	0.433	0.002
	L^A	70	0.020	0.000	0.980
61	Ni_3Sn_2_LT	20	0.577	0.422	0.001
	L^A	80	0.136	0.034	0.830

Table II.3.7 continuation

1	2	3	4	5	6
62	$NiBi_3$	30	0.244	0.000	0.756
	Ni_3Sn_2_LT	10	0.563	0.422	0.015
	L [A]	60	0.003	0.000	0.997
63	$NiBi_3$	10	0.252	0.002	0.746
	Ni_3Sn_2_LT	5	0.581	0.405	0.014
	L [A]	85	0.003	0.000	0.997
64	$NiBi_3$	10	0.248	0.000	0.752
	Ni_3Sn_2_LT	10	0.612	0.387	0.000
	L [A]	80	0.018	0.000	0.982
65	Ni_3Sn_4	50	0.460	0.532	0.008
	L [A]	50	0.000	0.022	0.978
	L [A]		0.002	0.973	0.025
66	Ni_3Sn_4	40	0.428	0.568	0.004
	L [A]	60	0.006	0.971	0.023
	L [A]		0.011	0.02	0.969
67	Ni_3Sn_4	30	0.433	0.567	0.000
	L [A]	70	0.000	0.982	0.018
	L [A]		0.005	0.025	0.970
68	Ni_3Sn_4	20	0.420	0.578	0.002
	L [A]	80	0.001	0.982	0.018
	L [A]		0.000	0.033	0.967
69	Ni_3Sn_4	30	0.447	0.553	0.000
	L [A]	70	0.000	0.976	0.024
	L [A]		0.005	0.020	0.975
70	Ni_3Sn_2_LT	30	0.557	0.443	0.000
	L [A]	70	0.015	0.008	0.977
71	$NiBi_3$	50	0.289	0.004	0.707
	NiBi	40	0.483	0.061	0.456
	Ni_3Sn_2_LT	10	0.611	0.379	0.010
72	(Ni)	20	0.999	0.001	0.000
	Ni_6Sn_2Bi	50	0.70±0.02	0.20±0.01	0.10±0.02
	NiBi	30	0.527	0.020	0.453
73	Ni_3Sn_HT	85	0.751	0.249	0.000
	L [A]	15	0.000	0.012	0.988
74	Ni_3Sn_HT	70	0.746	0.000	0.254
	L [A]	20	0.000	0.992	0.008

[A] – The liquid phase (L) decomposes at cooling to bismuth- and tin-rich crystals, thus its composition at the working temperatures could not be established accurately.

The results obtained with specimens used for calorimetric experiments (Nos. 59 – 74) and from the other side, with samples synthesized explicitly for phase equilibria studies coincide very well.

Calorimetric studies of liquid phases have been performed by direct reaction calorimetry at 833 K: nos. 75, 78 and 81; at 873 K: nos. 76, 79 and 82; at 933 K: nos. 77, 80 and 83 (Table II.3.8), using Setaram–Calvet 800 C. In order to check the temperature dependence of liquid phase enthalpies of formation, three different nominal compositions have been chosen. The masses of the specimens vary in the interval 0.12–0.29 g. The enthalpy values are average from five separate trials. The duration of one measurement was about 1.5–2.5 h. The specimen were withdrawn and slowly cooled in air.

Table II.3.8 Nominal compositions of the specimens used for calorimetric and phase equilibria studies of the system Ni–Sn–Bi (unpublished). No – consecutive number of the specimen; Nominal composition – chemical composition of the pertinent samples (X_{ij} – mole fractions of Ni, Sn and Bi); $\Delta_f H$ – enthalpy effects obtained by direct calorimetry, ($J \cdot g^{-1}$) and the corresponding standard deviations of the results. Reference state: fcc–Ni, liquid Bi and liquid Sn at the respective temperature.

№	Nominal composition			T K	$\Delta_f H^{L,T}$ $J \cdot g^{-1}$
	X_{Ni}	X_{Sn}	X_{Bi}		
75	0.05	0.70	0.25	833	−33±3
76				873	–34±4
77				933	−41±7
78	0.07	0.51	0.42	833	−41±1
79				873	−36±4
80				933	−37±5
81	0.1	0.27	0.63	833	−50±1
82				873	−55±5
83				933	−64±6

These specimens were investigated by EPMA in order to check up their chemical compositions and to identify the phases (Table II.3.9).

Table II.3.9 Results of the of the Ni–Bi–Sn system studies with specimens, obtained by direct reaction calorimetry experiments of liquid ternary solutions (nos 75, 78 and 81 at 833 K; nos. 76, 79 and 82 at 873 K; nos. 77, 80 and 83 at 933 K) (unpublished). No – consecutive number of the specimen; Phases – phases, observed in the corresponding specimen; Composition^{A} – chemical composition (X_{ij} – mole fractions of Ni, Sn and Bi) obtained by EPMA

No	Phases	Composition		
		X_{Ni}	X_{Sn}	X_{Bi}
1	2	3	4	5
75	Ni_3Sn_4	0.458	0.542	0.000
	L^B	0.000	0.021	0.979
	L^B	0.000	0.983	0.017
76	Ni_3Sn_4	0.435	0.565	0.000
	L^B	0.000	0.966	0.034
	L^B	0.000	0.007	0.993
77	Ni_3Sn_4	0.449	0.551	0.000
	L^B	0.000	0.976	0.024
	L^B	0.000	0.021	0.979
78	Ni_3Sn_4	0.466	0.536	0.000
	L^B	0.000	0.976	0.024
	L^B	0.000	0.025	0.975
79	Ni_3Sn_4	0.441	0.559	0.000
	L^B	0.000	0.973	0.027
	L^B	0.000	0.028	0.972
80	Ni_3Sn_4	0.449	0.549	0.002
	L^B	0.000	0.975	0.025
	L^B	0.000	0.008	0.992
81	Ni_3Sn_2	0.570	0.430	0.000
	L^B	0.000	0.973	0.027
	L^B	0.000	0.020	0.980

Table II.3.9 continuation

1	2	3	4	5
82	Ni_3Sn_2	0.561	0.439	0.000
	L^B	0.000	0.976	0.024
	L^B	0.004	0.093	0.903
83	Ni_3Sn_2	0.576	0.424	0.000
	L^B	0.000	0.987	0.013
	L^B	0.000	0.003	0.997

[A] – The lots of samples 75 – 77, 78 – 81 and 81 – 83 have identical chemical compositions as shown in Table II.3.8.

[B] – The liquid phase (L) decomposes at cooling to bismuth- and tin-rich crystals, thus its composition at the working temperatures could not be established accurately.

Taking into account, that standard deviation slightly increases with temperature, no temperature dependence was observed in this range.

➢ Conclusion

- The phase equilibria in the system Ni–Sn–Bi have been studied at 733, 773, 903 and 1273 K.
- The tie lines between two- and three-phase fields have been determined.
- Calorimetric studies of solid and liquid phases have been done at 733 K and 1273 K (solid phases); at 833 K, 873 K: and 933 K (liquid phases).
- The data show the existence of a ternary compound with approximate formula Ni_6Sn_2Bi. The chemical composition of the latter phase is $X_{Ni} = 0.66\pm0.03$, $X_{Sn} = 0.21\pm0.02$, $X_{Bi} = 0.13\pm0.02$ and it is either stoichiometric, either has a small homogeneity range. The melting temperature of the ternary phase is probably below 1273 K.
- A ternary eutectic reaction exists with the participation of the phases (Bi), (Sn) and Ni_3Sn_4. The solidification point of the ternary eutectic does not differ significantly (around 1 or 2 deg, probably) from that one of binary Bi–Sn eutectic. It was found that not only $NiBi_3$ or Ni_3Sn_4 could grow from Bi–Sn melts but Ni_3Sn_2 as well.

➢ Bibliography

[1] Lead-Free Solder Project Final Report, NCMS Report No. 0401 RE96 (Ann Arbor, MI:National Center for Manufacturing Sciences, 1997)

[2] Chen, C, C E Ho, A H Lin, Long-term aging study on the solid-state reaction between 58Bi42Sn solder and Ni substrate, Journal of electronic materials, Oct. 2000

[3] Hansen M. , K. Anderko, "Constitution of Binary Alloys", 2 edn., (1958) McGrow-Hill, NY.

[4] Massalski T., "CD ROM: Binary Alloy Phase Diagrams", (1996) ASM Intern., Ohio, USA.

[5] Magnus A., M. Mannheimer, Z. Physik. Chem 121, 267 (1926).

[6] Kawakami M., Z. Anorg. Allg. Chem. 167, 345 (1927).

[7] Samson-Himmelstjerna H., Z. Metallkde. 28, 197 (1936).

[8] Wittig F., F.Huber, Z. Electrochem. 60, 1181 (1956).

[9] Chiba Y., T. Matsushima, and K. Ono, Tohoku Daigaku Kagaku Keisoku, Kenkyusho Hokoku 20, 41 (1964).

[10] Aptekar I., V. Baskakova, USSR, Izv. Akad. Nauk SSSR, Metal. 6, 192 (1970).

[11] Blecic D., B. Dobovisek, Rud.-Metal. (Yugoslavia) 27, 291 (1980).

[12] Gladkikh N., S. Chizhik, V. Larin, L. Grigor'eva, A. Samsonik, and V. Sukhov, Izv. Akad. Nauk SSSR, Met. 1, 176 (1987).

[13] Savvin V., O. Mikhaleva, and A. Povzner, Ural. Gos. Tekh. Univ., Yekaterinburg, Russia, Rasplavy 2, 42 (2001).

[14] Lee B., C. Oh, and J. Shim, J. Electronic Mater. 25, 983 (1996).

[15] Asryan N, Mikula A (2004) Z Metallkd 95: 132

[16] Wittig FE, Huber F (1958) Z Phys Chem (Frankfurt) 18: 330

[17] Yazawa A, Kawashima T, Itagaki K (1968) J Jpn Inst Met 32: 1281

[18] Sharkey RL, Pool MJ (1972) Met Trans 3: 1773

[19] Seltz H, Dunkerley FJ (1942) J Am Chem Soc 64: 1392

[20] Flandorfer H, Sabbar A, Luef C, Ipser H (2005) Publication in preparation

[21] Dinsdale A., A. Watson, A. Kroupa, J. Vrestal, A. Zemanova, J. Vizdal COST 531 Thermodynamic Database for Lead-free Solder Alloys, Version 2.0 (2006)

[22] Ohtani H., K. Ishida: Journal of Electronic Materials, 1994, 23(8), 747-755

[23] Malakhov D, X. J. Liu, I. Ohnuma, R. Kainuma, H. Ohtani, K. Ishida, Mat. Trans. 2002, 43, 1879

[24] Dinsdale A., A. Watson, A. Kroupa, J. Vrestal, A. Zemanova, J. Vizdal COST 531 Thermodynamic Database for Lead-free Solder Alloys, Version 2.1b (2006)

[25] Predel B., in Landolt-Bornstein, Numerical Data and Functional Relationship in Scinece and Technology, New Series, O. Madelung , Ed., Group IV: Macroscopic and Technical Properties of Matter, Vol. 5, Phase Equilibria, Crystallograpchic and Thermodynamic Data of Binary Alloys, Subvolume b, B – Ba…C – Zr, Springer-Verlag, Berlin, 1992, p 211 – 212

[26] Nash P. , A. Nash, Phase Diagrams of Binary Nickel Alloys, E., ASM, 1991, p 310

[27] Portevin M. A., The Alloys of Nickel and Bismuth, Rev. Metall, Vol. 5, 1908, p 110 – 20

[28] Voss G., The Nickel – Bismuth System, Z. Anorg. Chem., Vol 57, 1908, p 52 – 58

[29] Iwase M., A. McLean: Met. Trans. B 14B (1983) 765–767.

[30] Predel B., H. Ruge: Thermochi. Acta 3 (1972) 411.

[31] Perring L., J. J. Kuntz, F. Bussy, J.C. Gachon: Intermetallics, 7 (1999) 1235.

[32] Yoshida H., T. Shima, T. Takahashi,T. Kaneko, T. Suzuki, H.M. Kimura, K. Asami, A. Inoue: J. Magnetism and Magnetic Materials 239 (2002) 5.

[33] Barin I. Thermochemical Data of Pure Substances, vol. I and II, VCH, Weinheim, 1993.

[34] Vassilev G.P., X.J. Liu, K. Ishida: J. Phase Equilibria and Diffusion (JPED) 26 (2005) 161.

[35] Vassilev G.P., J. Romanowska, G. Wnuk, IJMR (Z. Metllkde.) (2006) accepted

[36] Kang S.K., R.S. Rai, and S. Purushothaman, J. Electron. Mater. 25, 1113 (1996)

[37] Tao W. H., C. Chen, C. E. Ho, W. T. Chen, and C. R. Kao, Selective Interfacial Reaction between Ni and Eutectic SnBi Lead-Free Solder, Chem. Mater. 2001, 13, 1051-1056

[38] Lee, Jou-I, Chen, Sinn-Wen, Chang, Hsiu-Yu, Chen, Chih-Ming, Reactive wetting between molten Sn-Bi and Ni substrate, Journal of Electronic Materials, Mar 2003

[39] Vassilev G.P., K.I. Lilova, J.C. Gachon, Thermodynamic investigations of the Ni–Sn–Bi system, submitted to International Journal of Materials Research

[40] Kubaschewski O., C.B. Alcock: Metallurgical Thermochemistry. Perg. Press, Oxford (1972) 237.

[41] Vassilev G.P., K.I. Lilova, J.C. Gachon, Therm. Acta, 447 (1) (2006) 106–108

[42] Vassilev G.P., K.I. Lilova, J.C. Gachon, Calorimetric studies of the Ni-Sn system, In: Proceedings of VIIth Int. Workshop of Assoc. Phase Diagram and Thermod. Committee, Košice, Slovakia, 19 November 2005, Ed. W. Zakulski, ISBN 83-921845-5-6, Published by: Ins. Met. and Mat. Sc., Polish Academy of Sciences, Krakow, Poland, p. 27 – 34

[43] Ghosh G., Metall. Mater. Trans., 30A (1999) 1481

[44] Liu H., J. Wang, Z.P. Jin, CALPHAD 28 (2004) 363

[45] Vassilev G.P., Z. Metallkunde 95(9) (2004) 813-817

[46] Vassilev G.P., E. Dobrev , J.-C. Tedenac, JALCOM, 399 (2005) p. 118-125.

[47] Hägg G., G. Funke, Z. Phys. Chem. B 6, 272 (1929) (in German).

[48] Zhuravlev N., G. Zhdanov, E. Smirnova, Fizika metallov i metalloved (Russian journal of physical metallurgy) 13, 62 (1962) (in Russian).
[49] Villars P. (Editor), Pearson's Handbook Desk Edition, ASM International, 1997, ISBN 978-0-87170-603-4, OH, USA.

General Contributions

Systems constituted by transition metals (Co, Ni) with Sn and Bi were investigated by means of calorimetry, thermodynamic calculations and phase equilibria studies. These metals and alloys are prospective as:

A. components of new lead-free solders (Ni-Sn-Bi, Sn-Bi, Ni-Sn, Co-Sn);

B. substrates in electronic circuits (Ni)

C. electroplated layers (Ni-Sn, Co-Sn)

The most important contributions of the works are outlined bellow.

New thermochemical data

- Experimental calorimetric data about enthalpies of formation of the following solid phases of the binary systems Co–Sn, Ni–Sn: Co_3Sn_2, CoSn and $CoSn_2$, $CoSn_3$, Ni_3Sn_LT, Ni_3Sn_2_LT and Ni_3Sn_4, Ni_3Sn_HT, Ni_3Sn_2_HT. No thermochemical information was available in the literature for the latter two compounds.
- The enthalpies of formation of Bi-dotted Ni–Sn based solid phases were found to be comparable with these of the respective binary Ni-Sn compounds.
- Enthalpies of formation of liquid phases are measured in the systems Co–Sn, Ni–Sn–Bi. The existence of a temperature dependence of the Co–Sn enthalpy of mixing was confirmed.
- Thermodynamic re-optimization of the Co–Sn system was done and a set of optimized parameters was obtained. Good agreement is observed between experimental and calculated with optimized coefficients enthalpies of formation of this system. The deviations from ideal solutions behaviour are larger for the Ni-Sn system.

New topological data

- A formerly unknown ternary compound with approximate formula Ni_6Sn_2Bi was found in the system Ni-Sn-Bi.
- The willingness of the system Co-Sn to form metastable phases is confirmed. Namely, a metastable phase with formula Co_2Sn was observed.

- Three isothermal sections are constructed in the formerly known system Ni–Sn–Bi. Ternary eutectic point Ni–Sn–Bi is found thus showing the suitability of these alloys for lead-free solders.
- Topological and thermochemical data for phase transitions and phase equilibria in the systems Co-Sn, Ni-Sn and Ni-Sn-Bi were obtained: transition temperature (between low and high-temperature forms of Co_3Sn_2, $CoSn_3$, Ni_3Sn_2 compounds), enthalpy of transition (Co_3Sn_2, Ni_3Sn_2 compounds), etc.